RHEOLOGY AND PROCESSING OF BIODEGRADABLE POLY(ε-CAPROLACTONE) POLYESTERS AND THEIR BLENDS WITH POLYLACTIDES

by

Nazbanoo Noroozi

BSc. Amirkabir University of Technology Iran, 2002
MSc. Amirkabir University of Technology Iran, 2004

A THESIS SUBMITTED IN PARTIAL FULFILLMENT OF
THE REQUIREMENT FOR THE DEGREE OF

DOCTOR OF PHILOSOPHY

in

The Faculty of Graduate Studies

(Chemical and Biological Engineering)

THE UNIVERSITY OF BRITISH COLUMBIA

(Vancouver)

January 2013

Abstract

The solution rheological properties and melt viscoelastic behaviour of a number of commercial and newly synthesized PCLs with different molecular characteristics was investigated using both rotational and extensional rheometry. The variation of zero-shear viscosity and relaxation spectrum with molecular weight were found to be in agreement with theories for linear polymers. The classic Wagner model was found to represent the rheology of all PCL polymers quite well. In addition, the PCL processing instabilities were studied by capillary extrusion. Sharkskin and gross melt fracture was observed for the high molecular weight PCL at different shear rates. The onset of melt fracture occurred at 0.2 MPa at temperatures higher than 115°C. Moreover, addition of 0.5 wt% of a polylactide (PLA) into the PCL eliminated or delayed the onset of melt fracture to higher shear rates.

The thermodynamics and rheological behavior of PCL/PLA blends has been studied in an attempt to find ways to improve the mechanical properties of PCL. The effects of shear and heating rates on the determination of the phase separation boundary of the PCL/PLA blend system were studied in detail. The lower critical solution temperature (LCST) phase boundary for this system is shifted based on the frequency, heating rate and concentration of the components. Additionally, higher molecular weight amorphous PLA leads to phase separation boundary shifted to lower temperatures.

Differential scanning calorimetry (DSC) thermograms of PCL/PLA blends exhibit separate melting peaks, which are indicative of immiscible structure at all compositions in agreement with the phase diagram. Scanning electron microscopy (SEM) images have shown droplet morphology of PCL into PLA matrix up to 40wt% of PCL. Above this concentration the co-continuous morphology starts to appear, which becomes again droplet morphology for blends with PCL concentration above 60wt%. The viscoelastic studies in the phase separated region have shown the enhancement of the elastic modulus of blends at small frequencies, which is a signature behavior of immiscible systems due to the presence of interface and interfacial tension contribution to the stress. Emulsion models were found to be successful in the prediction of viscoelastic behavior at the compositions which corresponds to droplet morphology.

Preface

The work of this thesis consists of *four* different manuscripts.

Chapter 5 and part of chapter 6 are based on manuscript that has been published. Noroozi, N., Thomson, A.J., Noroozi, N., Schafer, L.L., Hatzikiriakos, S.G. (2012). "Viscoelastic behaviour and flow instabilities of biodegradable poly (ε-caprolactone) polyesters". *Rheologica Acta*, 51(2), 179-192.

Part of chapter 6 is based on a manuscript that has been accepted. Jazrawi, B., Noroozi, N., Ansari, M., Hatzikiriakos, S.G. (2012). "Processing Aids for Biodegradable Polymers". Accepted for publication in *Journal of Applied Polymer Science*.

The materials covered in chapters 7 has been prepared based on a submitted manuscript. Noroozi, N., Schafer, L.L., Hatzikiriakos, S.G. (2012). "Influence of dynamic conditions on phase separation of incompatible biodegradable blends".

Chapter 8 is based on a manuscript that has been published. Noroozi, N., Schafer, L.L., Hatzikiriakos, S.G. (2012). "Thermorheological properties of poly (ε-caprolactone)/polylactide blends". *Polymer Engineering & Science*, 52(11), 2348-2359.

All the experiments and data analysis have been performed by myself. Jaclyn A.Thomson synthesized the PCLs and performed the GPC measurements. Part of the Wagner modeling was performed in collaboration with Nader Noroozi. Part of the processing aid examination was performed by Bashar Jazrawi. The manuscripts were a collaborative effort between my supervisors Prof. Savvas G.Hatzikiriakos and Prof. Laurel Schafer and myself.

The initial and final drafts of this thesis were prepared by Nazbanoo Noroozi, with revisions edited and approved by Prof. Savvas G. Hatzikiriakos and Prof. Laurel Schafer.

Table of Contents

List of Tables

List of Figures

Nomenclature

A	cross-sectional area (m^2)
A_o	initial cross-sectional area (m^2)
a_T	horizontal shift factor
b	Rabinowitsch correction
b_T	vertical shift factor
D	capillary diameter (m)
D_b	diameter of barrel (m)
E_a	activation energy for flow (J/mol)
$F(t)$	instantaneous extensional force at time t (N)
F_F	frictional force (N)
$G(\gamma,t)$	stress relaxation modulus (Pa)
G'	storage modulus (Pa)
G''	loss modulus (Pa)
$\lvert G^* \rvert$	complex modulus (Pa)
G_N^o	plateau modulus (Pa)
g_i	generalized Maxwell model parameter, relaxation modulus (Pa)
$h(\gamma)$	damping function
ΔH_c	enthalpy of crystallization
ΔH_m	enthalpy of fusion
L/D	length to diameter ratio of the capillary die
L,Lo	capillary length; sample length (m)
M_c	critical molecular weight (kg/mol)
M_e	molecular weight between entanglements (kg/mol)
M_n	number average molecular weight (kg/mol)
M_w	weight average molecular weight (kg/mol)
M_w/M_n	Polydispersity index
P	absolute pressure (Pa)
P_d	driving pressure (Pa)

P_{end}	Bagley correction (Pa)
Δp	pressure drop (Pa)
Q	volumetric flow rate (m^3/s)
R	capillary radius (m)
R	radius of SER windup drums (m), gas constant (J/K.mol)
R_c	critical radius of nucleation (m)
R_g	radius of gyration (m)
R_h	hydrodynamic radius (m)
R_n	number average radii of droplets (m)
R_v	volume average radii of droplets (m)
R^*	Taylor break-up size
T	absolute temperature (k), torque (N.m)
T_b	binodal temperature (°C)
T_c	crystallization temperature (°C)
T_d	degradation temperature (°C)
T_g	glass transition temperature (°C)
T_m	melting temperature (°C)
T_s	spinodal temperature (°C)
T_0	reference temperature (°C)
t	time (s)
u_s	slip velocity (m/s)

Greek Letters

γ	shear strain, surface tension
$\dot{\gamma}$	shear rate (s^{-1})
$\dot{\gamma}_a$	apparent shear rate (s^{-1})
$\dot{\gamma}_{a,s}$	apparent shear rate corrected for slip (s^{-1})
$\dot{\gamma}_w$	wall shear rate (s^{-1})
γ_o	strain amplitude in oscillatory shear
δ	phase shift angle, solubility parameter

ε_b	elongation at break (%)
ε_H	Hencky strain
$\dot{\varepsilon}_H$	Hencky strain rate (s^{-1})
$[\eta]$	intrinsic viscosity (Pa.s)
η_o	zero-shear viscosity (Pa.s)
η^*	complex viscosity (Pa.s)
η^+	steady shear stress growth coefficient (Pa.s)
η_E^+	tensile stress growth coefficient (Pa.s)
λ_i	generalized Maxwell model parameter, relaxation time (s)
ρ	density (kg/m^3)
ζ	semi macroscopic length (m)
σ	shear stress (Pa)
σ_a	apparent shear stress (Pa)
σ_c	critical shear stress for the onset of melt fracture (Pa)
σ_w	wall shear stress (Pa)
ω	frequency (rad/s), angular speed (s^{-1})
Ω	Rotational rate of the SER shaft (s^{-1})
χ	Flory-Huggins interaction parameter

Abbreviations

ASTM	American society for testing and materials
DSC	differential scanning calorimeter
G-M	Gramespacher –Meissner equation
GPC	gel permeation chromatography
HBP	hyperbranched polymer
HDPE	high density polyethylene
ISO	international standardization organization
K-BKZ	Kaye-Bernstein, Kearsley and Zapas

KMHS	Kuhn-Mark-Houwink-Sakurada
LCST	lower critical solution temperature
LDPE	low density polyethylene
LTI	lysine triisocyanate
LVE	linear viscoelastic
PBS	polybutylene succinate
PBSA	poly(butylene succinate-co-butylene adipate)
PCL	poly(ε-caprolactone)
PE	polyethylene
PEG	polyethylene glycol
PEO	poly(ethylene oxide)
PES	poly(ethylene succinate)
PET	polyethylene terephthalate
PGA	poly(glycolic acid)
PHB	poly(β-hydroxybutyrate)
PLA	poly(lactide) or poly(lactic acid)
PP	polypropylene
PPO	polypropylene oxide
PS	polystyrene
POM	polarized optical microscopy
PVC	poly(vinyl chloride)
PVME	polyvinyl methacrylate
RG	renormalization group theory
ROP	ring-opening polymerization
THF	tetrahydrofuran
SEM	scanning electron microscopy
SER	Sentmanat Extensional Rheometer
WLF	Williams-Landel-Ferry

Acknowledgements

I would like to express my eternal gratitude to my supervisor, Prof. Savvas G. Hatzikiriakos and my co-supervisor, Prof. Laurel Schafer for their influential guidance, encouragement, patience and tremendous concern for the success of this research work. Additionally, I would like to acknowledge my supervisory committee members, Prof. Anthony Lau and Prof. Parisa Mehrkhodavandi.

It was a great pleasure working with a diverse group of people in the Rheology lab. I would like to thank them, both past and present colleagues for their support. I also thank Jaclyn A. Thomson from the Chemistry Department for synthesizing the polymer samples.

I would like to gratefully acknowledge NSERC for the financial support of this research project. Also I thank Perstorp and Natureworks LLC for providing the materials.

Most importantly, my heartfelt gratitude to those who matter to me the most, my parents and my brother.

To my wonderful parents,
Homeira and Saeid,
and the best brother, Nader,
whose support, encouragement, sacrifice and love
made all this possible...

1 Introduction

Production of more than 130 million ton/year of synthetic plastics and the disposal of over 10 million ton/year of synthetic plastics makes disposal management a major concern (Kolybaba et al. 2003). Biodegradable polymers are possible solution to control the non-biodegradable waste disposal problem associated with petroleum-derived plastics. This has raised great interest in research about these materials (Mohanty et al. 2000, Nair and Laurencin 2007). Biodegradable polymers can be defined as macromolecules that undergo degradation through the action of living organisms. The most important biodegradable polymers of defined chemical structure are aliphatic polyesters including poly-lactides (PLA), poly (ε-caprolactone)s (PCL), poly(ethylene oxide) (PEO) and poly(β-hydroxybutyrates) (PHB) (Mohanty et al. 2000).

PCL (poly ε-caprolactone) is a semi-crystalline aliphatic polyester with high flexibility and biocompatibility. It is produced by ring opening polymerization (ROP) of cyclic ester monomer, lactone (Mohanty et al. 2000). In the past decade, great interest has been given back to PCL not only as a replacement of non-degradable polymers for common applications but also as a specific plastic for select applications in the medical and agricultural sector (Ray and Bousmina 2005, Grossvenor and Staniforth 1996, Khatiwala et al. 2008). PCL has been reported in the literature to have several applications such as powder coating of pharmaceutical tablets, controlled release drug carriers, interfacial agent in the fluoropolymers process aids formulation (Oriani and Chapman 2003), microparticles for drug delivery and polymeric scaffolds for tissue engineering (Hutmacher 2000). PCL is of great importance due to biodegradability, biocompatibility, low glass transition temperature and low melting point (Nair and Laurencin 2007, Hutmacher 2000). In this study, commercial PCLs as well as controlled macrostructure PCL samples synthesized *via* ROP using novel homoleptic amidate complexes of yttrium were investigated (Stanlake et al. 2008).

In spite of its great technological importance very few studies exist particularly on its rheological and processing behaviour. Investigation of viscoelastic properties of PCL is necessary to address the possible flow instabilities in processing such as wall slip and various types of melt fracture (Hatzikiriakos and Dealy 1991, 1992a).

As mentioned above, biodegradable polymers such as poly(ε-caprolactone) (PCL) and polylactides (PLA) are considered as potential substitutes for conventional plastics. However

some drawbacks such as the brittleness of PLA and low modulus of PCL are prohibiting factors for a wide range of applications and processing of these materials (Ray and Bousmina 2005, Nair and Laurencin 2007). Blending of these polymers with other biodegradable polymers offers a way to maintain the best attributes of these polymers without compromising the biodegradability. Blending offers more simplicity in tailoring resulting properties compared to other strategies such as copolymerization and addition of nanoparticles. Moreover, blending PCL with PLA improves the mechanical properties compared to individual components (Broz et al. 2003, Chen et al. 2003, Lopez-Rodriguez et al. 2006). In multicomponent systems, the final properties are highly influenced by the properties of the individual constituents and miscibility between these components. In spite of the close solubility parameters (δ) of PCL and PLA, 9.2 $(cal/cm^3)^{1/2}$ and 10.1$(cal/cm^3)^{1/2}$ respectively (Coleman et al. 1990), lack of specific interactions between PCL and PLA leads to immiscibility in PCL/PLA blends, which highlight the role of interfacial tension on the properties of these blends (Lopez-Rodriguez et al. 2006). PCL/PLA blends are composed of at least one crystalline component, which results in complex phase behavior. The lower critical solution temperature (LCST) phase behavior at a temperature range above the melting point of PCL has been previously reported for PLA and PCL system (Meredith and Amis 2000). However, to the best of our knowledge, the rheological behavior of these blends in the transitional region has never been reported. Moreover, there are no studies addressing the effects of molecular characteristics on the phase diagram of these systems. In addition, the influence of shear flow on the phase transition has not been studied yet into much detail. The rheological response in the transitional area of bi-component systems has been employed before to study their thermodynamics and to obtain the critical solution temperature of various blend systems (Ajji and Choplin 1991a, Vlassopolous et al. 1997, Chopra et al. 1998, Zhang et al. 2001). A number of theoretical models generally called emulsion models have been developed to predict the viscoelastic properties of the immiscible polymer blends from the properties of the pure components (Gramespacher and Meissner 1992, Graebling et al. 1993, Bousmina 1999). These models are based on the assumptions made for the case of Newtonian emulsions considering the linear viscoelastic properties of the phases and the contribution of the interfacial tension effect to the stress tensor.

The main objective of this thesis is to extensively study the rheological and processing properties of several controlled macrostructure PCL homopolymers as well as some commercial PCLs over a wide range of molecular weights. The phase separation of PCL/PLA blend system will also be investigated by using a rheological approach for different molecular weights of the individual components. The rheological behavior of the blends in the transitional and the phase separated regions will also be studied. In addition, the effect of PLA and/or PCL on the crystallinity, thermal characteristics and the mechanical properties of the other component will be investigated as well. Morphological studies will also be performed to determine the morphology of the blends as a function of blend composition. A number of emulsion models will be used to predict the viscoelastic response of the blends. The effect of molecular weight of the components and viscosity ratio on the applicability of these emulsion models will also be addressed.

2 Literature Review

2.1 Biodegradable Polymers

Conventional plastics such as polyolefins, polystyrene (PS) and poly (vinyl chloride) (PVC) have found many applications in packaging, automotive and medical sectors. However, the short term application of these plastics compared to their overall life time, raises serious concerns related to environmental contamination (Gross and Kalra 2002). Although recycling has been addressed in the past as a way to control the plastic waste accumulation, only a few types of plastics such as polyethylene terephthalate (PET) and poly (vinyl chloride) (PVC) have successfully been recycled.

In the past two decades the approach to have highly resistant plastics for many applications turned into biodegradable plastics as a sustainable choice to manage the enormous amount of plastic waste in the environment. Indeed, biodegradable polymers become a rapidly growing field of academic and industrial interest. However, commercialization of biodegradable polymers in competition with conventional plastics remains a challenge.

According to the international organizations such as the International Standardization Organization (ISO) and the American Society for Testing and Materials (ASTM), there are different definitions and criteria for biodegradable polymers and biodegradability. ASTM D6400, D6868 and D7081 specify that biodegradable polymers are the materials that undergo biodegradation and change in chemical structure through the action of enzymes and active microorganisms such as bacteria, fungi and actinomycetes. Biodegradation happens in the temperature range of 20 to 60°C and in neutral or slightly acidic environment (Kolybaba et al. 2003). Full biodegradation corresponds to the full transformation of polymer into the low-molecular-weight molecules of water, carbon dioxide and microbial biomass. Based on ASTM D6400, 90% degradation of the polymer in less than 180 days is required as a criterion for a polymer to be accepted as a biodegradable material (Song et al. 2009). The products of biodegradation are nontoxic and integrate into the living cycle of other organisms as a survival resource (Narayan 2006).

The biodegradation process or erosion of polymer chains into short fragments includes hydrolytic or enzymatic cleavage of selected bonds in the polymer chain and also physical bond break down (Nair and Laurencin 2007). Polymer characteristics such as

crystallinity and molecular weight affect the biodegradation significantly (Ikada and Tsuji 2000).

Biodegradable polymers can be classified into two categories based on their origin: Natural and synthetic biodegradable polymers. Natural biodegradable polymers can be sub classified into the natural polymers, and modified natural polymers. Synthetic biodegradable polymers can be synthesized from monomers obtained from petroleum products or monomers with natural origin (Ray and Bousmina 2005).

2.1.1 Natural Biodegradable Polymers

Natural biodegradable polymers are materials of natural origin such as naturally available polysaccharides, proteins and poly(β-hydroxyalkanoates) or naturally modified such as cellulose acetate. The modified polymers have improved processability and mechanical properties compared to the natural polymers. Poly(β-hydroxyalkanoate)s are synthesized from microbial fermentation of bacteria.

Table 2.1 Natural Biodegradable Polymers, adapted from Ikada et al. (Ikada and Tsuji 2000)

Natural	***Natural Modified***
Plant origin polysaccharides: Cellulose, Starch, Alginate	Cellulose acetate
Animal origin polysaccharides: Chitin (Chitosan), Hyaluronate	Starch Plastics
Microbe origin polysaccharides: Hyaluronate	
Microbe origin polyesters: Poly(β-hydroxyalkanoate)	
Proteins: Collagen (Gelatin), Albumin	

The most notable poly(β-hydroxyalkanoate) is poly(β-hydroxybutyrate) (PHB) which is commercially available in a limited way. However, weak processability and high brittleness are major drawbacks of this material. Examples of natural biodegradable polymers are summarized in Table 2.1 (Ikada and Tsuji 2000, Mohanty et al. 2000).

2.1.2 Synthetic Biodegradable Polymers

Aliphatic polyesters are one of the most important classes of synthetic biodegradable polymers. They can be classified into poly(α-hydroxy acid)s, poly(ω-hydroxyalkanoate) which consist of hydroxy acids as a repeating unit, and poly(alkylene dicarboxylate) which are products of polycondensation polymerization of diols and dicarboxylic acid. Polyester amides are another class of synthetic biodegradable polymers (Mohanty et al. 2000, Flieger et al. 2003). Synthetic biodegradable polymers can be synthesized from petroleum-based or renewable-based monomers.

Poly(α-hydroxy acid)s such as poly(lactic acid) (PLA) and poly(glycolic acid) (PGA) are thermoplastic polyesters with high melting points which can be synthesized by condensation polymerization or ring opening polymerization (ROP) to obtain high molecular weight polymers (Reddy et al. 2003). PLA has attracted high interest because of the possibility of synthesizing it from renewable resources such as corn. PLA is a hydrophobic polymer that can be degraded in the presence of enzymes and via a hydrolytic degradation process of the ester backbone. Lactides are available in different isomers of L or D which results crystalline PLLA and PDLA and amorphous PDLLA polymers. PLLA has a melting temperature of about 175°C and a glass transition temperature of 60°C. PLLA has higher tensile strength compared to the amorphous PDLLA (Nair and Laurencin 2007).

Poly(alkylene dicarboxylate) is commercially available as Bionolle® in various grades such as polybutylene succinate (PBS), poly(butylene succinate-co-butylene adipate) (PBSA) and poly(ethylene succinate) (PES) which are available in high molecular weights. Bionolle® polymers are synthesized by polycondensation of glycols and aliphatic dicarboxylic acids. Bionolle® polymers resemble with polyolefins, with a glass transition temperature (T_g) between those of polyethylene (PE) and polypropylene (PP), which are -45°C to -10°C and good processability in the same temperature range as polyolefins (160-200°C).

The poly(ω-hydroxyalkanoate) group is another aliphatic polyester which is mostly known by poly(ε-caprolactone) (PCL). PCL is discussed in detail hereafter.

2.1.3 Poly(ε-caprolactone) (PCL)

Poly(ε-caprolactone) (PCL) is a 6-carbon numbered polymer from the family of poly (ω-hydroxyalkanoate)s aliphatic polyesters. Figure 2.1 illustrates the chemical structure of poly(ε-caprolactone) polymer. PCL consists of hexanoate as a repeating unit. PCL is semi-crystalline, hydrophobic, biodegradable linear polyester, which has low glass transition (T_g) of –60ºC and melting temperature (T_m) of 60ºC. At room temperature, it is a tough polymer with low tensile modulus between those of low density polyethylene (LDPE) and high density polyethylene (HDPE) and high elongation at break (ε_b) >400% (Arraiza et al. 2007). The degree of crystallinity of PCL can reach the level of 69% (Labet and Thielemans 2009). It has been reported that the degree of crystallinity of PCL decreases with increasing molecular weight (Woodruff and Hutmacher 2010).

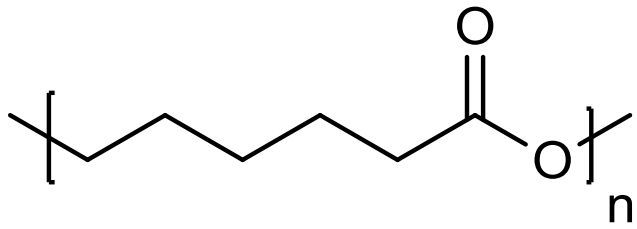

Figure 2.1 Structure of poly(ε-caprolactone)

The degradation time for PCL varies between several months to several years (up to 4 years), which depends on the molecular weight, degree of crystallinity and the conditions of the exposed environment. Full degradation of PCL may happen in the presence of microorganisms (Shimao 2001). Degrading agents attack the amorphous phase first, which leads to increasing crystallinity, while the molecular weight remains unchanged. Following that, ester cleavage results in loss of molecular weight (Gross and Kalra 2002, Ikada and Tsuji 2000). PCL degrades in hydrolytic as well as the enzymatic process by the random ester cleavage of carbonyl groups and then enzymatic surface erosion (Jenkins and Harrison 2006). PCL is soluble in many solvents such as chloroform, dichloromethane, toluene and

benzene at room temperature. In addition, PCL has partial solubility in acetone and dimethylformamide (Labet and Thielemans 2009).

Miscibility, biodegradability and biocompatibility of PCL are rare properties that makes PCL a significant polymer to investigate. PCL is miscible with a number of polymers such as poly (vinyl chloride) (PVC) and is a good candidate for blending and tailoring its properties (Woodruff and Hutmacher 2010). Currently PCL is sold under two major trademarks of Capa® and Tone® produced by Perstorp and Union Carbide, respectively. Some of the typical thermophysical and mechanical properties of PCL are reported in Table 2.2 (Labet and Thielemans 2009).

Table 2.2 Thermophysical mechanical properties of PCL, adapted from Labet et al. (Labet and Thielemans 2009).

Property	***Value***
Density, ρ (gcm^{-3})	1.071–1.200
Glass transition temperature, T_g (°C)	(-65)–(-60)
Melting temperature, T_m (°C)	56–65
Decomposition temperature, T_d (°C)	350
Tensile strength, σ (MPa)	4–785
Young modulus, E (GPa)	0.21–0.44
Elongation at break, ε_b (%)	20–1000

2.1.4 Polymerization of Poly(ε-caprolactone)

There are two main polymerization methods for polyesters including poly(ε-caprolactone), namely: polycondensation polymerization and ring opening polymerization (ROP). The polycondensation polymerization has been reported as early as the 1930s by the esterification process of diols and dicarboxylic acids. Producing polymers with molecular weights even up to 30,000 g/mol with this technique requires high temperature and long reaction time. This level of molecular weight results in moderate mechanical properties. Also control over the polydispersity and obtaining nearly monodisperse polymer with this method is hardly achievable. In addition, byproducts of polycondensation such as water should be constantly removed during the reaction (Okada 2002). Dong et al. (1998) reported the synthesis of a

PCL with the molecular weight of 5400 g/mol and polydispersity of 2.2 produced in a polycondensation reaction of ethyl 6-hydroxyhexanoate after 20 days (Dong et al. 1998, Labet and Thielemans 2009).

Ring opening polymerization is an alternative efficient method to produce biodegradable polyesters in shorter reaction time and at a lower polymerization temperature with the ability to have control over the molecular weight and molecular weight distribution. This method mainly involves ring opening polymerization (ROP) of the cyclic ester monomer, lactone. The structure of lactone monomer is shown in Figure 2.2. Based on the catalytic system, ROP can be classified into the following groups: Cationic, anionic, monomer activated and coordination-insertion ROP.

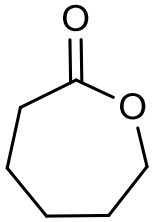

Figure 2.2 The molecular structure of ε-caprolactone

Cationic and anionic ring opening polymerization proceeds by the formation of cationic and anionic species. Scandium triflouromethanesulfonate, $Sc(OTf)_3$ has been used as a catalyst for cationic living ring opening polymerization (Okada 2002) as shown in Figure 2.3. ROP of monomer activated method proceeds by the activation of the monomer molecules by a catalyst. Coordination-insertion ring opening polymerization is known as the most common technique for this type of polymerization, which occurs by the coordination of the monomer to the catalyst and insertion of the metal-oxygen bond of the catalyst.

The presence of catalyst and initiator in a polymerization system can be associated with the intermolecular and intramolecular transesterification as side reactions. These reactions may lessen the molecular weight and broaden the molecular weight distribution. The occurrence of these side reactions is normally at the later stages of polymerization (Labet and Thielemans 2009).

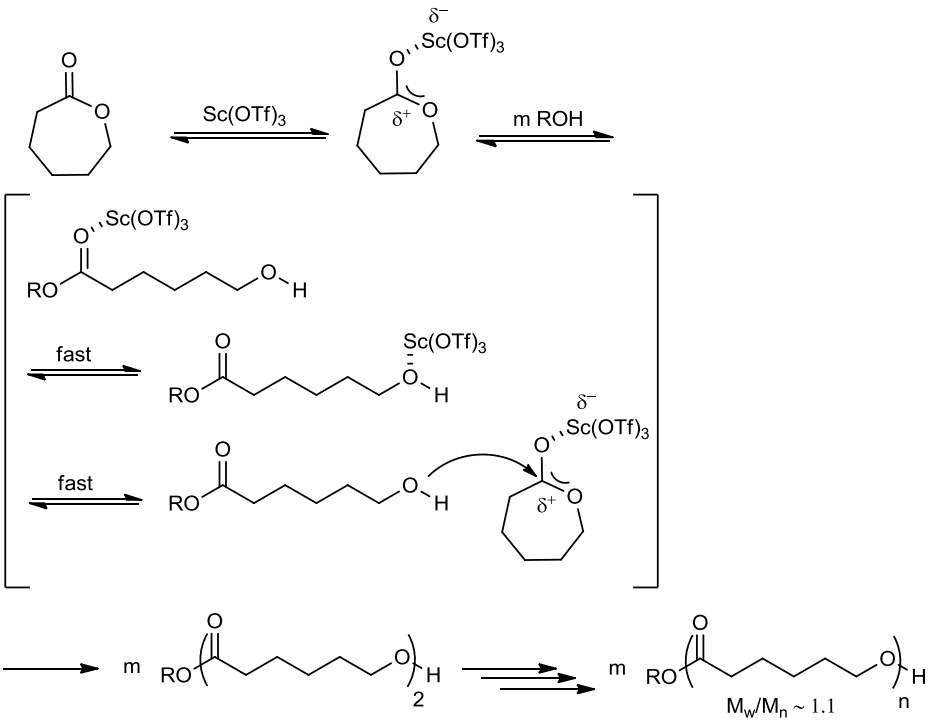

Figure 2.3 Possible mechanism of cationic living ring opening polymerization of ε-caprolactone by $Sc(OTf)_3$ as a catalyst, adapted from Okada (2002).

Figure 2.4 depicts the schematic of intermolecular and intramolecular tranesterification reactions.

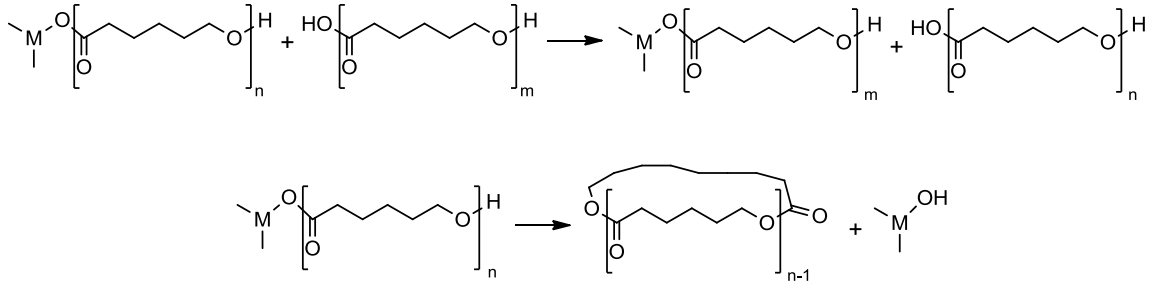

Figure 2.4 Intermolecular and intramolecular transesterification reactions in the PCL polymerization process, adapted from Labet 2009 (Labet and Thielemans 2009).

Various types of catalytic systems are used for ring opening polymerization namely metal based, organic and enzymatic catalysts. Metal-based catalysts includes alkali-based compounds, which are anionic compounds used in anionic ROP method. Transesterification side reactions results in the loss of molecular weight control in this type of catalyst (Labet and Thielemans 2009). Satisfactory results have been obtained by using metal alkoxides such as Lanthanide boronhydride complexes as a catalyst in polymerization of ε-caprolactone

(Bonnet 2005). Alkaline earth-based catalysts, poor metal-based catalysts such as aluminum based and tin-based, transition metal-based such as zirconium-based and rare earth metal-based catalysts such as scandium, lanthanum and yttrium are other catalyst systems for ring opening polymerization (ROP). Rare-earth catalysts have attracted significant attention as highly efficient catalysts that enable good control over the polymerization reaction. Rare-earth tris(amidate) complexes of yttrium have been used as initiators for the ring opening polymerization of ε-caprolactone (Stanlake and Schafer 2008). These complexes have shown significant ability to produce high molecular weight polyesters.

2.2 Rheological Analysis

Rheology is the science of flow and deformation of matter. It studies relationships between force and deformation and/or rate of deformation in the form of mathematical models (rheological constitutive equations). For molten polymers as viscoelastic complex fluids, their rheological properties are key elements in defining the processing and mechanical properties of final products (Larson 1999). An important role of rheology is to establish a relation between rheological properties and molecular structure (Malkin 1994). This can be done by means of rheometers which are devices that apply forces and measure the response of the material as a function of rate of deformation in the form of shear or extensional flow.

Shear flow is imposed in the form of drag flow or pressure-driven flow. Among different geometries generating drag flow, the concentric cylinder (Couette flow), parallel-plate and cone-and-plate rheometers are more commonly used for the molten polymers. In terms of pressure-driven flows, capillary rheometer is commonly used. In the following section, the parallel-plate, cone and plate and extensional geometries used in rheometry will be discussed in detail.

2.2.1 Rotational Rheometry

The parallel-plate geometry consists of two concentric plates with an adjustable gap between them. The lower plate is fixed and the upper plate can be rotated by a specific rotational speed (Figure 2.5). In parallel-plate, the shear rate varies within this geometry and it cannot generate uniform shearing flow (Larson 1999). Instead the cone-and-plate geometry (Figure 2.5) can be used to generate a uniform shear flow of constant shear rate using cones with a

small angle (2-5°). This geometry is able to generate a constant rate of shear and measure the first normal stress difference (Dealy and Wissbrun 1990). The measured torque by the rheometer is related to the shear stress based on different equations related to the geometry. Many types of rheological testing can be performed by the use of these geometries.

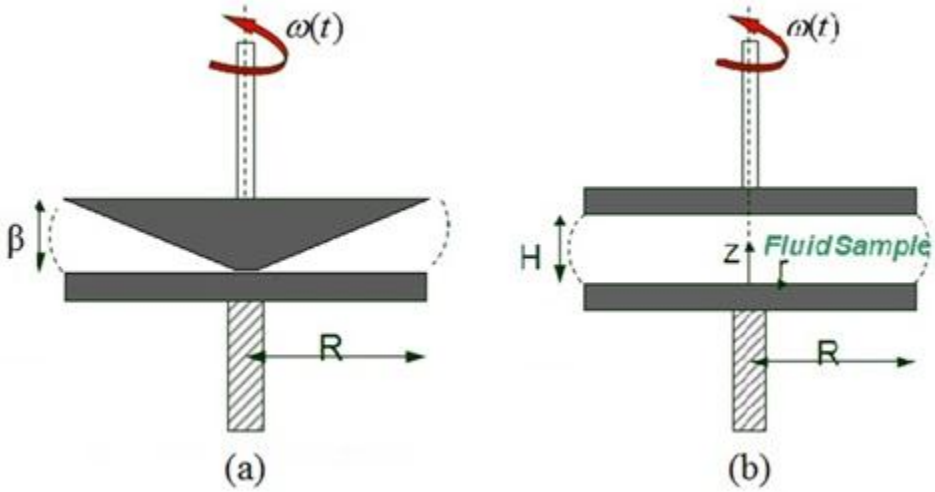

Figure 2.5 Schematics of (a) cone and plate and (b) parallel plate geometries.

One of the most commonly used experiments to determine the viscoelastic properties of polymers is the small-amplitude oscillatory shearing (SAOS). The strain, γ, varies sinusoidally with time using various angular velocities and the shear stress is measured. The applied strain is as follows:

$$\gamma(t) = \gamma_0 \sin(\omega t) \tag{2-1}$$

where γ_0 is the strain amplitude and ω is the frequency of oscillation. It can be proven for small levels of applied strains that the shear stress is also a sinusoidal function of time and the applied frequency with a phase shift angle, δ. Then the shear stress can be expressed as follows:

$$\sigma(t) = \sigma_0 \sin(\omega t + \delta) \tag{2-2}$$

The shear stress can be decomposed into the following expression by defining δ as $\tan\delta = \frac{G''}{G'}$:

$$\sigma(t) = \gamma_o \left[G'(\omega)\sin(\omega t) + G''(\omega)\cos(\omega t) \right] \tag{2-3}$$

In Equation 2.3, the first term corresponds to the in-phase response with the strain which is defined as the storage or elastic modulus (*G'*). The second term is related to the out-of-phase response or the loss or viscous modulus (*G"*). The complex modulus, G^*, is another parameter containing the elastic and viscous modulus and its magnitude is:

$$\left|G^*\right| = \sqrt{G'^2 + G''^2} \tag{2-4}$$

The complex viscosity can also be defined according to the complex modulus, containing the viscous and elastic parts, $\left|\eta^*\right| = \frac{\left|G^*\right|}{\omega}$ (Macosko 1994).

2.2.2 Extensional Rheometry

Extensional deformation has a significant role in many industrial polymer processing operations such as film blowing, blow molding, foaming, fiber spinning and thermoforming. In all dies and molds, large extensional deformation exists at the diverging and converging areas. Moreover, most products are formed outside of the die when polymer melts exits, where strong extensional conditions prevail. Uniaxial extensional flow is the simplest extensional flow that can be used in the lab to study the extensional rheological properties of molten polymers. In such an experiment, the Hencky strain is defined as the logarithmic change of the length of the sample (cylindrical or planar), *L(t)*, over time as follows:

$$\varepsilon_H(t) = \ln \frac{L(t)}{L_0} \tag{2-5}$$

where ε_H is the Hencky strain and L_0 is the initial length of the sample. Similarly, the Hencky strain rate is defined by:

$$\dot{\varepsilon}_H = \frac{1}{L_0}\frac{dL}{dt} \tag{2-6}$$

The force required to stretch the sample normalized by the instantaneous area is defined as the tensile stress by:

$$\sigma_E(t,\dot{\varepsilon}) = \frac{F(t)}{A(t)} \tag{2-7}$$

When the tensile stress is normalized by the Hencky strain rate, the tensile stress growth coefficient is obtained, defined as follows:

$$\eta_E^+(t) = \frac{\sigma_E(t,\dot{\varepsilon})}{\dot{\varepsilon}_H} \tag{2-8}$$

For Newtonian fluid the tensile stress growth coefficient is three times the shear stress growth coefficient. This ratio is called the Trouton ratio:

$$\frac{\eta_E^+(t)}{\eta^+(t)} = 3 \tag{2-9}$$

In polymeric melts this ratio is valid at low rates. Some polymers that contain branches such as low density polyethylene (LDPE), the tensile stress growth coefficient increases beyond what is indicated by Equation 2.9, a phenomenon known as strain hardening or extensional thickening and exhibits deviation from the linear viscoelastic response (Macosko 1994). It is well accepted that the extensional viscosity is highly sensitive to the molecular structure of the polymer significantly more than shear viscosity. However, generating uniform elongational deformation and accurate measurement of the extensional viscosity is a challenge especially for low viscosity polymers.

The Sentmanat Extensional Rheometer (SER) is a dual wind-up extensional rheometer with the ability to generate uniform extensional deformation with high values of Hencky strain rate up to $20s^{-1}$ under a higher environment in terms of controlled temperature (Sentmanat 2004). The sample is subjected to extensional deformation by two counter-rotating drums. Figure 2.6 demonstrates the SER schematically.

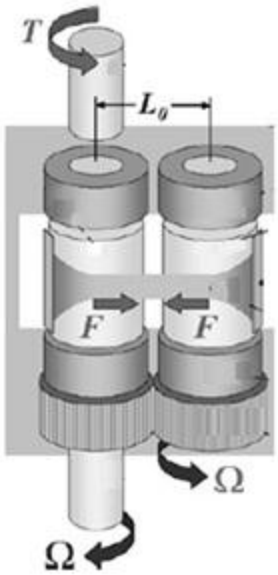

Figure 2.6 Schematic of a Sentmanat extensional fixture, adapted from Sentmanat (2004).

The Hencky strain rate can be calculated from the rotation rate of the shaft as follows:

$$\dot{\varepsilon}_H = \frac{2\Omega R}{L_0} \tag{2-10}$$

where R is the radius of wind-up drums. The torque can be measured from the applied force by the following relation:

$$T = 2(F + F_F)R \tag{2-11}$$

Due to the small share of frictional force (F_F) (less than 2%), it can be neglected. The cross sectional area of the sample changes during the measurement by the following expression:

$$A(t) = A_0 \exp(-\dot{\varepsilon}_H t) \tag{2-12}$$

According to the above-mentioned relations, at constant Hencky strain rate, the tensile stress growth coefficient can be calculated by the following equation:

$$\eta_E^+(t) = \frac{F(t)}{\dot{\varepsilon}_H A(t)} \tag{2-13}$$

where $F(t)$ is the extensional force at time t measured by the instrument from the torque signal.

2.2.3 Time-Temperature Superposition

The main idea of superposition is that the identical value of any viscoelastic function can be obtained either by changing time or by changing temperature (Malkin 1994). To fully describe the viscoelastic properties of polymers, these properties should be known over a wide range of time scales (frequencies). In practice, viscoelastic data are collected at several temperatures over a certain range of frequencies (machine limitation) and are shifted to a reference temperature to produce a master curve. This concept is called time-temperature superposition principle (Macosko 1994). The fluids that follow this principle are called thermorheologically simple fluids.

In generating the master curve, the plotted properties/parameters having a unit of time are shifted horizontally or unit of stress are shifted vertically. Figure 2.8 represents a master curve of the storage modulus for a PCL polymer constructed from the storage modulus data at different temperatures shown in Figure 2.7. The data at temperatures of 70°C and 130°C are shifted to the reference temperature of 100°C. Thus the master curve covers now a wider range of frequency. The horizontal shift factor, a_T or temperature coefficient is a factor that shows the temperature dependence of viscoelastic properties.

A commonly used relation for a_T to show its dependence on temperature is the empirical Arrhenius equation:

$$a_T = \exp\left[\frac{E_a}{R}\left(\frac{1}{T}-\frac{1}{T_0}\right)\right] \tag{2-14}$$

where T_0 is the reference temperature and E_a is the activation energy for the flow.

For temperatures well above the glass transition temperature of the polymer, the Arrhenius relationship may successfully fit the linear viscoelastic data. For temperatures close to glass transition temperature, the horizontal shift factor (a_T) can be best modeled by the William-Landel-Ferry Equation (WLF) with the empirical constants of c_1 and c_2 that can be calculated by fitting experimental data:

$$\log a_T = \frac{-c_1(T-T_0)}{c_2+(T-T_0)} \tag{2-15}$$

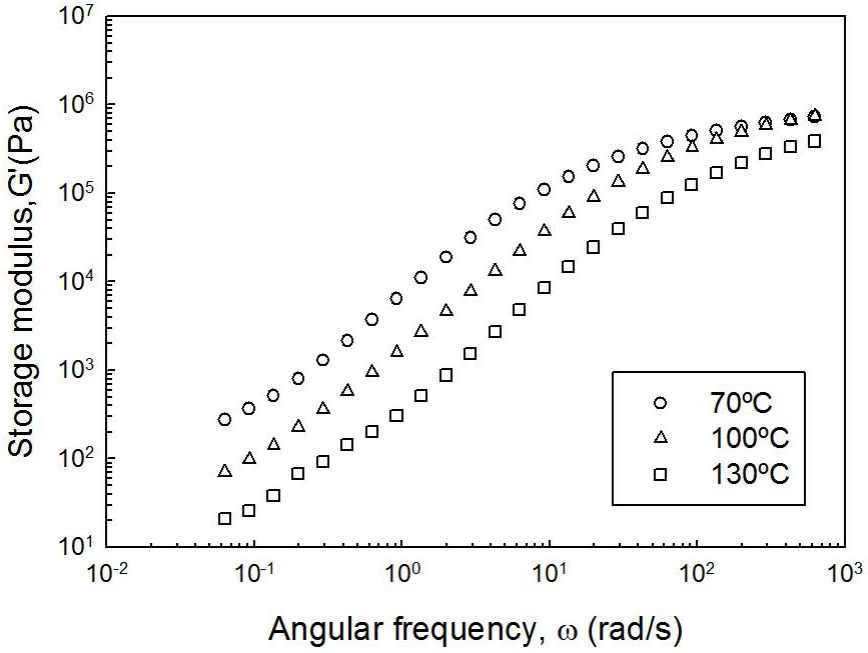

Figure 2.7 Storage modulus measured at temperatures of 70°C, 100°C and 130°C for a typical PCL melt.

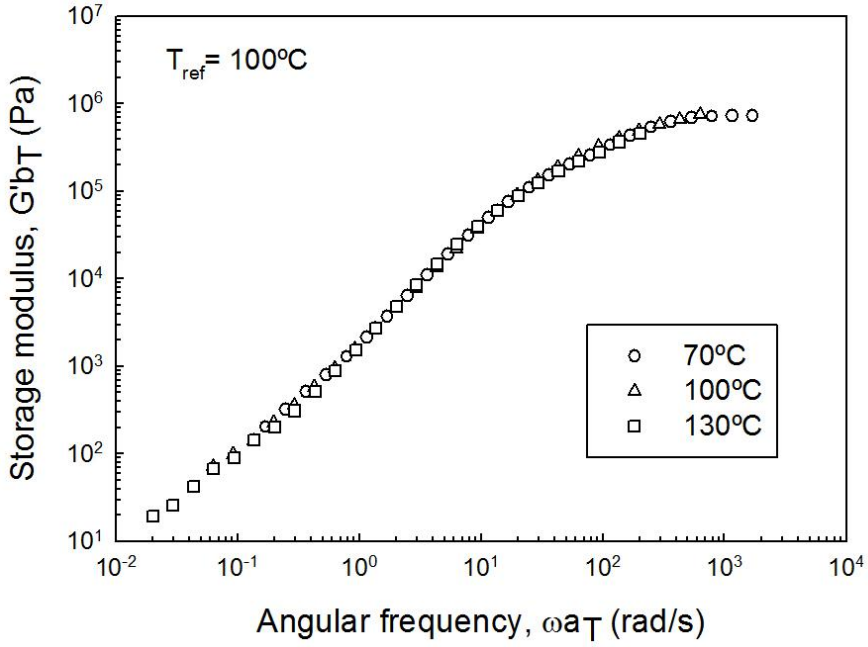

Figure 2.8 The master curve of the data presented in Figure 2.7 at the reference temperature of 100°C.

Sometimes a vertical shift factor (b_T) should be applied to the data to obtain perfect superposition of the rheological data. This reflects the temperature dependence of plateau modulus and the temperature dependence of the density of polymers. The values of vertical shift factors are typically close to unity (Dealy and Wissbrun 1999).

2.2.4 Rheological studies on Poly(ε-caprolactone)

Rheological studies on PCL have been performed by many groups although no rheological study exists to address systematically the effects of molecular parameters (Ramkumar and Bhattacharya 1998, Kapoor and Bhattacharya 1999, Grosvenor and Staniforth 1996, Acierno et al. 2006, Gimenez et al. 2000, Arraiza et al. 2007). The linear viscoelastic properties of two different molecular weight PCLs were evaluated by Kapoor and Bhattacharya (1999) exhibiting shear thinning behavior, while their viscosity curves have clearly shown a plateau at low shear rates (zero-shear viscosity). Higher molecular weight PCL started to exhibit a higher degree of shear thinning at a lower shear rate as normally expected for linear polymers. Grosvenor et al. (1996) have characterized PCLs with different molecular weights in the range of 16,900 to 35,500 g/mol. Non-linear shear thinning (pseudoplastic) behavior has been observed as a result of change in chain configuration.

The stress relaxation of PCLs has been investigated at different temperatures by Kapoor and Bhattacharya (1999). It has been reported that at higher temperature and higher shear stress values, the relaxation occurs more rapidly. In addition, it has been found that below strain values of 0.1 which are within the linear viscoelastic regime, the relaxation moduli are superposed and are independent of the strain magnitudes.

One of the first extensional rheological studies of biodegradable polymers has been performed by Kapoor and Bhattacharya (1999) by using the Meissner elongational rheometer. At low extensional rates (Hencky strain rates), linear behavior has been detected. At higher extensional rates, the transient extensional viscosity exhibited deviation from linear viscoelasticity faster than at lower rates. These observations were more pronounced at higher temperatures (130°C).

Based on rheological measurements at different temperatures, PCL has shown a shear thinning (pseudoplastic) behavior with a clear Newtonian zone at low frequencies in the temperature range of 100-160°C (Arraiza et al. 2007). In contrast Arraiza et al (2007)

reported the unusual viscosity behavior of PLA at low shear rates by the appearance of a maximum instead of a constant region corresponding to some kind of thermal instability of PLA. PCL demonstrates higher thermal stability compared to PLA.

The Fox and Loshaek equation (Fox and Loshaek 1955) describing the relationship between zero shear viscosity and molecular weight for linear amorphous polymers is as follows:

$$\eta_0 = KM_w^a \tag{2-16}$$

According to literature "*a*" has a universal value of 3.4-3.6 for narrow molecular weight distribution and for molecular weights above the critical molecular weight (M_c), although higher values have been reported up to about 4. Gimenez et al. (2000) have investigated this relationship for PCLs with molecular weights ranging from 35,800 to 59,300 g/mol and reported the following relationship at 140°C:

$$\eta_0 = 6.9 \times 10^{-20} M_w^{4.6} \tag{2-17}$$

Based on Bagley and West results in 1958, M_c is 16,900 for PCL. At very low shear rates, PCL behaves like a Newtonian liquid similar to other polymer melts and the dependence of viscosity on temperature obeys the Arrhenius law (Equation 2.14). Typical master curves for the linear viscoelastic properties including complex viscosity (η^*), storage modulus (G') and loss modulus (G'') for PCL having M_w= 120,000 g/mol are presented in Figure 2.9 over four decades of frequency at the reference temperature of 60°C (Acierno et al. 2006). This is typical for linear polydisperse polymers of high molecular weight. To obtain the master curve, time-temperature superposition principle has been used by using the shift factor a_T which in turn follows the Arrhenius equation (Equation 2.14).

The value of 40.0 ± 0.5 kJ/mol for the flow activation energy of PCL has been reported by Gimenez et al. (2000) which is in close agreement with the value of 35 KJ/mol reported by Ramkumar and Bhattacharya study (1998).

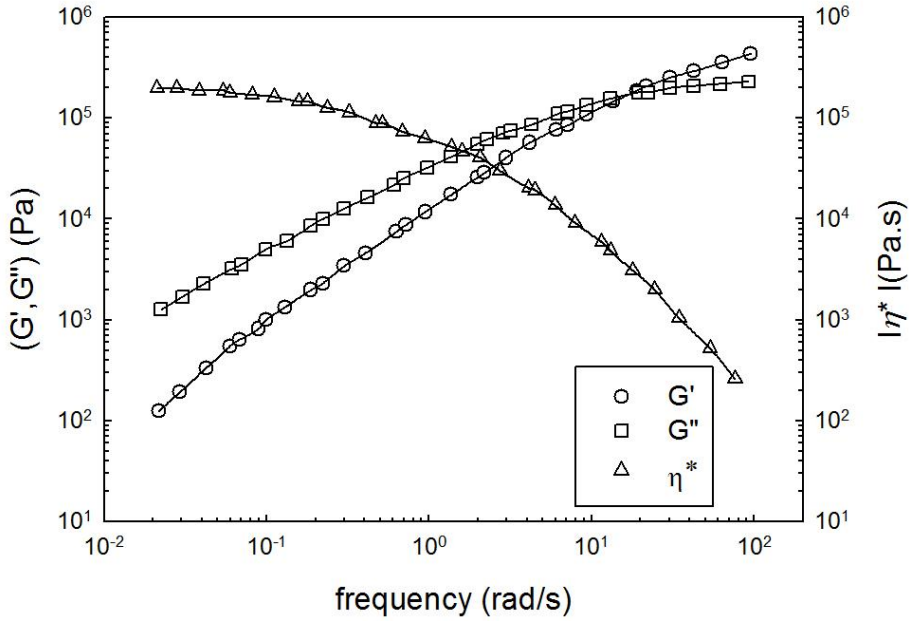

Figure 2.9 Master Curve of Complex viscosity and viscoelastic moduli as a function of frequency at the reference temperature of 60 ºC, adapted from Acierno et al. (Acierno et al. 2006).

The plateau modulus (G_N^0) of PCL was measured to be 1 MPa ± 0.1. The molecular weight between the entanglements (M_e) was reported as 3,000 g/mol based on the Ferry equation ($M_c \cong 2M_e$) at the temperature of 140°C and the melt density of 0.9 g/cm^3 (Gimenez et al. 2002).

2.3 Processing of Biodegradable Polymers

2.3.1 Capillary Extrusion of Biodegradable Polymers

Capillary flow is a pressure-driven flow that is generated by means of a capillary rheometer. Apart from a large pressure drop in the capillary, there are also pressure drops in the entrance and exit regions to the capillary. A capillary rheometer has the ability to produce high shear rates to measure the shear stress and the viscosity of a molten polymer (Dealy and Wissbrun 1999). Capillary extrusion can also be employed as an effective tool to evaluate the processability of polymers.

The capillary rheometer consists of a heated reservoir (barrel) where the polymer is placed and once in a molten state it is forced to flow through the die by means of a plunger

(piston). The die is located at the end of the barrel, having a specified length (L), and diameter (D) parameters, that affect processability of polymers. Figure 2.10 is a schematic of the capillary rheometer.

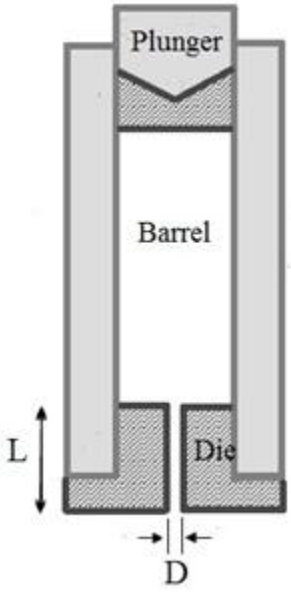

Figure 2.10 Schematic of a capillary rheometer.

The measurable parameters by the rheometer are the required force or the total pressure (ΔP) to move the plunger and the velocity of the plunger or the volumetric flow rate (Q). The total pressure and the volumetric flow rate can be transformed into the apparent shear stress (σ_a) and apparent shear rate ($\dot{\gamma}_a$) by the following equations:

$$\sigma_a = \frac{D\Delta P}{4L} \tag{2-18}$$

$$\dot{\gamma}_a = \frac{32Q}{\pi D^3} \tag{2-19}$$

Figure 2.11 depicts the typical variation of pressure along a capillary die including the entrance and exit pressures. It can be clearly observed that the total pressure drop includes the pressure drop over the whole length of the capillary die (ΔP_{cap}) in addition to the pressure drop at the entrance (ΔP_{ent}) and the pressure drop at the exit area (ΔP_{exit}) (Mitsoulis and Hatzikiriakos 2003).

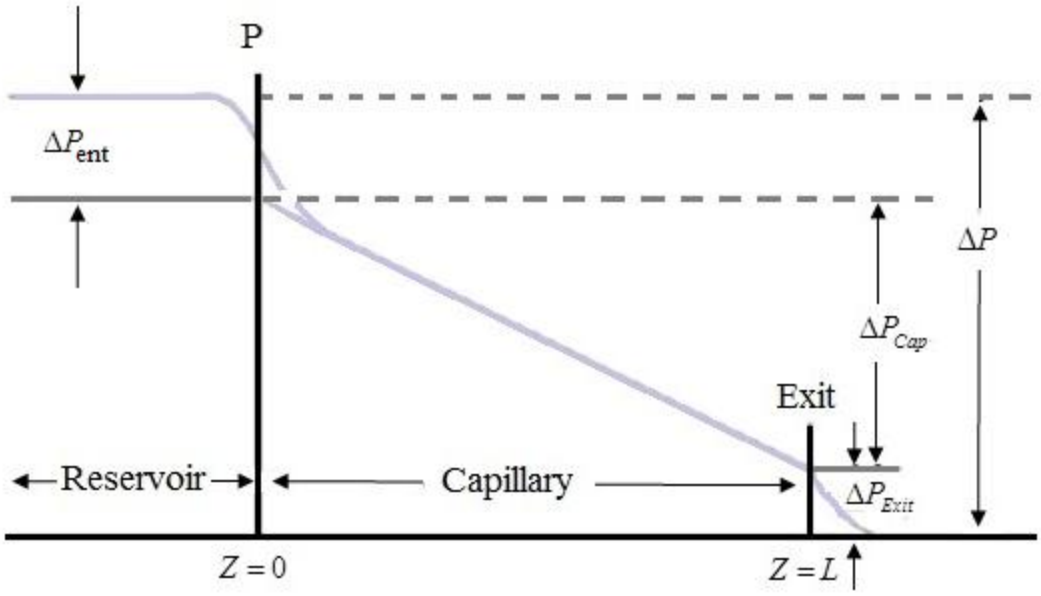

Figure 2.11 Typical diagram of the pressure drop along the length of a capillary die, adapted from Mitsoulis et al. (Mitsoulis and Hatzikiriakos 2003).

In order to calculate the true shear stress, the end pressure drop which is the summation of entrance pressure and exit pressure drops should be extracted from the total pressure drop measured by the rheometer (Dealy and Wissbrun 1999). The true shear stress (σ_w) can then be calculated by the following expression:

$$\sigma_w = \frac{\Delta P - \Delta P_{end}}{4(L/D)} \tag{2-20}$$

In this equation ΔP_{end} which includes both ΔP_{ent} and ΔP_{exit} can be determined by means of the Bagley plot i.e. by plotting ΔP versus L/D ratio at a fixed apparent shear rate and extrapolating a fitted straight line to zero L/D. For this matter, experiments should be performed for at least three dies having different lengths and the same diameter.

The apparent shear rate also needs to be corrected to result the true shear rate, ($\dot{\gamma}_w$) by applying Rabinowistch correction (Dealy and Wissbrun 1999).

$$\gamma_w = \frac{3n+1}{4n}\dot{\gamma}_a \tag{2-21}$$

Where n is the power law exponent which is defined as $\frac{d(\log \sigma_w)}{d(\log \dot{\gamma}_a)}$.

2.3.2 Processability of Biodegradable Polymers

It is known that in the extrusion of thermoplastics, the desirable products should be free of any surface defects. From the production efficiency point of view, it is also desirable to keep the extrusion rates as high as possible and the extrusion pressure as low as possible in order to make efficient use of the processing machinery with the least cost. Therefore, the ultimate goal is to minimize the cost of operation without compromising the quality of production. However, in the extrusion process (particularly for linear polymers) small amplitude periodic distortion and irregularities appear on the surface of the extrudates, once the flow rate (throughput) exceeds a critical value, thus limiting the rate of production at uneconomical levels (Hatzikiriakos and Migler 2005, Rosenbaum et al. 2000). Understanding the flow instabilities that may occur in the extrusion operations of commercial biodegradable polyesters is crucial for the design of processing equipment and processing operations. In particular, understanding the origin and occurrence of sharkskin melt fracture is important in identifying methods to eliminate or reduce these irregularities, and thus to minimizing costs by producing high volumes (Dealy and Wissbrun, 1990).

The different types of flow instabilities are generally known collectively as melt fracture. The surface instabilities can be classified into sharkskin, stick-slip (oscillating melt fracture) and gross melt fracture. Sharkskin is usually the first instability that occurs when the wall shear stress exceeds a first critical value. This value is reported as 0.1 MPa for a number of polymers (Migler 2005). Sharkskin is characterized by the appearance of the small amplitude periodic distortions on the surface at relatively low shear rates. The mechanism of the rupture of the extrudate at the die exit due to the change in the velocity profile (significant stretching) of the polymer is more accepted for the origin of sharkskin (Cogswell 1977, Achilleos et al. 2002). The other instability is called stick-slip which is associated to the presence of alternate smooth and distorted portions on the surface as the extrusion

pressure oscillates between two extreme values (Georgiou 2005). By increasing the shear rate, gross irregular distortions known as gross melt fracture are obtained (Dealy and Kim 2005). Gross melt fracture deforms the extrudate severely affecting the volume of the extrudate. It should be noted that some polymers such as polystyrene and branched polymers show gross melt fracture at high shear rates without sharkskin instability at lower shear rates. Parameters such as die geometrical dimensions, temperature and molecular parameters and structure of polymers affect the occurrence of processing instabilities described above. Figure 2.12 illustrates typical images of extrudates exhibiting the various types of irregularities (Migler 2005).

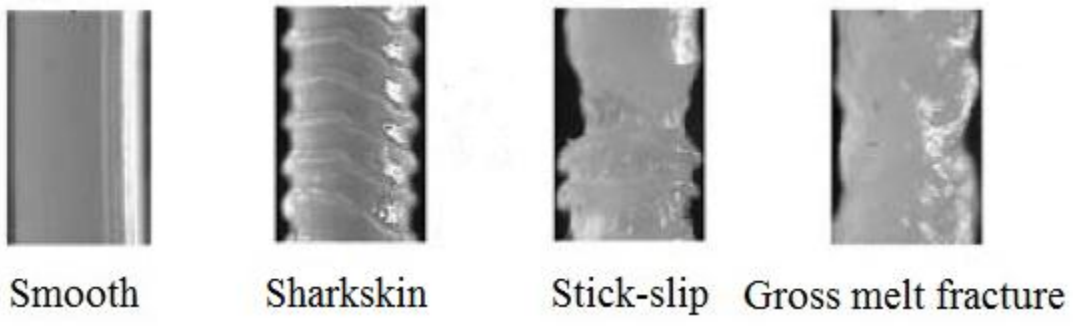

Figure 2.12 Typical surface irregularities, adapted from Migler (2005).

Another important phenomenon that needs attention in polymer processing is the possible occurrence of wall slip (violation of the classical no-slip boundary condition of fluid mechanics). It is well documented in the literature that when the wall shear stress exceeds a critical value, polymer shows slip (Ramamurthy 1986, Archer 2005, Hatzikiriakos 2012). Theoretical developments by de Gennes and Brochard-Wyart (1992) imply that molten polymers always slip no matter how small is the applied shear stress level; however, at a critical level of shear stress, slip changes from weak to strong. Under slip conditions, the following expression can be easily derived for capillary flow and be used consequently to perform the slip calculations (Mooney 1931, Ramamurthy 1986):

$$\dot{\gamma}_a = \dot{\gamma}_{a,s} + \frac{8u_s}{D} \tag{2-22}$$

where $\dot{\gamma}_{a,s}$ is the apparent shear rate under no-slip conditions, u_s is the slip velocity and D is the diameter of the capillary die. The technique used to obtain the slip velocity is called

Mooney analysis. Plotting $\dot{\gamma}_a$ versus 1/D at a constant shear stress value results a straight line with slope equal to $8u_s$. The intercept in such a plot results the apparent shear rate under no-slip conditions, $\dot{\gamma}_{a,s}$ (Mooney 1931). This method has been extensively employed by many research groups to generate slip data needed in numerical simulations of polymer processing operations (Hatzikiriakos and Dealy 1992a).

Kanev et al. (2007) were the first to report on the processing of biodegradable polymers. They observed that by increasing the shear rate, sharkskin and gross melt fracture defects appear on the extrudate surface. The values of the critical shear stress for the onset of sharkskin are 140 to 180 KPa and 360 to 400 KPa for gross melt fracture. These critical values are in agreement with the values reported for HDPE and LDPE (Migler 2005). Another recent relevant study on the processing of biodegradable polymers was reported by Othman et al (2012). Slip was found for PLAs above a certain level of molecular weight. It was also observed that the slip velocity increases by decreasing the molecular weight of PLA, then became zero for the low molecular weight PLA (M_w=55,400). For the high molecular weight PLA (M_w=110,100) the critical shear stress for the onset of melt fracture was found to be between 0.2 to 0.3 MPa. This value was temperature independent, and it was reported to depend on the die geometry. Moreover, addition of 0.5 wt% PCL was highly effective as a processing aid to delay the occurrence of surface instabilities to higher shear stress values.

2.3.3 Processing aids

Significant amount of work has been directed into identifying processing aids to overcome the challenge of surface instabilities and gross melt fracture during the polymer processing (Achilleos et al. 2002, Amos et al. 2001). Various types of materials have been used as processing aids. Fluoropolymers and stearates have been used as processing aid for polyolefins such as high-density polyethylene and low-density polyethylene up to 0.1 wt% and 0.3 wt%, respectively (Achilleos et al. 2002). These materials act as lubricants or slip promoters, reducing the pressure drop and postponing the occurrence of surface defects to higher shear rates. It was found that fluoropolymers mainly affect the sharkskin and stick-slip rather than gross melt fracture (Hatzikiriakos and Migler 2005). The disadvantage of these materials is the long induction time (up to 2 hours) to establish a stable coating on the wall.

Silicon-based chemicals and also liquid crystalline polymers were attempted as possible processing aids for polyethylene in the literature (La Mantia et al. 1989). In the case of liquid crystalline polymers, the very high processing temperature and weak compatibility with polyethylene prevented further studies on these materials. Hyperbranched polymers (HBPs) have also been reported as effective processing aid for low-density polyethylene. HBPs have the ability to migrate to the wall, thus providing a lubricating effect. Around 0.5 wt% HBP eliminate instabilities effectively (Hong et al. 2000). Boron nitride has also been reported as a processing aid to eliminate not only sharkskin but gross melt fracture as well (Rosenbaum et al. 2000, Hatzikiriakos 2005). The role of processing aids is to have a lubrication effect on the wall that promotes slip, thus reducing pressure drop and shear stress levels.

Processing aids for biodegradable polymers (specifically PCL) do not exist. Therefore, methods to enhance the rate of production by eliminating or postponing these phenomena (if they occur) to higher shear rates in the case of biodegradable polymers are desirable from an industrial point of view.

2.4 Polymer Blends

Polymer blend is a mixture of at least two polymeric or copolymeric components. Blends have been widely used for many years to tailor the properties and processability of homopolymers and control the cost for different applications. Blending is found to be more practical and less expensive to modify the properties of both components compared to the copolymerization. Blends can be characterized by their phase behavior or miscibility. Miscibility strongly affects the thermal, mechanical, rheological and morphology properties of the blend. Immiscible blends have multiple phases. On the other hand, partially immiscible blends contain part of each component in each phase. Miscibility occurs as a result of the exothermic interactions between the components (negative Gibbs free energy) which lead to a single glass transition temperature (T_g) for a blend (Barlow and Paul 1981). A study by Coleman et al. (1990) reported that the least difference in the non-hydrogen bonded solubility parameters and the highly favorable intermolecular interactions between the components strengthen the possibility of miscibility.

In multicomponent immiscible systems the role of interfacial tension in the morphology and consequently in the final properties is crucial. If the surface tension of the components are known, interfacial tension can be obtained based on the reciprocal mean of the surface tensions (Wu 1971). There are various experimental methods to measure the interfacial tension such as pendant droplet and imbedded-fiber retraction (Biresaw and Carriere 2002). The molecular weights of the components also influence the interfacial tension of immiscible blends (Anastasiadis et al. 1988). In general, in an immiscible blend, the lower mass fraction component tends to form a droplet morphology. By increasing the mass fraction of that component, droplets tend to coalesce and transform into co-continuous morphology (Broz et al. 2003). Viscoelastic properties of the components along with the interfacial tension largely affect the morphology and final properties of the blend.

2.4.1 Poly(ε-caprolactone) and Poly(lactide) Blends

Many studies have been reported in the literature on the poly(ε-caprolactone) and polylactide blends as an interesting combination of biodegradable polymeric blends. As discussed earlier in section 2.1.2, polylactides can be polymerized to possess an amorphous or crystalline structure. However, both structures exhibit high brittleness at ambient temperature which is a major drawback for many applications (Lopez-Rodriguez et al. 2006). PCL due to the specific characteristics (see section 2.2) is a good candidate to toughen PLA in a blend. Also tuning the biodegradation time is another target of studying PCL and PLA blends.

Studies on the PLA and PCL blends revealed the immiscibility in this system (Wang et al. 1998, Meredith and Amis 2000, Broz et al. 2003, Dell'erba et al. 2001, Wu et al. 2008, Wu et al. 2010, Yang et al. 1997, Zhang et al. 2009). Application of the PCL and PLA blends in membranes has been studied by Aslan et al. (2000). In the presence of 10wt% of PDLLA, membranes with better mechanical properties were obtained. Due to the immiscibility of these polymers, PDLLA-co-PCL has been used as compatibilizer up to 5 wt% resulted into the homogenous porous network.

Mechanical properties such as Young modulus, elongation at break and yield stress of PCL (M_w=80,000) and PDLLA (M_w=100,000) blend have been investigated for different compositions of the components (Broz et al. 2003). It is mentioned that above 40 wt% PDLLA, the modulus increased linearly by PDLLA content up to 2.5 GPa. In contrast,

elongation at break decreased by the PDLLA content up to 60 wt%. The percolation threshold (the droplet coalescence) has been predicted to be 50 wt% of PDLLA.

Another study on mechanical properties of PCL (M_w≅ 28,000) and PLLA (M_w≅ 115,000) has been performed by Chen et al. (2003). Copolymer of ethylene oxide (PEO) and propylene oxide (PPO) has been entered to the blend as surfactant to improve the miscibility. Results indicate that the elongation at break has been improved by addition of PCL and surfactants but yield stress and modulus has been decreased.

Investigation of thermal properties of PCL (M_n=55,000) and PLLA (M_n=100,000) blends exhibit the improvement of crystallinity of PLLA in the presence of PCL component. The microscopy studies of the morphology show the phase boundary in this system. PLLA-PCL diblock and PLLA-PCL-PLLA triblocks has been employed as interfacial agent to elevate the level of compatibility in the PCL and PLA blend. It is reported that in spite of the immiscibility of PCL and PLA, these polymers are not highly incompatible (Dell'erba et al. 2001). Diblock copolymer of polyethylene glycol (PEG) and poly(ε-caprolactone) (PCL) has been successfully employed as a compatibilizer in the PCL and PLA blend to increase the phase adhesion, showing improvement in mechanical properties. PEG block in the compatibilizer is miscible with PLA (Na et al. 2002, Tsuji and Horikawa 2007). Mechanical properties of PCL and PLA blends are highly affected by the composition ratio and can be predicted by the rule of mixtures (Simoes et al. 2009, Park and Todo 2011). Addition of dicumyl peroxide (DCP) that form crosslinked structure, significantly improves the interfacial adhesion and tensile strain of PLA and PCL blend (Semba et al. 2006). Lysine triisocyanate (LTI) has been used as an additive by the aim of compatibilizing and improving the miscibility of PCL and PLA blend. Furthermore, 1 wt% LTI improve the impact fracture of PCL and PLA blend significantly (Takayama and Todo 2006). The effect of PDLLA content on the crystallization of PCL has also been investigated. PDLLA did not have a drastic effect on the crystallization of PCL. However, the radius of spherulites of PCL has been larger in the blend than the PCL homopolymer (Tsuji and Ikada 1998).

Processing conditions of preparation of the PCL and PLLA blend such as shear rate and time drastically affect the biodegradation. It is mentioned that higher processing time and shear rate of melt blending accelerate the enzymatic degradation of PCL and PLLA blend (Tsuji et al. 2007).

3 Thesis Objectives and Organization

3.1 Thesis Objectives

The objective of this PhD thesis is to study the rheological behavior of a series of newly synthesized controlled macrostructure and some commercial poly (ε-caprolactone) (PCL) as well as their blends with various polylactides (PLA). More specifically, the main objective is to develop molecular structure-property relationship for the rheological, processing and mechanical properties of PCL polymers and its blends with a representative PLA polymer. The particular objectives can be summarized as follows:

1. Evaluate the rheological behavior of PCLs in a systematic way as a function of molecular parameters. First, the linear viscoelastic properties of the PCLs will be analyzed over a wide range of temperatures and frequencies. The nonlinear rheological properties such as stress relaxation and viscosity functions will be determined by means of a rotational rheometer. Extensional rheology will also be studied in order to determine the degree of strain hardening if any. The solution properties of these polymers will also be studied and related to molecular parameters for a better documentation of their structure.
2. Study the processing properties of PCL homopolymers and the critical conditions for the occurrence of melt fracture phenomena; investigate possible flow instabilities as a function of temperature and molecular weight of PCL; and develop processing aids to eliminate/minimize the impact of flow instabilities on processing.
3. Investigate the thermal and rheological behavior of blends of various PLAs with a representative PCL in a series of blends with different composition ratios. Study the effect of PLA on mechanical properties of PCL namely the Young modulus, tensile strength, and elongation at break.
4. Study the thermodynamics of PCL and PLA blends by the use of rheological methods. Evaluate the effect of dynamic conditions on the phase boundary behavior of PCL and PLA blends.

3.2 Thesis Organization

This thesis is organized as follows. The introduction and motivation of this study is briefly described in chapter 1. The literature review on PCL related to the present study is provided in chapter2. This chapter includes a review of different classes of biodegradable polymers

with particularly emphasis on PCL polymers. Polymerization methods for PCL are summarized and previous rheological and processing studies on PCL are discussed in detail. In other parts of this chapter, polymer blends and in particular the thermorheological properties of the PCL/PLA blend system are reviewed. In this chapter a number of fundamental concepts related to rheological measurements of this work are also explained. Chapter 3 presents the objectives and the organization of this thesis. In chapter 4, the materials and methodology used in this research are discussed in detail. In chapter 5, the linear viscoelasticity of the newly synthesized as well as of a number of commercial PCLs is presented in addition to the extensional rheological behavior of the commercial PCLs. Also a constitutive model for prediction of the rheological data is presented. The solution properties of the homopolymers are also discussed in this chapter and related to their molecular structure. Chapter 6 includes the processability of the PCL homopolymers at different conditions in addition to the presentation of processing aids for PCLs. The phase behavior of the PCL/ PLA blend system is discussed in chapter 7. The morphological characteristics of the various blends in the phase separated region are also presented. Chapter 8 includes the thermal properties of the PCL/PLA blends. The viscoelastic properties of the blends are also reported in this chapter. Furthermore, predictions of emulsion models of the viscoelastic properties of the various blends are finally examined. The conclusions and recommendations for future research are presented in the final chapter 9.

4 Materials and Methodology

4.1 Materials

Commercial poly (ε-caprolactone) polymers (Capa®6800, Capa®6500, Capa®6430, Capa®6250), from Perstorp (Capa® technology) with various molecular weights ranging from 23,000 to 72,000 g/mol and with approximately constant polydispersity of 1.23 were studied. These are listed in Table 4.1 along with their molecular characteristics. In addition, controlled macrostructure PCLs were synthesized *via* ring opening polymerization of cyclic monomer of ε-caprolactone using novel homoleptic amidate complexes of yttrium in room temperature (Stanlake et al. 2008, Thomson and Schafer 2012). This type of high activity rare-earth amidate complexes, produce PCLs with high molecular weight and relatively narrow molecular weight distribution. The chemical structure of yttrium amidate complexes are displayed in Figure 4.1 and 4.2 which are referred to as initiator A and B in this thesis, respectively. The polymers synthesized and studied are listed in Table 4.2 along with their molecular characteristics.

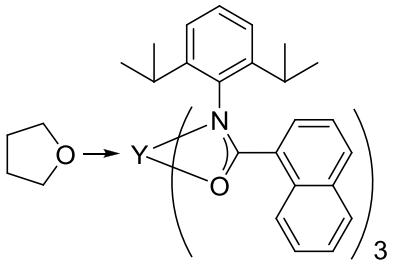

Figure 4.1 Yttrium tris(amidate) complex (Initiator A).

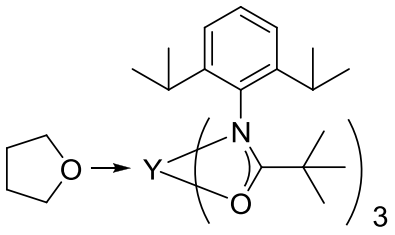

Figure 4.2 Yttrium amidate complex (Initiator B).

PCLs were synthesized by the following procedure reported by Stanlake et al (2008): inside a nitrogen filled glovebox, an yttrium (amidate) complex (0.0112 mmol) was dissolved in 10 mL of toluene (measured by volumetric flask). The colorless solution was transferred to a 20 mL vial, equipped with a stir bar. ε-Caprolactone (0.28 mL, 2.5 mmol) was transferred by

syringe directly into the rapidly stirring solution of yttrium(amidate) complex. The reaction was stirred for 15 min within the glovebox and then exposed to air and quenched with 1 mL of 1 M aqueous HCl solution. The polymer was precipitated from cold petroleum ether. The polymer was isolated by vacuum filtration, and then dried overnight *in vacuo*.

Table 4.1 Molecular weights and molecular weight distribution of commercial PCLs.

Sample	M_n (10^5 g.mol^{-1})	M_w (10^5 g.mol^{-1})	M_w/M_n
Capa 6800	0.722	0.884	1.224
Capa 6500	0.456	0.555	1.219
Capa 6430	0.379	0.456	1.227
Capa 6250	0.236	0.289	1.225

Table 4.2 PCL homopolymers synthesized and studied in this work.

Sample	***Initiator***	***% Yield*** [b]	M_n (10^5 g.mol^{-1})	M_w (10^5 g.mol^{-1})	M_w/M_n
JT-4-151	A	95	1.130	1.311	1.160
JT-6-65[c]	A	95	1.042	1.267	1.216
JT-4-149	A	97	0.943	1.098	1.165
JT-3-67	A	93	0.812	1.020	1.255
JT-3-87	B	99	0.668	0.971	1.453
JT-3-163	B	99	0.639	0.963	1.507
JT-4-145	B	99	0.600	0.942	1.571
JT-4-141	B	97	0.499	0.807	1.616
JT-3-161	A	93	0.572	0.728	1.275
JT-4-15	B	99	0.363	0.657	1.812
JT-4-137	B	95	0.354	0.560	1.584

[a] general polymerization conditions: toluene, 15 minutes, 25 °C. [b] yield = weight of polymer obtained/weight of monomer used. [c] reaction temperature 60 °C.

In addition to the mentioned PCL homopolymers, commercial poly(lactide) polymers (PLA) (PLA 2002D, PLA 3051D and PLA 3251D), NatureWorks products, of various molecular weights ranging from 55,400 to 110,100 g/mol and approximately constant

polydispersity (1.6 to 1.82) were studied in this work as blends with the commercial PCLs listed in Table 4.1. The molecular weights and molecular weight distribution of PLAs are presented in Table 4.3.

Table 4.3 Molecular weight and molecular weight distribution of commercial PLAs.

Sample	M_n (10^5 g.mol^{-1})	M_w (10^5 g.mol^{-1})	M_w/M_n
PLA 7001D	0.692	1.101	1.59
PLA 2002D	0.587	1.069	1.82
PLA 3051D	0.508	0.925	1.82
PLA 3251D	0.342	0.554	1.62

Three diblock copolymers PLA-*b*-PCL with narrow molecular weight distribution were synthesized with different block length ratios (Table 4.4). Diblock copolymers (PCL/PLA ratio = 40/60, 75/25, 80/20) were synthesized by PhD student in Dr.Schafer's group by the following procedure: Inside a nitrogen filled glovebox, an yttrium (amidate) complex (0.3056 g, 0.2652 mmol) was dissolved in 50 mL of THF to make a standard solution. 1 mL of the standard solution was then dissolved in more THF (40/60(1.00 mL), 75/25(1.80 mL), 80/20(2.10 mL)) and transferred to a 20 mL vial, equipped with a stir bar. ε-caprolactone (40/60(0.10 mL, 0.90 mmol), 75/25(0.20 mL, 1.8 mmol), 80/20(0.25 mL, 2.3 mmol)) was transferred by syringe directly into the rapidly stirring solution of an yttrium (amidate) complex. The reaction was stirred for 15 min within the glovebox. A standard solution of rac-lactide (6.1189g, 42.45 mmol) was made in a 50 mL volumetric flask. The rac-lactide solution 40/60(2.50 mL, 2.12 mmol), 75/25(2.20 mL, 1.87 mmol), 80/20(1.90 mL, 1.61 mmol)) was added all at once to the solution of PCL and left to stir for an additional 15 min. In some cases, manual stirring was required. The mixture was then exposed to air and quenched with 1 mL of 1 M aqueous HCl solution. The polymer was precipitated from cold petroleum ether. The polymer was isolated by vacuum filtration, and then dried overnight *in vacuo*.

Table 4.4 Diblock copolymers synthesized and studied in this work.

Sample	*% Yield*	M_n (10^5 g.mol^{-1})	M_w (10^5 g.mol^{-1})	M_w/M_n
PLA60-*b*-PCL40	62	0.995	1.243	1.27
PLA25-*b*-PCL75	56	1.413	1.718	1.23
PLA20-*b*-PCL80	62	1.132	1.431	1.26

4.2 Characterization Techniques

4.2.1 Gel Permeation Chromatography (GPC)

The molecular weights (M_w and M_n), molecular weight distribution (polydispersity index) and solution properties namely, radius of gyration (R_g), hydrodynamic radius (R_h) and intrinsic viscosity ([η]) of the newly synthesized PCLs were measured by triple detection gel permeation chromatography by using Waters liquid chromatograph equipped with a Waters 515 HPLC pump, Waters 717 plus autosampler, Waters Styragel columns (4.6 x 300 mm) HR5E, HR4, and HR2, Waters 2410 differential refractometer, Wyatt tristar miniDAWN (laser light scattering detector) and a Wyatt ViscoStar viscometer. Tetrahydrofuran (THF) as a mobile phase was used with a solvent flow rate of 0.5ml/min. Measurements were performed at laser wavelength of 690 nm and at room temperature. Absolute molecular weights were determined using a dn/dc (change in refractive index/change in concentration) of 0.079 mL•g^{-1} (Thomas et al. 2012). The data were processed using Astra software provided by Wyatt Technology Corp.

4.2.2 Differential Scanning Calorimeter (DSC)

Thermal properties of the blends were measured by using a differential scanning calorimeter, TA instruments Q2000 calibrated by indium. In order to obtain the glass transition (T_g), the crystallization (T_c) and the melting temperatures (T_m) of the homopolymers and the blends, Differential Scanning Calorimetry (DSC) was performed in an inert atmosphere (nitrogen) with approximately 2.3-2.5 mg of sample in an aluminum pan. Samples were heated quickly to 200°C and they were held isothermally there for 5 min in order to eliminate any thermal history and remove any residual crystals. Then, they were gradually cooled down to -10°C with a cooling rate of 10°C/min. The samples were reheated to 200°C with a heating rate of

10°C/min. The crystallization and melting temperatures were determined from exothermic and the second endothermic peak values.

4.2.3 Scanning Electron Microscopy (SEM)

The morphological studies of the blends were carried out by using scanning electron microscope (SEM), HITACHI S-3000 N with 5 KV accelerating voltage. The microscope is equipped with Quartz Xone-X-Ray Microanalysis System. The cross section of the cryogenically brittle fractured samples was etched with acetic acid in order to dissolve the PCL phase selectively and to obtain a better image contrast. The etching procedure has been conducted at different etching times of 10s, 30s, 1 min and 5 min. The optimum time for etching was observed to be 30 s in order not to affect the morphology of the fractured surface. The fractured etched surface was gold coated by S150A Sputter Coater, Edwards with gold deposition rate of 15 nm per min for 35 s.

4.2.4 Polarized Optical Microscopy (POM)

The optical microscopy was carried out by Mitutoyo microscope set up equipped with Lumenera LU 165 color CCD camera and accompanied with the hot stage. The microscope has the 20x magnification and captures images with typical dimensions of 160x220 μm. The microscope has the capability of providing the polarized as well as non-polarized light. The thickness of the samples for the optical microscopy analysis was around 9μm. At this thickness, the phase separation is independent of thickness (Reich and Cohen 1981).

4.3 Homopolymers Sample Preparation for Rheological Testing

Newly synthesized PCLs were solution casted in 8 wt% chloroform due to the limited amounts produced. The solutions were stored in Petri dishes in a fume hood overnight and then dried under vacuum for four days at 35°C to ensure the gradual removal of the solvent and moisture from the samples. Due to the high propensity of poly(ε-caprolactone)s to absorb moisture and hydrolytic degradation, the commercial and synthesized PCLs were dried in a vacuum oven for an additional 24 hrs at 35°C prior to molding. To prepare suitable samples for rheological measurements, dried samples were compression molded at 80°C for 10 min

before cooling. The molding temperature is selected well above the melting temperature of PCL, which is determined by DSC.

4.4 Blends Preparation

Blends of PCL/PLA blends of various composition ratios were prepared by continuous solution mixing and casting of 8wt% solutions in chloroform for 2 hrs in order to obtain mixing at the molecular level. Similar to the homopolymers, the solutions were kept in Petri dishes in a fume hood overnight and then gradually dried under vacuum for four days at 45°C to allow complete evaporation of both solvent and moisture.

The samples were additionally dried in a vacuum oven at 35°C for 24 hrs, prior to the rheological testing. Samples for rheological measurements were compression-molded at 180°C for 5 min before cooling, resulting in sheets with thickness of about 1 mm. The compression molding temperature was selected based on the melting temperature of the polymers obtained from DSC.

4.5 Rheological Measurements

4.5.1 Linear Viscoelasticity

Homopolymers: The linear viscoelastic properties of PCL homopolymers have been determined by a rotational rheometer (Anton-Paar, MCR 501) equipped with a cone-and-plate geometry (diameter of 25 mm and cone angle of 4°). Amplitude sweep tests were performed at constant frequency of 1 Hz (6.28 rad/s), to determine the limit of linear viscoelasticity (LVE). Small amplitude frequency sweep tests were performed at frequencies in the range from 0.01 to 100 rad/s, with a strain of 5% and several temperatures above the melting point in the range of 62 to 160°C. Dynamic time sweep tests were carried out at an angular frequency of 1 rad/s and 100°C to evaluate the thermal stability of the samples. Variation of viscoelastic properties over time has shown excellent thermal stability of the samples in the time frame of measurements (typically up to 1,500 s). The shear damping function of the PCLs was determined by relaxation experiments after the imposition of sudden step shear strain tests at 100°C and 160°C. The measured damping function was employed in the constitutive modeling of the viscoelastic behavior.

Blends: The rheological properties of the PCL/PLA blends were determined by using the Bohlin Gemini HR Nano rotational rheometer equipped with a cone-and-plate geometry (diameter of 25mm and cone angle of 2.5°) in nitrogen atmosphere to prevent thermal degradation of the PCL and PLA components. Similar to PCL homopolymers, amplitude sweep tests were performed at constant frequency of 1 Hz (6.28 rad/s), to determine the limit of linear viscoelasticity. The thermal stability of the blends was confirmed by dynamic time sweep tests at an angular frequency of 1 rad/s at 170°C. Furthermore, small amplitude frequency sweep tests were performed at frequencies in the range from 0.01 to 100 rad/s, with a strain of 5% at 170°C.

Isochronal dynamic temperature ramp tests were carried out at different frequencies of 0.007 Hz (0.044 rad/s), 0.05 Hz (0.314 rad/s), 0.1 Hz (0.628 rad/s), 1 Hz (6.28 rad/s) and 10 Hz (62.8 rad/s) and different heating rates of 0.2, 0.5 and 1 °C/min. The measurements were repeated 3 times for each type of experiment. The temperature range in this study was 70-130°C covering the miscible and phase separated region in these blends. The measurements were all performed in oscillatory shear mode and constant shear stress of 20 Pa.

4.5.2 Extensional Rheology

Uniaxial extensional flow measurements were conducted using the Sentmanat Extensional Rheometer (SER-2) which is a fixture to the MCR 501 (Anton-Paar) rheometer. Details of the SER setup can be found in section 2.2.2. Samples were prepared by compression molding as explained in the previous section. The extensional stress growth coefficients were measured at 62°C, which is a few degrees above the melting point of PCL to have high enough viscosity in order to avoid sagging. Measurements were carried out at different Hencky strain rates ($\dot{\varepsilon}_H$) ranging from 0.01 to 10 s^{-1}. All measurements were done under a nitrogen atmosphere to avoid degradation.

4.5.3 Constitutive Rheological Modeling of Poly(ε-caprolactone)

The Wagner integral constitutive model, Kaye-Bernstein, Kearsley and Zapas (K-BKZ) model was used to analyze the linear and nonlinear viscoelastic behavior of PCL (Bernstein et al. 1963, Kaye 1962, Wagner 1976, Rolon-Garrido and Wagner 2009). The damping and memory functions were evaluated based on the results of the stress relaxation experiments

and the linear and nonlinear viscoelastic behavior of PCL. The ability of the above mentioned model in predicting the nonlinear behavior of PCL was studied using the experimental data from the start-up of steady state shear, and oscillatory flow experiments.

4.5.4 Rheological Modeling of the Blends

The emulsion models of Gramespacher and Meissner (G-M) and modified Palierne were employed to predict the viscoelastic response of the PCL and PLA blends with different composition ratios (Graebling et al. 1993, Gramespacher and Meissner 1992).

4.6 Processing Study

The processability and shear viscosity at high apparent shear rates were investigated by a pressure-driven Instron capillary rheometer equipped with a barrel having a diameter of 0.9525 cm. Measurements were carried out by using several capillary dies with various diameters (*D*) and length-to-diameter ratios (*L/D*). A series of dies with the same diameter and various length-to-diameter ratios, *L/D* were used to correct for the entry effects by using the Bagley method and also to assess the effect of pressure on viscosity. Another series of dies having different diameters and the same *L/D* ratios were used to detect slip effects through the Mooney analysis (Hatzikiriakos and Dealy 1992a; Ramamurthy 1986). All dies had an entry angle (2α) of 180°. The Bagley and Rabinowitsch corrections were applied to the data to obtain the true viscosity of the samples (Dealy and Wissbrun 1990) in order to compare them with viscosity data from the cone-and-plate rheometer. The extrudates from the capillary extrusion experiments were inspected by means of scanning electron microscopy to detect any visual defects known as melt fracture phenomena (Ramamurthy 1986, Hatzikiriakos and Dealy 1992a, b). The reproducibility of the data measured by Instron capillary rheometer is within ±10%. Dimensional characteristics of the dies used in this study are reported in Table 4.5.

Table 4.5 Characteristics of the capillary dies.

D (mm)	*L/D*	*2α (°)*
0.43	15	180
0.43	30	180
0.43	47	180
0.76	5	180
0.76	15	180
0.76	30	180

4.7 Tensile Measurements

Tensile tests were carried out using the COM-TEN 95 series tensile testing equipment (COM-TEN Industries) at ambient temperature. Tensile specimens were cut from compression-molded films. Specimen of 36.6 mm in width and 90 mm in length were cut from the middle portion of the compressed films to avoid edge effects and edge imperfections. The films were compressed in a hot press at 80°C for homopolymers PCL and at 180°C for the PCL/PLA blends for 10 min before being cooled. A gage length of 10 mm, crosshead speed of 25 mm/min and a 40 pound (178 N) capacity of load cell was used for testing all samples. To eliminate specimen slippage from the grips, double adhesive masking tape was used to wrap around the top and bottom portions of the sample. For each sample five tests were run. The average modulus, tensile stress and elongation at break were calculated from the resultant stress-strain measurements and these are reported below along with standard deviations shown by the plotted error bars.

5 Rheology of Poly(ε-caprolactone) Homopolymers

This chapter summarizes the rheological study of a series of commercial PCLs and synthesized controlled macrostructure PCLs (Stanlake et al. 2008, Thomson and Schafer 2012) summarized in Tables 4.1 and 4.2 respectively. The melt viscoelastic properties and the solution properties of the PCLs are investigated in relation to the molecular characteristics and also compared with previous resources in literature (Gimenez et al. 2000). The extensional viscosity measurements for PCL are presented at higher Hencky strain rate and lower temperature than previously reported (Kapoor and Bhattacharya 1999). Moreover, the rheological behavior of PCL is modeled by using the classic K-BKZ Wagner constitutive equation based on the viscoelastic data.

5.1 Solution Properties

The average values of intrinsic viscosity of all the PCLs used in this work as a function of weight-average molecular weight (M_w) are depicted in Figure 5.1.

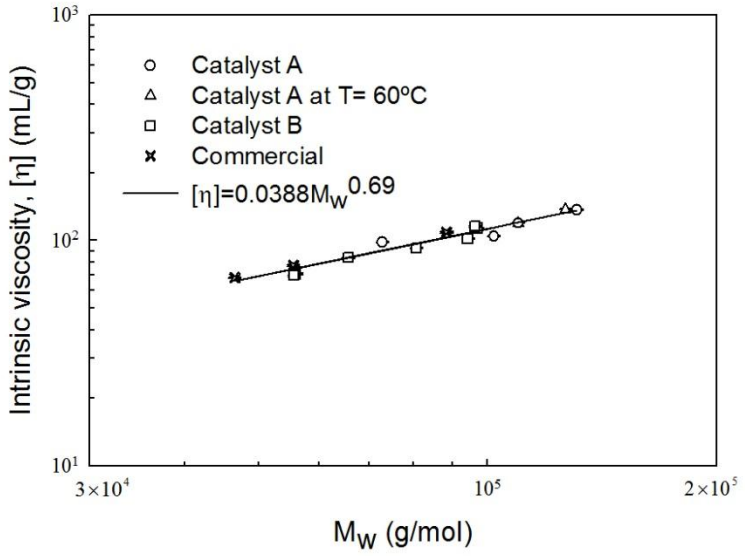

Figure 5.1 The intrinsic viscosities of newly synthesized and commercial PCLs as a function of molecular weight at 25°C. The solid line represents the Mark-Houwink equation with the exponent of 0.69.

As can be inferred from the plot, the intrinsic viscosity follows the Kuhn-Mark-Houwink-Sakurada (KMHS) equation, $[\eta] = K.M_w^a$, with the exponent of 0.69 which is very close to

the value of 0.73 of PCLs in dimethylformamide solvent and 0.82 in benzene, reported by Koleske et al., 1969. According to the Flory-Fox theory, values of the Mark-Houwink exponent below 0.8 are an indication of linear flexible polymer chains in a good solvent (Flory and Fox 1954).

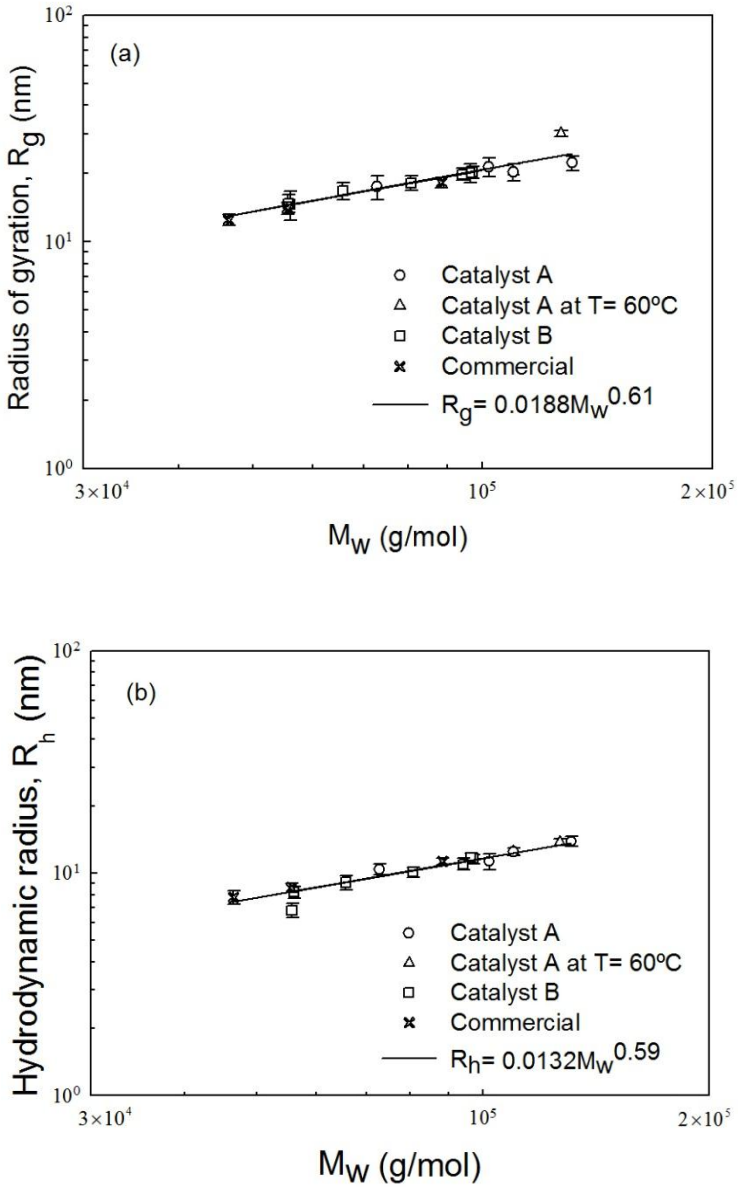

Figure 5.2 (a) Root-mean-square radius of gyration (R_g) as a function of molecular weight for the newly synthesized and commercial PCLs at 25°C. Solid lines correspond to the power law relationship with the exponent of 0.61. (b) Hydrodynamic radius (R_h) of PCLs as a function of molecular weight.

The characteristic radii of chains, namely the radius of gyration (R_g) and the hydrodynamic radius (R_h) are plotted in Figure 5.2a and 5.2b, respectively. Z-average root-mean-square radius of gyration, R_g is a measure of the chain dimension, defined as the 2nd moment around the center of the mass of the chain (Teraoka, 2002). The hydrodynamic radius is defined as the 1st moment of the size distribution, and an average over all the possible conformations. It is related to the hydrodynamic interactions of the monomers of the polymer chain in the solvent medium which reduces the friction coefficient (Burchard, 1999). The molecular weight dependence of the radius of gyration follows a power law relationship of $R_g=0.0188M_w^{0.61}$. All data for PCLs are generally well described by this power law scaling except from some slight scattering for the PCLs produced by initiator A at 60°C. The exponent of 0.61 is in good agreement with the renormalization theory predicted value of 0.588 for linear polymers in good solvent (Auhl et al., 2006). In addition, the molecular weight dependence of the hydrodynamic radius also follows a power law scaling of $R_h=0.0132M_w^{0.59}$ which has very similar exponent to the radius of gyration and intrinsic viscosity.

5.2 Linear Viscoelastic Properties of Poly(ε-caprolactone) Homopolymers

The thermal stability of PCLs has been investigated by dynamic time sweep measurements at the constant frequency of 1 rad/s and the temperature of 100°C. Representative results of the commercial PCL and synthesized PCLs using different catalytic system (referred to Table 4.2) are plotted in Figure 5.3. The consistency of dynamic viscosity over time is an indication of no degradation. The commercial samples were thermally stable up to 10,000 s since they include thermal stabilizers. The synthesized PCLs were found to be sufficiently thermally stable up to at least 1,700 s, a time enough to carry out our typical rheological experiments which last up to 1,500 s. The difference in thermal stability of PCLs is related to the presence of thermal stabilizer in commercial PCLs which may affect the rheological properties as well.

Linear viscoelastic moduli of the highest molecular weight PCL among the commercial PCLs (Capa®6800) were measured at different temperatures from 62°C to 160°C, well above the glass transition temperature of PCL (-60°C, as provided by Perstorp®).

The measurements were carried out in the frequency range of 0.01 to 100 rad/s. Figure 5.4 exhibits the storage modulus (*G'*) and loss modulus (*G"*) of Capa®6800 at different temperatures.

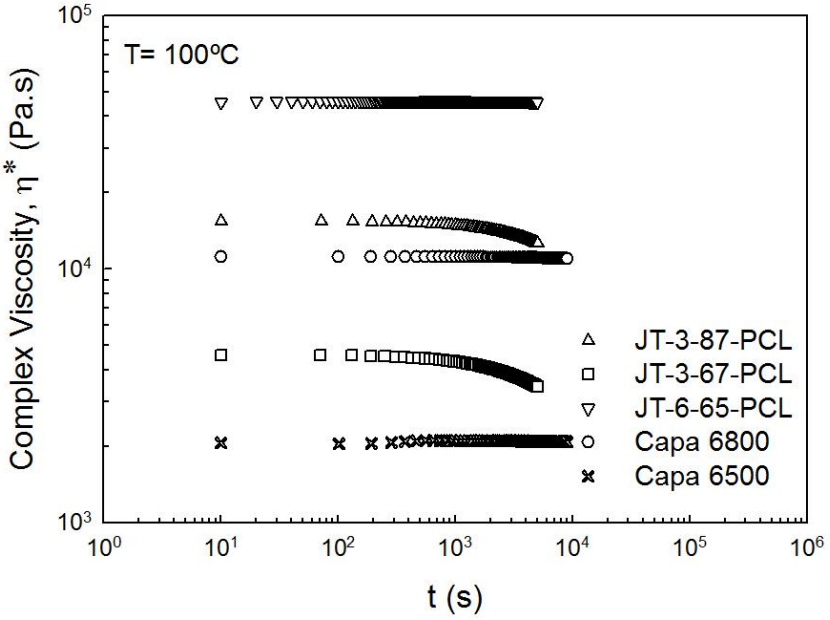

Figure 5.3 Thermal stability of representative PCL samples at 100°C.

Based on the time-temperature superposition principle (more details can be found in section 2.2.3), the rheological data of Figure 5.4 at different temperatures were superposed to the selected reference temperature of 100°C by means of vertical and horizontal shift factors to construct the master curves. The master curves of linear viscoelastic properties of Capa®6800 namely, storage modulus (*G'*), loss modulus (*G"*) and complex viscosity ($|\eta^*|$) are presented in Figure 5.5 at the reference temperature of 100°C.

The master curves were produced employing the RHEOL PLUS software. The complex viscosity ($|\eta^*|$) curve shows the zero shear viscosity value at small frequencies. It should be noted that at small frequencies, the terminal zone has been reached with the characteristic slope of storage modulus (*G'*) and loss modulus (*G"*) with frequency, to be 2 and 1, respectively. The continuous lines in Figure 5.5 represents fits of relaxation spectrum (g_i,λ_i) discussed below (Ferri 1980).

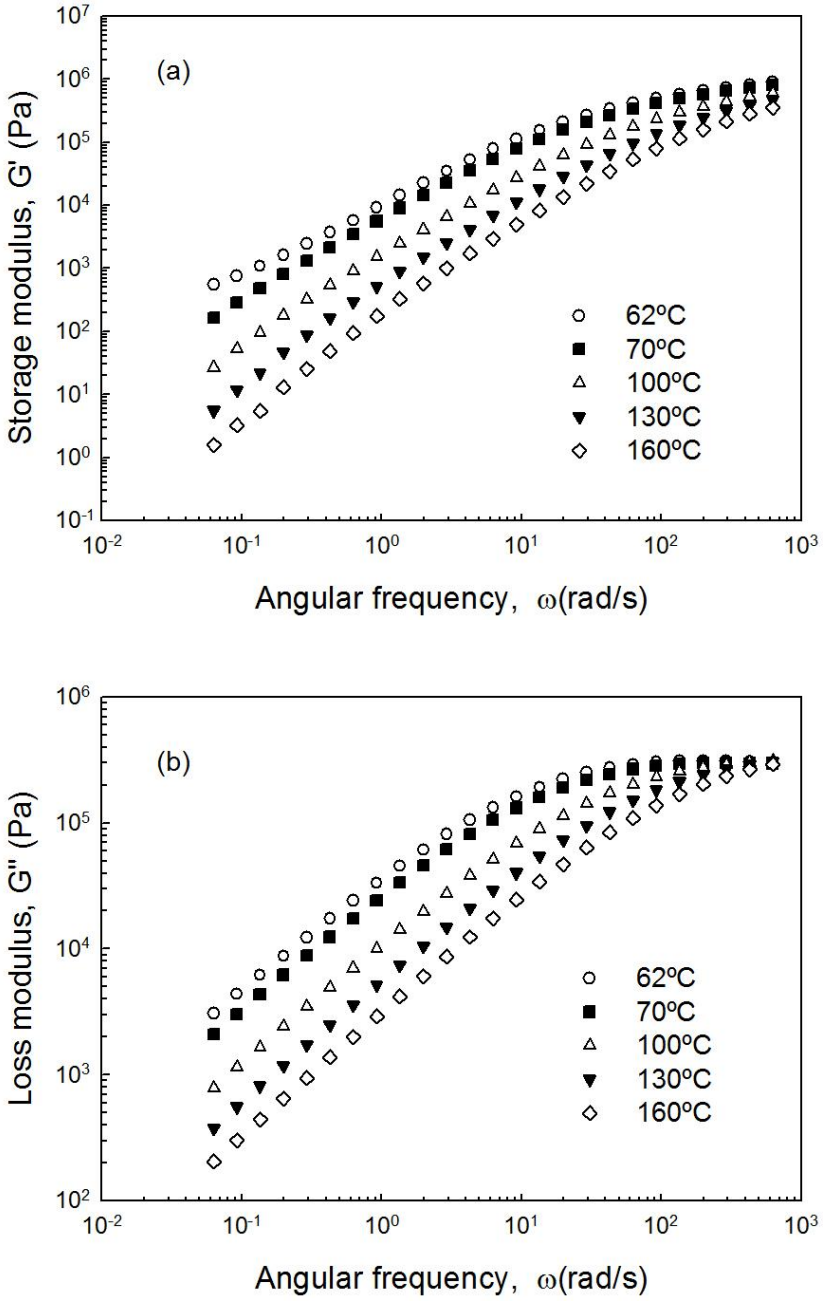

Figure 5.4 (a) Storage modulus (*G'*) (b) Loss modulus (*G"*) of Capa®6800 at the temperature range of 62°C to 160°C.

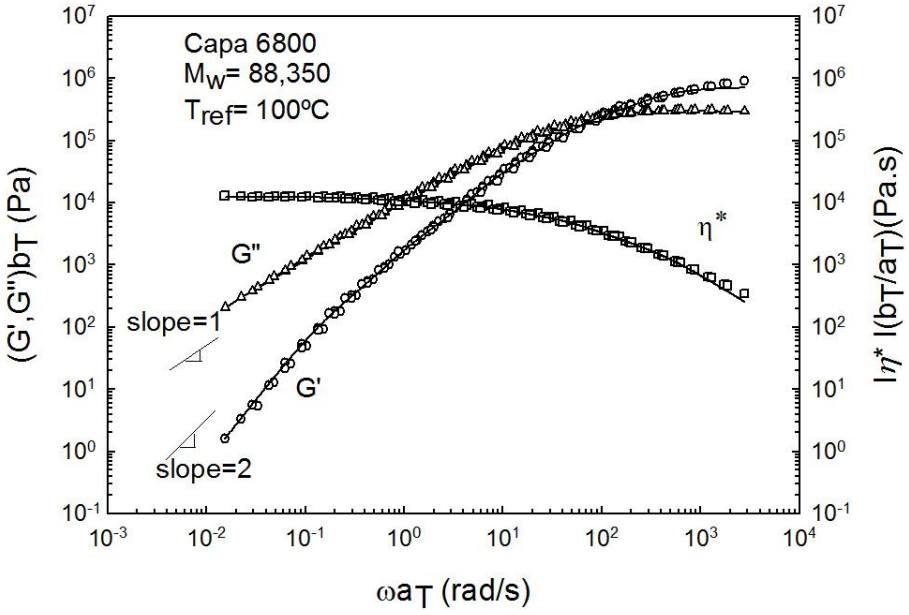

Figure 5.5 Master curve of linear viscoelastic moduli, G' and G" and complex viscosity ($|\eta^*|$) of commercial PCL (Capa®6800) as a function of frequency at the reference temperature of 100°C.

Moreover, the van Gurp-Palmen plot which represents the phase angle (δ) as a function of complex modulus (G^*), is also a strong test of the validity of time-temperature superposition principle. This plot for Capa®6800 is shown in Figure 5.6. The data show perfect superposition which confirms the thermorheological simplicity of Capa®6800.

Figure 5.7 depicts the linear viscoelastic moduli of one the synthesized PCLs (JT-4-15). The viscoelastic functions of the moduli are similar to the master curve presented in Figure 5.5. The origin of the slight increase of viscosity at low shear rates is due to a low level of physical crosslinking or even possibly to experimental error. Figure 5.7 shows narrower range of frequencies that linear viscoelastic data could be measured having the characteristic slope of 2 for elastic modulus (G') compare to the commercial Capa®6800.

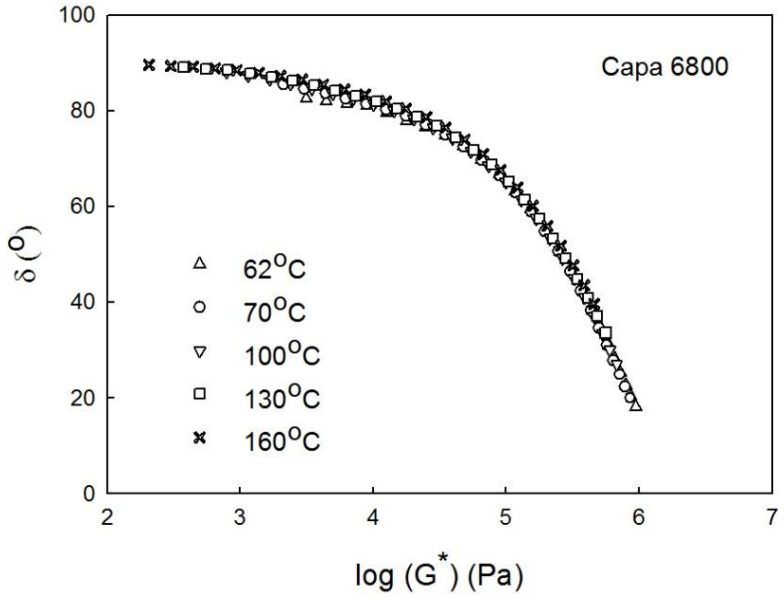

Figure 5.6 The phase angle (δ) as a function of complex modulus at different temperatures for Capa®6800.

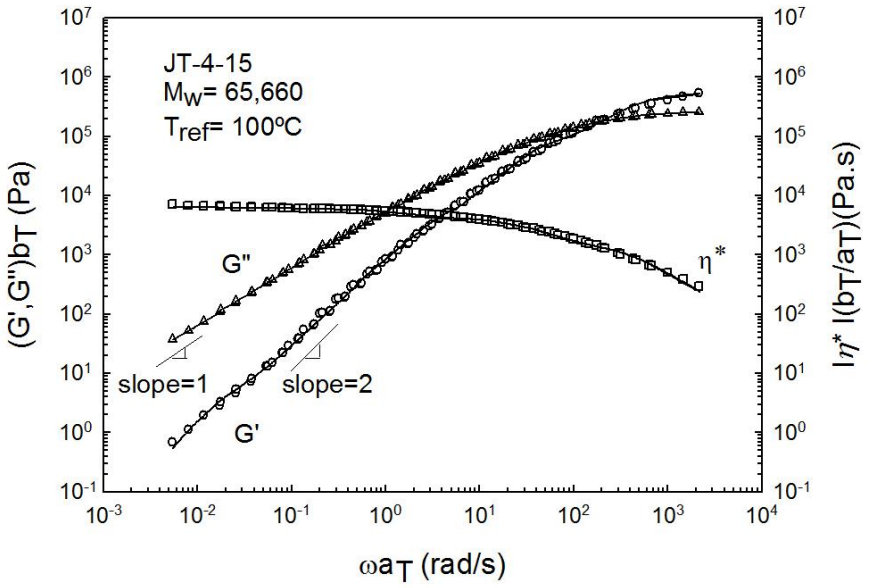

Figure 5.7 Master curve of linear viscoelastic moduli and dynamic viscosity ($|\eta^*|$) of PCL (JT-4-15) as a function of frequency at the reference temperature of 100°C.

Master curves of the linear viscoelastic moduli and complex viscosity were produced for all the homopolymer PCLs and they are presented in Appendix A. Deviation of the

characteristic slope at low frequencies for some of PCLs can be related to physical crosslinking.

The storage and loss moduli of commercial PCLs of various molecular weight are plotted in Figure 5.8.a and 5.8b respectively. The same viscoelastic properties are shown for different molecular weight synthesized PCLs in Figure 5.9a and 5.9b as a function of reduced frequency. Continuous lines represent fits of the Maxwell relaxation spectrum (g_i, λ_i).

$$G'(\omega) = \sum_{i=1}^{N} \frac{g_i \lambda_i^2 \omega^2}{1 + \lambda_i^2 \omega^2} \tag{5-1}$$

$$G''(\omega) = \sum_{i=1}^{N} \frac{g_i \lambda_i \omega}{1 + \lambda_1^2 \omega^2} \tag{5-2}$$

From Figures 5.8 and 5.9, it can be inferred that with increase of the molecular weight, the dynamic moduli (storage and loss modulus) reach the terminal zone at lower frequencies. High molecular weight PCLs (commercial and synthesized) exhibit a tendency to a plateau region at high frequencies. It should be noted that at high frequencies, storage and loss modulus are nearly independent of molecular weight and the measurements as expected for linear polymers (Dealy and Larson 2006, Dealy and Wissbrun 1990).

The shift factors determined to superpose the linear viscoelastic data are indicative of temperature dependence of viscoelastic properties. As discussed before the horizontal shift factor (a_T) demonstrates the temperature dependence of viscosity as well that of the relaxation times. For semi-crystalline polymers more than 100°C above the glass transition temperature, a_T follows the Arrhenius equation (Equation 2.14) (Dealy and Wissbrun 1990). The values of activation energy, a_T determined for commercial and synthesized homopolymers were found to be mostly in the range of 32.5 to 40.8 KJ/mol with no particular trend and dependencies on molecular parameters. These values are in good agreement with the previously reported values of 35-38 KJ/mol for the activation energy of PCL in the literature (Kapoor and Bhattacharya 1999). It should be noted that the corresponding activation energy values for the newly synthesized PCL are higher than those of the commercial PCLs, which might be an indication of structural differences.

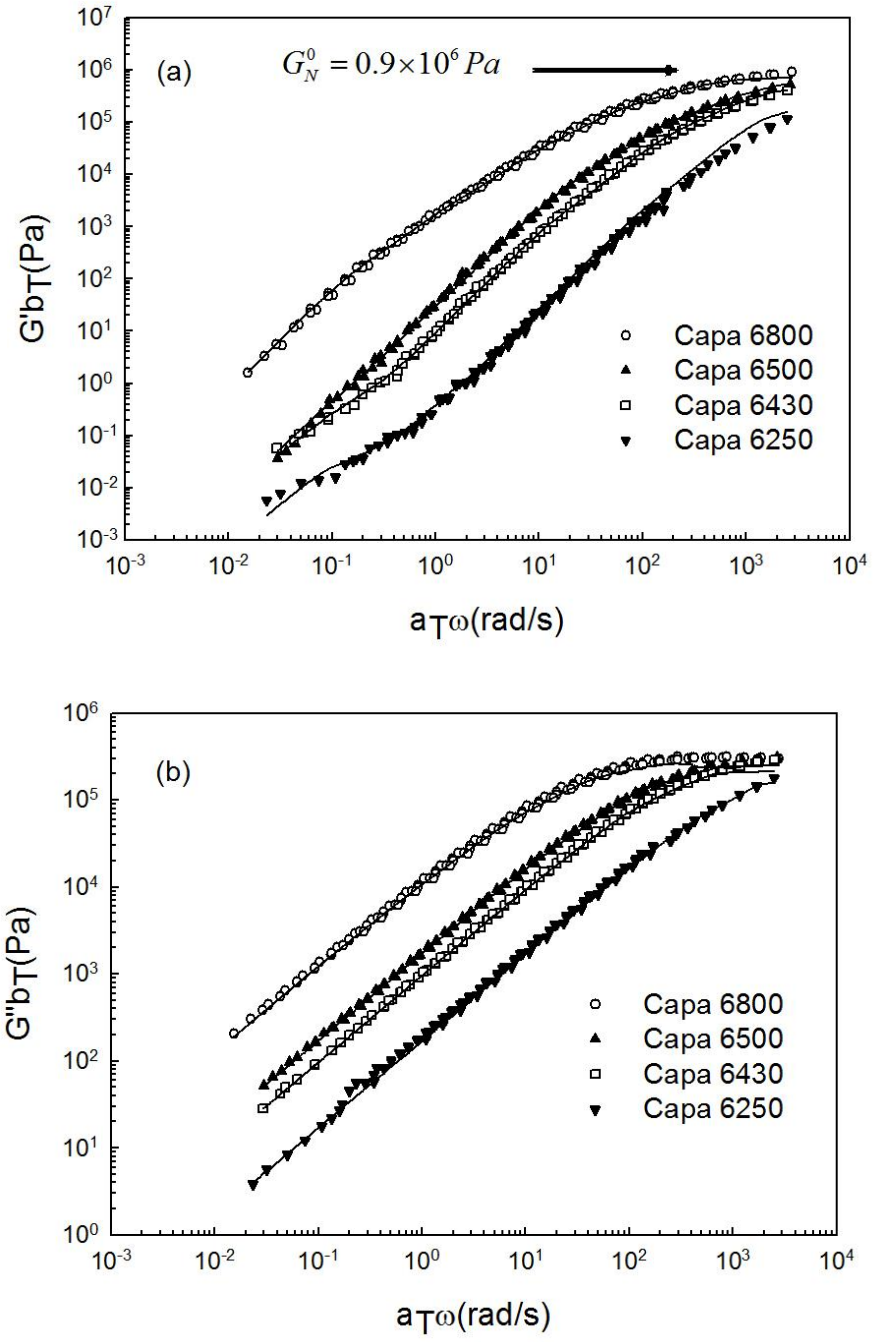

Figure 5.8 Effect of molecular weight on (a) Storage modulus and (b) Loss modulus of commercial PCLs at the reference temperature of 100°C.

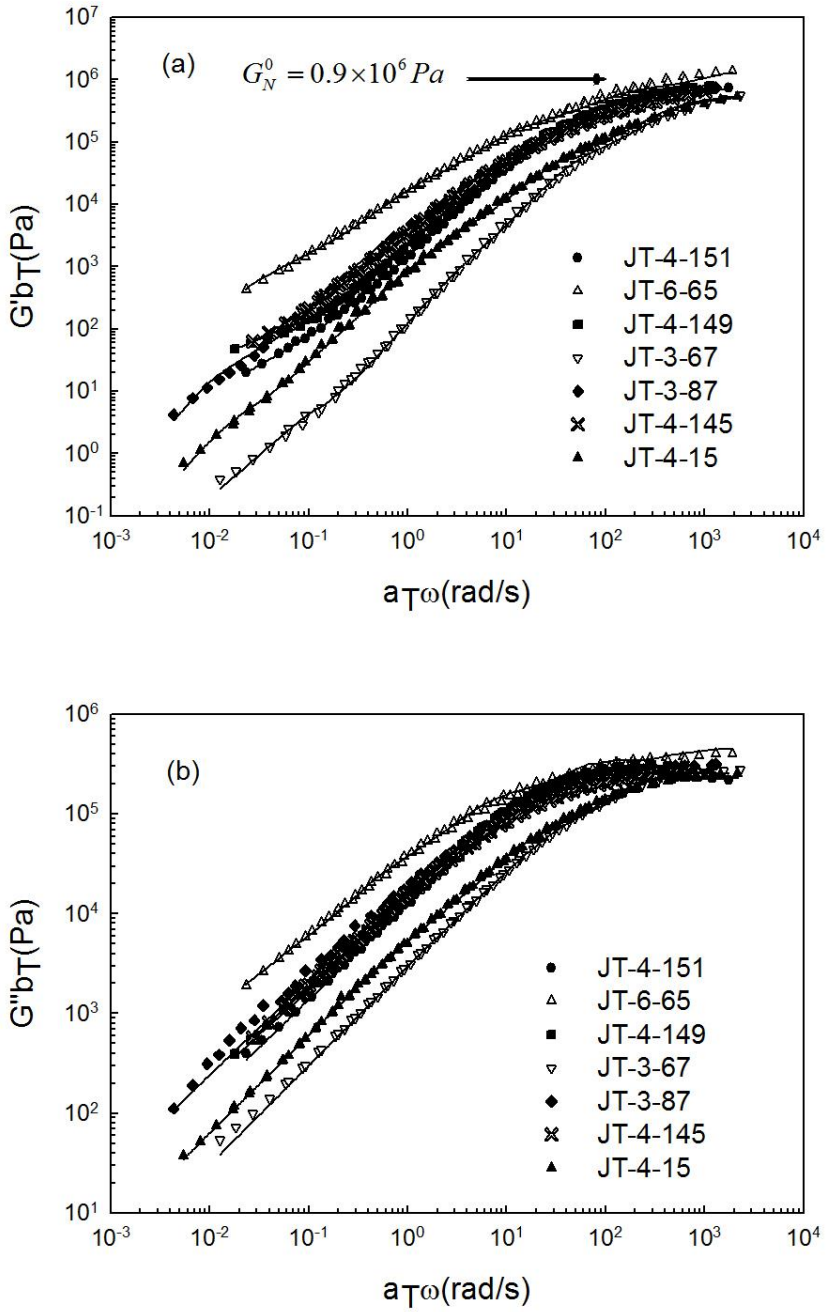

Figure 5.9 Effect of molecular weight on (a) Storage modulus and (b) Loss modulus of synthesized PCLs at the reference temperature of 100°C.

The values of vertical shift factor (b_T) used to superpose data varied from 0.95 to 1.12, which indicates the weak dependence of modulus on temperature. Values of vertical shift factors close to 1 are typical for linear polymers. The variation of horizontal shift factors (a_T) of

different molecular weight PCLs with temperature is depicted in Figure 5.10. These values are almost the same for commercial PCLs and independent of the molecular weight as also discussed above. The dotted line in Figure 5.10 represents the Arrhenius equation for commercial PCL with the slope of 35.76 kJ/mol.

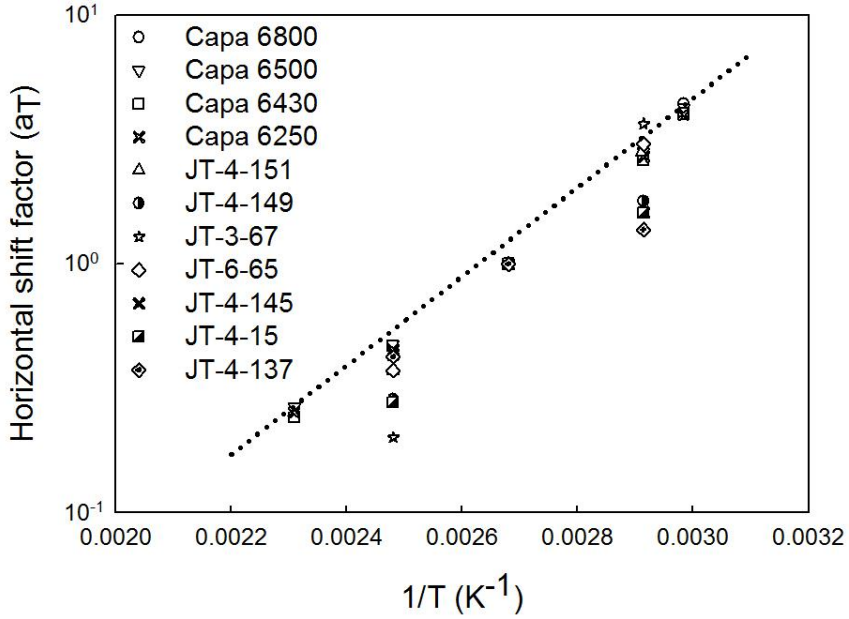

Figure 5.10 The horizontal shift factors calculated from time-temperature superposition to obtain the master curve of the linear viscoelastic properties at the reference temperature of 100°C.

At high shear rates, the degree of shear thinning can be assessed by fitting a viscous model. For this study the Carreau-Yasuda model was employed which can be written as follows (Carreau 1972, Bird et al. 1987):

$$\eta = \frac{\eta_0}{\left[1+(\lambda\dot{\gamma})^{\alpha}\right]^{\frac{1-n}{\alpha}}} \tag{5-3}$$

In the Carreau-Yasuda model, η is the viscosity function, η_0 is the zero-shear viscosity, $\dot{\gamma}$ is the shear rate, α and n are fitting parameters with n representing the degree of shear thinning. The fitted parameters of the Carreau-Yasuda model for the PCL homopolymers are summarized in Table 5.1. As seen the power law exponent, n, correlates

well with molecular weight. The higher the molecular weight of PCL polymer, the higher the degree of shear thinning and the smaller the exponent *n* (Dealy and Larson 2006).

Table 5.1 Zero shear viscosity and activation energy of the PCL homopolymers in descending order of M_w at the reference temperature of 100°C.

Sample	***Zero shear viscosity 100°C, η_0 Discrete relaxation spectrum (Pa.s)***	***Carreau-Yasuda parameters***			***Activation energy for flow, E_a (kJ/mol)***
		η_0 (Pa.s)	***n***	***α***	
JT-4-151[a]	15,437	15,518	0.0494	0.6034	38.7
JT-6-65[c]	91,247	91,880	0.0001	0.5557	40.1
JT-4-149[a]	22,451	23,224	0.0521	0.6359	34.8
JT-3-67[a]	3,071	3,194	0.0557	0.6789	55.3
JT-3-87[b]	21,480	22,535	0.0259	0.4917	39.5
JT-4-145[b]	22,788	22,424	0.0367	0.4855	25.0
Capa6800	12,416	12,902	0.0420	0.5304	32.5
JT-4-15[b]	6,231	6,408	0.0924	0.5064	40.8
Capa6500	1,670	1,759	0.3999	0.9531	33.9
Capa6430	841	992	0.4809	1.0744	34.0
JT-4-137[b]	2,630	2,578	0.1606	0.6228	22.2
Capa6250	119	157	0.7149	1.6286	33.9

[a]: PCLs synthesized by initiator A, [b]: PCLs synthesized by initiator B and [c]: PCL synthesized by initiator A at temperature 60°C.

Figure 5.11 shows the complex viscosity of PCLs along with the Carreau-Yasuda model fits to obtain the zero-shear viscosities as a model parameter. Note that the zero-shear viscosity could not be reached experimentally for all the PCLs. The values of zero-shear viscosity for all polymers are listed in Table 5.1 at the reference temperature of 100°C. These are also in agreement with the values obtained by the discrete relaxation spectrum obtained by fitting the linear viscoelastic moduli (Equations 5.1 and 5.2) (Baumgaertel and Winter 1989, Baumgaertel et al. 1990).

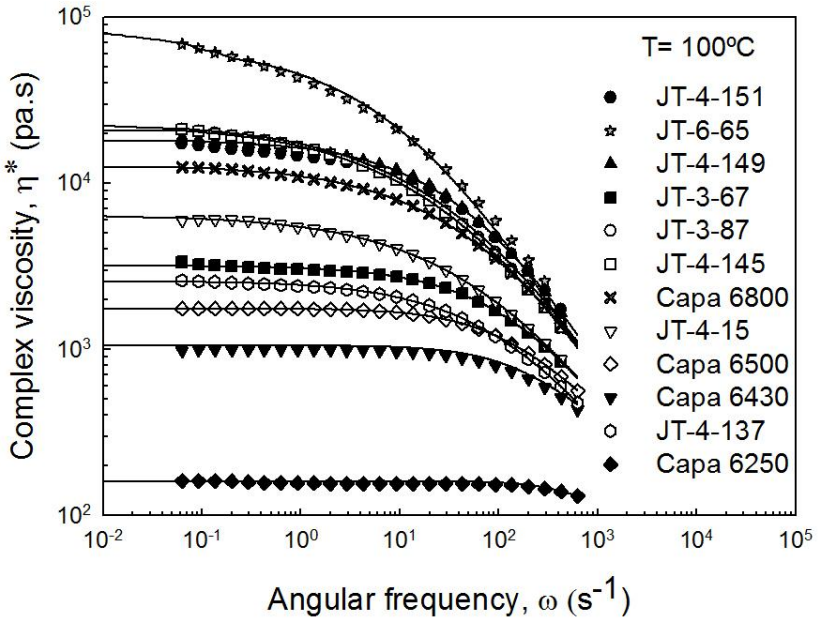

Figure 5.11 The complex viscosity of PCLs at the reference temperature of 100°C. The solid lines represent the Carreau-Yasuda model fitting.

The plateau modulus was calculated numerically from the loss modulus values obtained from the master curve according to the following equation (Dealy and Wissbrun 1990):

$$G_N^0 = \frac{2}{\pi}\int_{-\infty}^{\infty} G''(\omega)\, d\ln\omega \qquad (5\text{-}4)$$

The integration resulted in the value of plateau modulus of $G_N^0 = 0.9107\times10^6\, Pa$ for Capa® 6800 at 100°C. This is relatively higher than the values reported in the literature previously ($G_N^0 = 0.552\times10^6$ and $0.146\times10^6\, Pa$; Ramkumar and Bhattacharya 1998).

It can be clearly observed from Figures 5.8 and 5.9 that at higher molecular weights, the storage and loss moduli have reached more defined plateau regions. At higher shear rates, the storage and loss moduli are relatively independent of molecular weight due to the key role of short segment relaxation.

The molecular weight between entanglements can be determined from the plateau modulus using the following equation:

$$M_e = \frac{\rho RT}{G_N^0} \tag{5-5}$$

Based on Equation 5.5, the value of molecular weight between entanglements (M_e) is 3,900 g/mol for PCLs having density of 1.145 g/cm^3 at 100°C provided by Perstorp.

Figure 5.12 depicts the relationship between the zero-shear viscosity and the molecular weight for the PCLs listed in Tables 4.1 and 4.2. The data can be described by the following equation at 100°C:

$$\eta_0 = 2.0 \times 10^{-16} M_w^{4.0306} \tag{5-6}$$

where M_w is the weight average molecular weight in g/mol and η_0 is the zero-shear viscosity in Pa.s. The dotted line in Figure 5.12 corresponds to Equation 5.6. Most linear nearly monodisperse polymers with molecular weights above the critical molecular weight (M_c) exhibits zero-shear viscosity versus molecular weight relationships with slopes in the range of 3.4-3.6. However, higher slopes around 4 have been reported for a number of polymeric systems, including PCLs and PLAs (Gimenez et al. 2000 and Othman et al. 2011). A power law relationship of $\eta_0 \propto M_w^{4.6}$ has been reported for poly(ε-caprolactone) by Gimenez et al. (2000). Taking into account all data previously reported and those measured in the present study, the following relationship can be derived:

$$\eta_0 = 2.0 \times 10^{-19} M_w^{4.6396} \tag{5-7}$$

The values of molecular weights reported in Figure 5.12 are the values measured after the rheological analysis to consider the possible thermal degradation. Based on the results of complex viscosity plot (Figure 5.11) and zero-sear viscosity plot (Figure 5.12), it can be concluded that the synthesized PCLs by the catalytic system A are less thermally stable compare to the other PCLs except for the polymer that synthesized by the same initiator at 60°C.

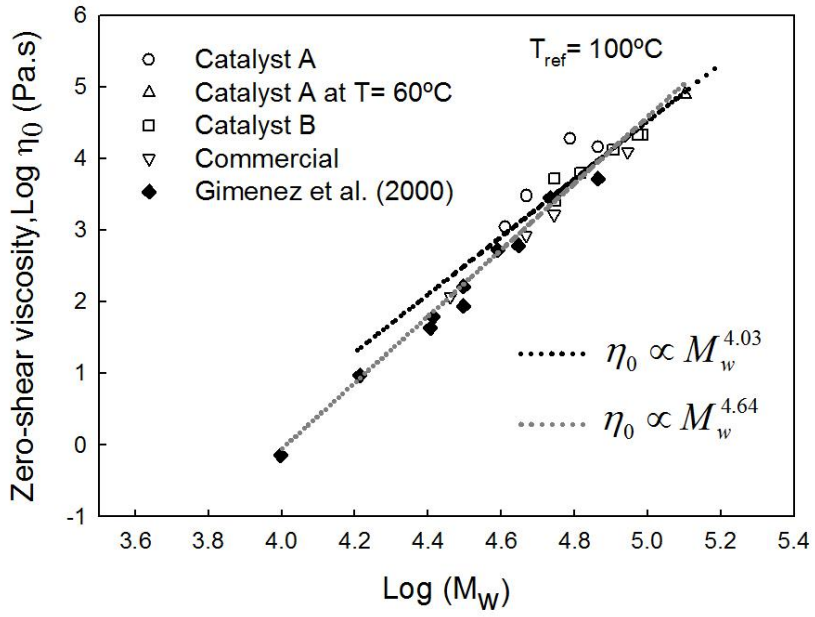

Figure 5.12 Zero-shear viscosity (η_0) as a function of molecular weight (M_w) at the reference temperature of 100°C.

5.3 Stress Relaxation and Damping Function of Homopolymers

Stress relaxation experiments were performed to determine the damping function required for the constitutive modeling. A series of such experiments for Capa® 6800 are plotted in Figure 5.13 in terms of the relaxation modulus, $G(\gamma,t)$ for shear strain values up to 3. The measurements were performed at 160°C since at low temperatures, wall slip possibly occurs which limits the accuracy. Wall slip in such experiments at low temperatures has also been reported previously for the case of polyisoprenes (Ferri and Greco 2006). Up to strains of about γ=0.4, the measurements superpose well since such small strains lie within the linear viscoelastic region. Figure 5.14 exhibits the superposition of stress relaxation curves. The curves in Figure 5.13 are similar and their perfect superposition (Figure 5.14) suggest that the time-dependent relaxation modulus and strain-dependent damping function are separable and the classic simplified K-BKZ model (referred to as Wagner model) can be used for their constitutive modeling (Ferri 1980, Bernstein et al. 1963, Kaye 1962, Wagner 1976, Rolon-Garrido and Wagner 2009).

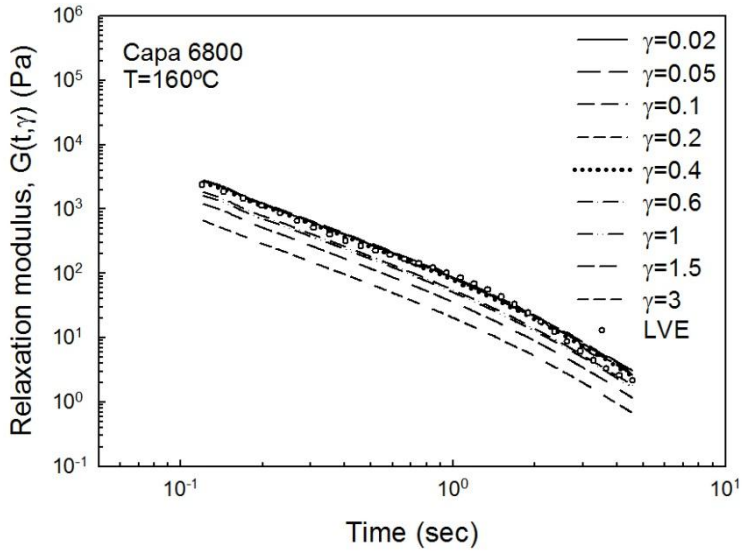

Figure 5.13 Step-strain stress relaxation tests for Capa®6800 at 160°C. Circles represent the linear relaxation modulus (LVE) calculated from the discrete relaxation spectrum.

The linear viscoelastic modulus can be determined from the parsimonious relaxation spectrum by fitting the linear viscoelastic moduli as follows (Ferri 1980):

$$G(t) = \sum_{i=1}^{N} g_i e^{\frac{-t}{\lambda_i}} \tag{5-8}$$

The values of g_i and λ_i are the generalized Maxwell model parameters extracted from the discrete spectrum by Equations 5.1 and 5.2.

The values of g_i and λ_i for Capa®6800 are summarized in Table 5.2 at various temperatures ranging from 62°C to 160°C. The values of g_i and λ_i at a single temperature and the activation energy would be sufficient to represent the data at all temperatures. However, for the sake of higher accuracy, these should be given at all temperatures due to the existence of the vertical shift factor b_T. The continuous lines in Figures 5.5 and 5.7 represents the parsimonious relaxation spectrum obtained from Equations 5.1 and 5.2.

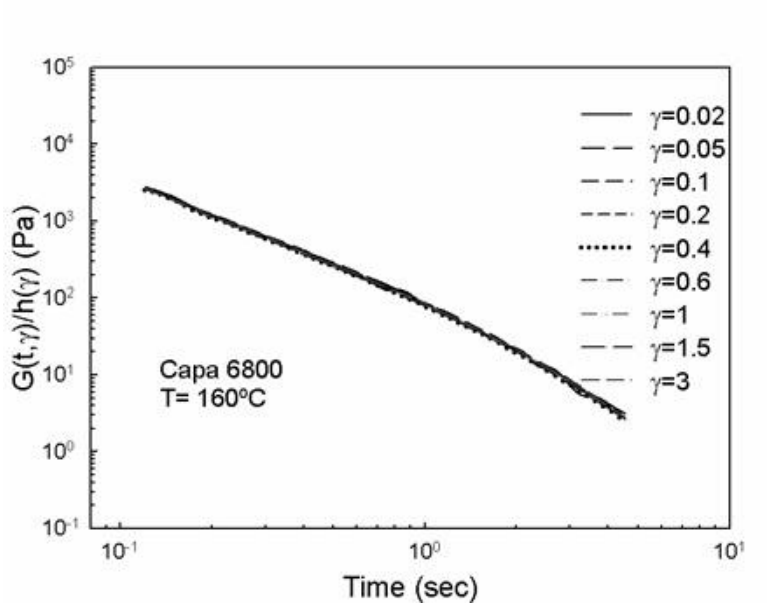

Figure 5.14 Superposed stress relaxation curves of Capa®6800 at 160°C to determine the damping function.

Table 5.2 Generalized Maxwell parameters, g_i (relaxation modulus) and λ_i (relaxation time) for Capa®6800 at various temperatures.

70°C		***100°C***	
g_i ***(Pa)***	λ_i ***(s)***	g_i ***(Pa)***	λ_i ***(s)***
1.92×10^{5}	6.34×10^{-2}	4.12×10^{5}	3.22×10^{-3}
3.69×10^{5}	2.20×10^{-3}	2.11×10^{5}	1.82×10^{-2}
3.47×10^{5}	1.17×10^{-2}	0.39×10^{5}	0.1×10^{0}
0.24×10^{5}	4.65×10^{-3}	0.02×10^{5}	7.34×10^{-1}
0.01×10^{5}	5.8×10^{0}	0.002×10^{5}	4.76×10^{0}
130°C		***160°C***	
g_i ***(Pa)***	λ_i ***(s)***	g_i ***(Pa)***	λ_i ***(s)***
1.57×10^{5}	1.32×10^{-2}	0.89×10^{5}	1.36×10^{-2}
3.98×10^{5}	2.47×10^{-2}	3.58×10^{5}	2.43×10^{-3}
0.23×10^{5}	7.16×10^{-2}	0.07×10^{5}	8.52×10^{-2}
0.01×10^{5}	4.98×10^{-1}	0.004×10^{5}	6.04×10^{-1}
0.0009×10^{5}	2.89×10^{0}	0.00003×10^{5}	6.37×10^{0}

The damping function, $h(\gamma)$ is plotted in Figure 5.15. It is found that the Papanastasiou model (Papanastasiou et al. 1983) with a single fitting parameter can represent the data well with α=0.58. The general form of this model is as follows:

$$h(\gamma) = \frac{1}{1+\alpha\gamma^2} \tag{5-9}$$

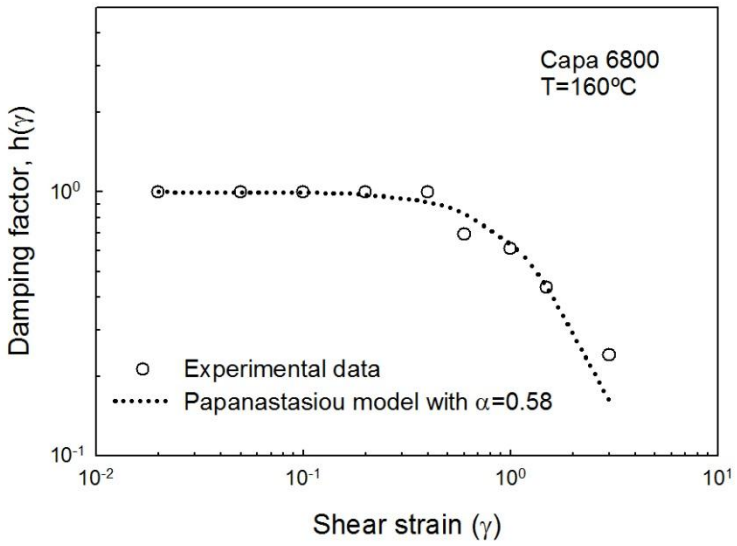

Figure 5.15 The damping function of Capa®6800 at 160°C.

5.4 Extensional Rheology

The behavior of poly(ε-caprolactone) in uniaxial extensional deformation is shown in Figure 5.16. The measurements were carried out at several Hencky strain rates from 0.01 to $10s^{-1}$ at the low temperature of 62°C. This temperature was selected to avoid sagging caused by the low viscosity of PCL at higher temperatures. Figure 5.16 depicts the tensile stress growth coefficient of Capa®6800, η_E^+, at 62°C at a number of Hencky strain rates, $\dot{\varepsilon}_H$. The behavior presented in Figure 5.16 is typical for linear polymers and the response at all rates follows the linear viscoelastic envelope of $3\eta_E^+$ (Ferri 1980). The shear stress growth coefficient can

be determined from the parsimonious relaxation spectrum (g_i,λ_i) using the following equation:

$$\eta^+(t) = \sum_{i=1}^{N} \frac{g_i}{\lambda_i}\left(1 - e^{\frac{-t}{\lambda_i}}\right) \tag{5-10}$$

Also the relaxation time of the chain is very small compared to the deformation time scale, which cannot lead to strain hardening behavior.

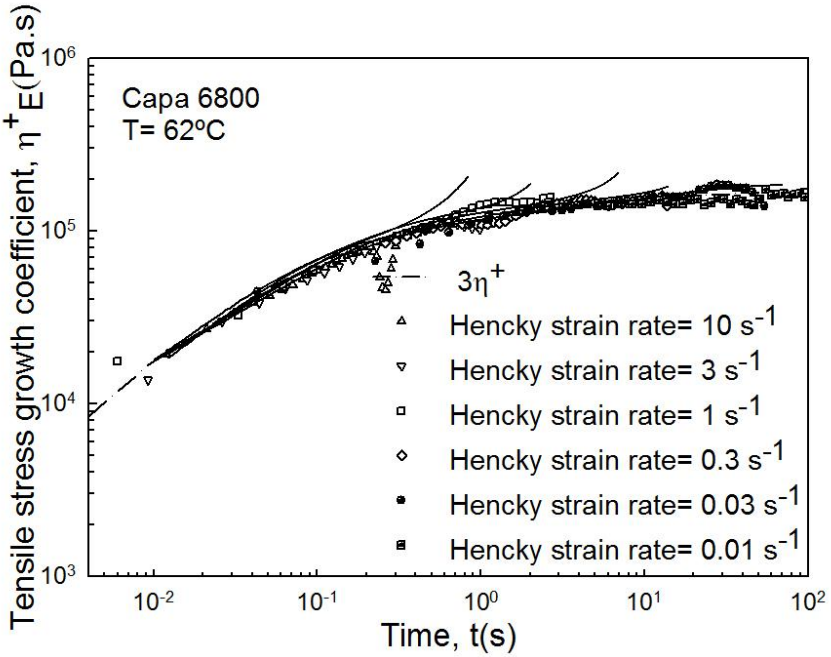

Figure 5.16 The tensile stress growth coefficient of Capa®6800 at various Hencky strain rates at 62°C.

5.5 Constitutive Modeling

To gain a better understanding of the behavior of poly(ε-caprolactone) in shear and extensional flow, a simplified version of the K-BKZ equation (Kaye-Bernstein, Kearsley and Zapas) (Bernstein et al. 1963, Kaye 1962) also known as the classic Wagner constitutive model has been employed (Wagner 1976, Rolon-Garrido and Wagner 2009). This Wagner model can be written as follows:

$$\sigma(t) = \int_{-\infty}^{t} m(t-t')h(\mathrm{I}_1, \mathrm{I}_2)B(t,t')dt \tag{5-11}$$

where $\boldsymbol{\sigma}(t)$ is the stress tensor, $\boldsymbol{B}(t,t')$ is the Finger tensor, $m(t-t')$ is the memory function and $h(I_1,I_2)$ is the damping function. The damping function is typically a function of first and second invariant of deformation tensor, in this case the Finger tensor. The memory function is related to linear relaxation modulus, and it can be described as a summation of the exponentials obtained from the relaxation spectrum parameters (g_i,λ_i). These parameters and their determination were discussed earlier in Equations 5.1 and Equation 5.2.

$$m(t-t') = \frac{dG(t-t')}{dt'} = \sum_i \frac{g_i}{\lambda_i} \exp\left(-\frac{(t-t')}{\lambda_i}\right) \tag{5-12}$$

As discussed above, the damping function was determined experimentally by the step-strain relaxation tests (Figure 5.15) and was represented by Equation 5.9; however, a more general expression is needed to include all types of flow such as extensional. In case of the start-up of steady shear, Equation 5.11 can be written as:

$$\eta^+(t) = tG(t)\left(\frac{1}{1+\alpha(\dot{\gamma}t)^2}\right) + \int_0^t sm(s)\left(\frac{1}{1+\alpha(\dot{\gamma}s)^2}\right)ds \tag{5-13}$$

Figure 5.17 depicts a comparison between the viscoelastic response of start-up of steady shear experiments at 160°C and the Wagner model predictions of Equation 5.13. Using the damping function given by Equation 5.9 with the value of α=0.58 determined by shear experiments (Figures 5.13, 5.14 and 5.15), the predictions were within ±8% of the experimental results in Figure 5.17. The same results have been previously reported specially for highly entangled polymers (Kasehagen and Macosko 1998). Therefore, the start-up of steady shear experimental results have been used directly to determine the optimum value of α of the damping function. The optimum value of α was found to be 0.256 that is different from the value of 0.58 determined from stress relaxation experiments. The same value of $1/\alpha$ = 3.9 has been reported before for linear polymers by Kasehagen and Macosko (1998). The undershoot exhibited by the solid lines is a consequence of the discrete relaxation spectra calculated.

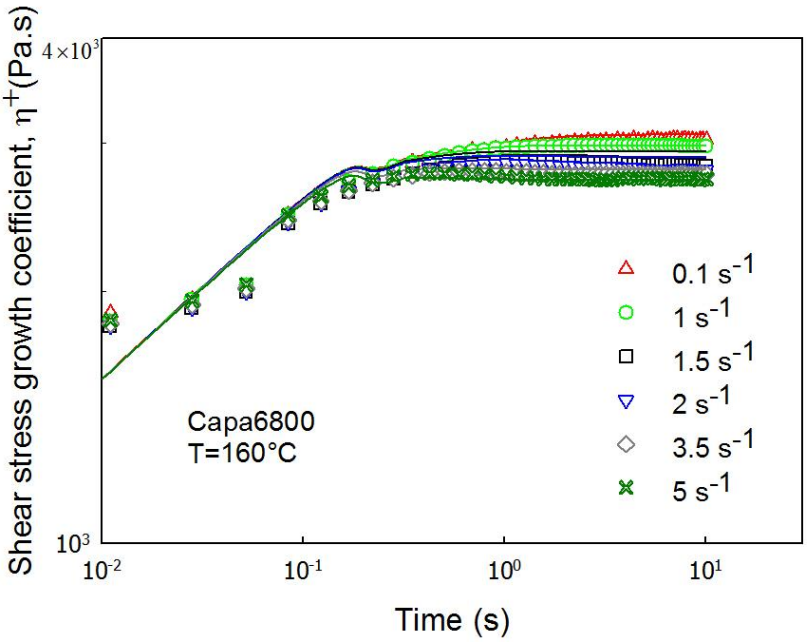

Figure 5.17 Steady shear stress growth coefficient of Capa®6800 for various shear rates at 160°C. The solid lines represent the Wagner model predictions.

There are a few attempts to measure uniaxial extension directly due to the experimental limitations of applying step strain (Rolon-Garrido and Wagner 2009). Wagner calculated the damping function in uniaxial extension by using the constitutive equation inversely. By this approach, the Wagner model (Equation 5.11) can be rearranged into the following equation for the case of tensile stress relaxation after imposition of a sudden Hencky strain (Urakawa et al. 1995):

$$h(\varepsilon) = \frac{\dfrac{\sigma(t)}{G(t)} - \dfrac{1}{\dot{\varepsilon}}\displaystyle\int_0^{\varepsilon} \sigma(s)\frac{m(s)}{G^2(s)}\,ds}{e^{2\varepsilon} - e^{-2(1+m)\varepsilon}} \tag{5-14}$$

For uniaxial extension, m = 0.5. In this case a different form of the damping function has been used, namely:

$$h(I_1, I_2) = \frac{1}{1+\alpha\sqrt{(I_1-3)(I_2-3)}} \tag{5-15}$$

By substituting the invariants of the Finger tensor, the damping function takes the following form:

$$h(\varepsilon) = \frac{1}{1 + \alpha\sqrt{(e^{2\varepsilon} + 2e^{-\varepsilon} - 3)(2e^{\varepsilon} + e^{-2\varepsilon} - 3)}} \tag{5-16}$$

The value of α can be obtained by fitting the extensional stress growth coefficient using the same values of shear relaxation modulus and relaxation time. However, the model shows satisfactory predictions with the same value of parameter α equal to 0.256 that was obtained from shear experiments. The solid lines in Figure 5.16 show the Wagner model predictions for Hencky Strain rates of 0.03, 0.3,1, 3 and 10 s^{-1}.

5.6 Summary

The solution and melt rheological properties of PCLs having different molecular weights have been investigated. First for the solution rheological properties it was found that Mark Houwink parameters and the characteristic radii agreed well with values reported for other linear flexible polymers confirming the linear macrostructure of PCL molecules.

For the melt properties, it was found that the time-temperature superposition applies well on the linear viscoelastic data of all PCLs examined, indicating that PCLs are thermorheologically simple fluids. The plateau modulus of PCLs was found to be 0.9×10^{6} Pa, which is independent of molecular weight. The molecular weight between entanglements for PCL was found to be approximately 3,900 g/mol that was determined from their plateau modulus and well established relationships in literature. The zero-shear viscosities of PCLs have shown a power law scaling exponent of 4.0 with the molecular weight, which is higher than the exponent of 3.4-3.6 typically reported for linear well-entangled nearly monodisperse polymers. Furthermore, no strain hardening was observed under extensional flow. A simplified version of the K-BKZ rheological constitutive equation known as the Wagner constitutive equation was successfully used to predict the viscoelastic behavior of PCLs under shear and extensional flows.

6 Processing and flow instabilities of Poly(ε-caprolactone) Homopolymers

In this chapter, the processing and flow instabilities of commercial PCLs are studied. Specifically, their processing behavior in capillary flow is examined in terms of critical conditions for the onset of melt fracture. Finally, processing aids that can be used to postpone the onset of melt fracture to high shear rates are identified and proposed (Achilleos et al., 2002; Amos et al., 2001).

6.1 Capillary Extrusion

The processability of commercial PCLs has been studied by capillary rheometry. As discussed above the raw data obtained from such a piece of equipment (pressure drop, ΔP versus volumetric flow rate, Q) can be transformed into fundamental rheological data (apparent wall shear stress, $\sigma_{w,a}$ if the Bagley correction has not been applied or wall shear stress, $\sigma_{w,a}$ and apparent shear rate, $\dot{\gamma}_a$) by the use of Equations 2.19 and 2.10.

Capillary experiments for Capa®6800 were performed for two series of dies with diameters, D = 0.43 mm and 0.76 mm and three length-to-diameter ratios at several temperatures ranging from 80–160°C. Figure 6.1 depicts the flow curves of Capa®6800 for three capillary dies having a diameter of 0.43 mm and three different length-to-diameter ratios. Figure 6.2 shows the Bagley correction plots corresponding to the flow curves of Figure 6.1. The entry pressure drop was obtained by applying linear regression to the data. Determining the Bagley (entry pressure drop) and Rabinowitsch corrections and replotting the data of Figure 6.1, an excellent superposition is obtained (Figure 6.3). Since the data for various L/D superpose well, it implies that the effect of pressure on viscosity is negligible and it is similar to that reported for HDPE (Hatzikiriakos and Dealy 1994). Similar results were obtained for the second series of dies having a diameter of 0.76 mm. The apparent flow curve, Bagley plot and the Bagley corrected flow curve obtained with capillary dies having a diameter of 0.76 mm are included in Appendix B.

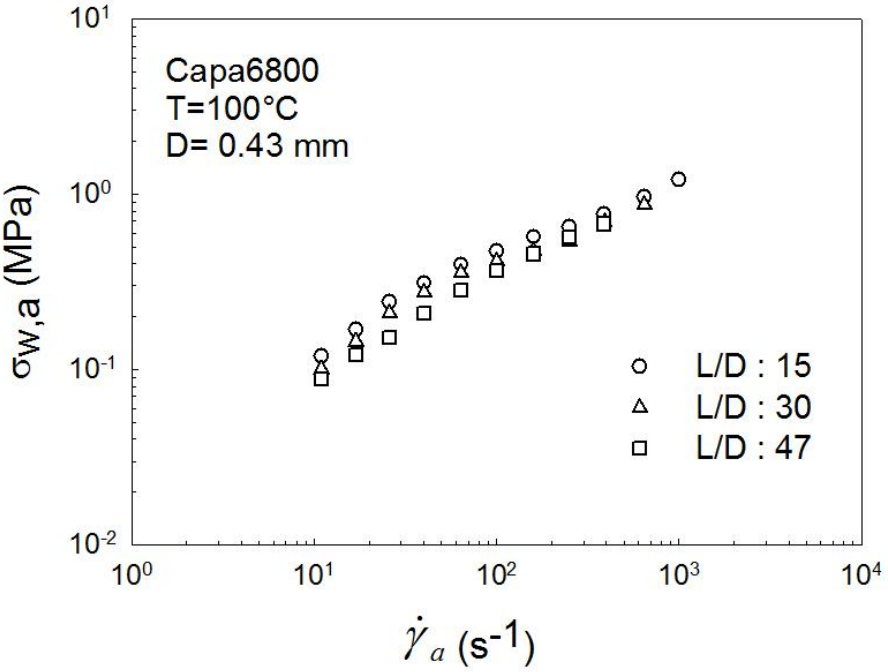

Figure 6.1 The apparent flow curves of PCL Capa®6800 at 100°C using three capillary dies having a constant diameter of 0.43 mm and different *L*/*D* ratio to determine the effect of pressure on viscosity.

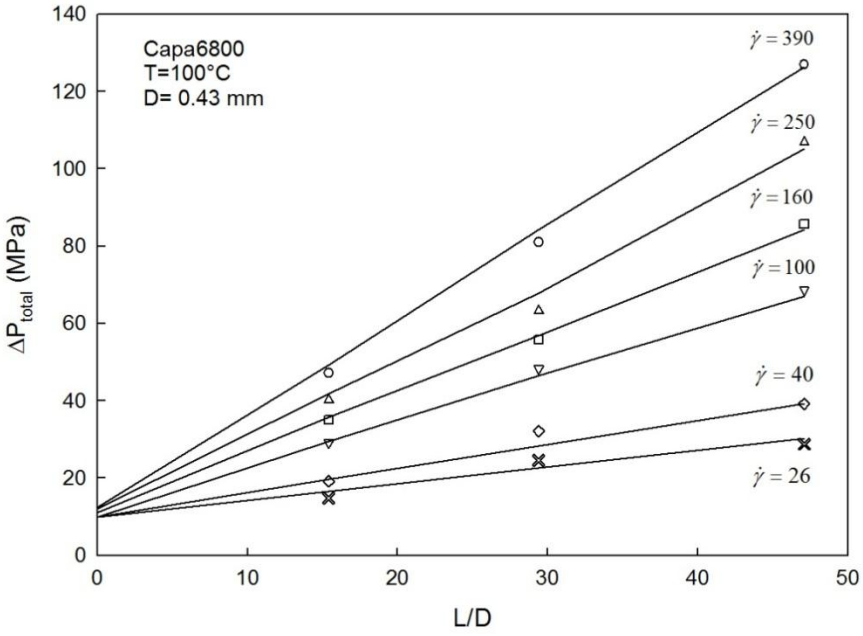

Figure 6.2 Bagley plot to determine the end pressure for Capa®6800 at 100°C.

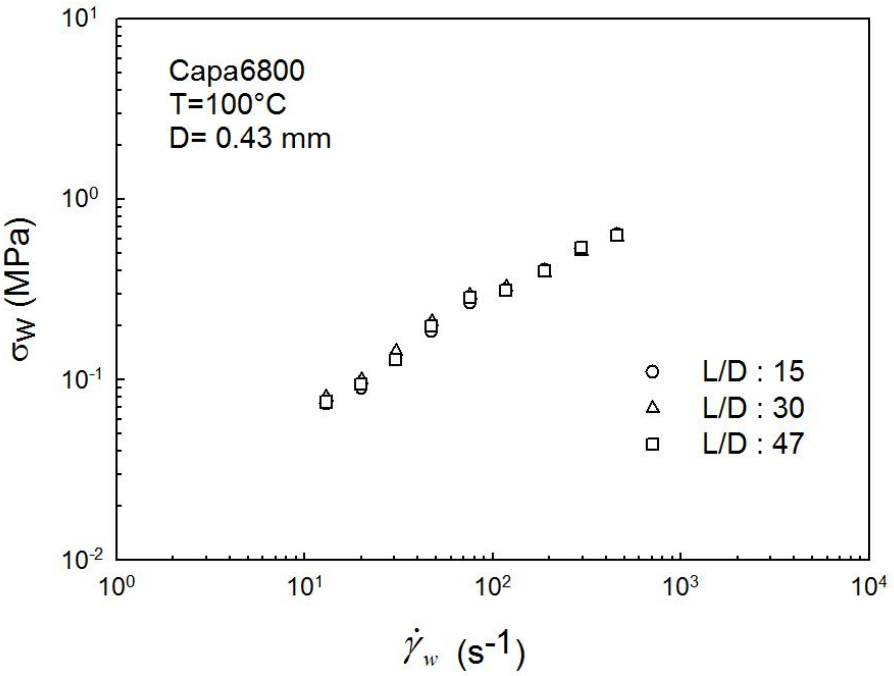

Figure 6.3 The Bagley-corrected flow curves of PCL Capa®6800 at 100°C using three capillary dies having a constant diameter of 0.43mm and different *L*/*D* ratio. Superposition of the data implies that the effect of pressure on viscosity is insignificant.

Figure 6.4 depicts the Bagley-corrected flow curves for two capillary dies having a constant *L*/*D* = 30 (keep the effect of pressure constant) and two different diameters, namely 0.43 and 0.76 mm. Since the data superpose well, it can be concluded that slip does not occur in the flow of PCL, at least not up to levels of stress reached in this work that is approximately 0.5 MPa.

The validity of the Cox–Merz rule is shown in Figure 6.5 for the two PCLs having the highest molecular weight at 100°C. This also implies the absence of slip. Detailed capillary experiments for the two PCLs having the lowest molecular weight, namely Capa®6430 and Capa®6250 listed in Table 4.1, were not performed due to the lack of interest. It is noted that these two low molecular weight polymers exhibit no flow instabilities as is explained in the next section.

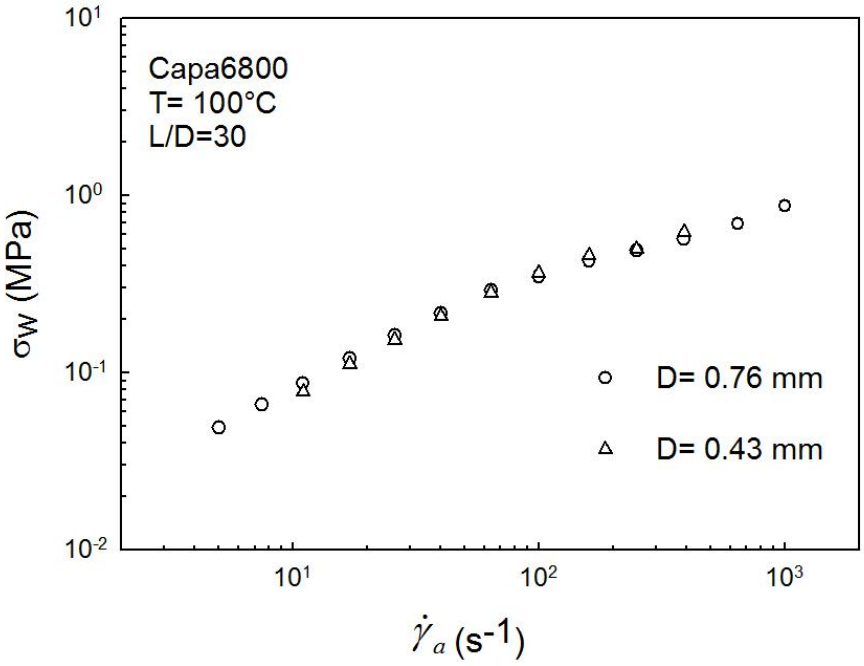

Figure 6.4 The Bagley-corrected flow curves of Capa®6800 obtained for two sets of capillaries with the same *L*/*D* and different diameters to examine slip effects. Good superposition implies the absence of slip.

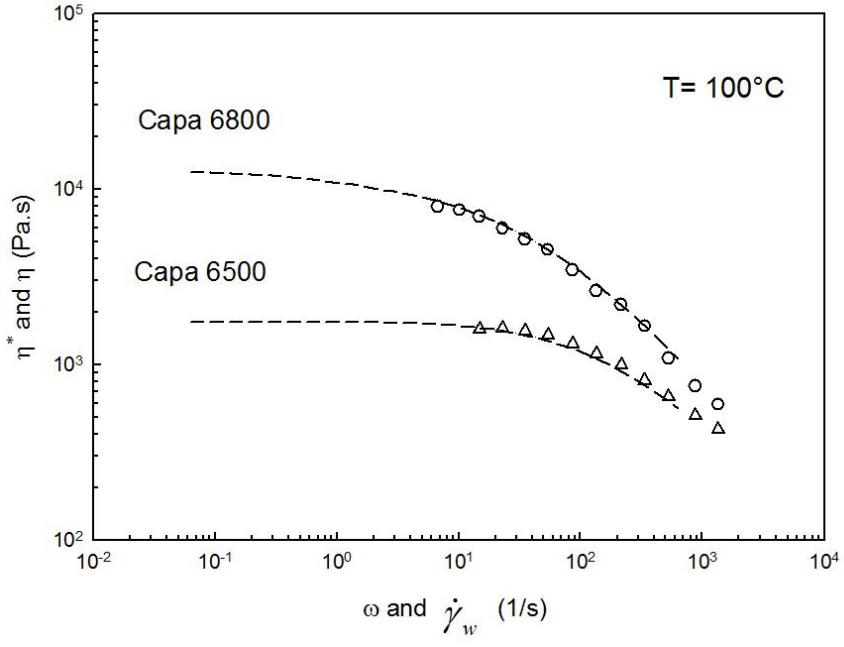

Figure 6.5 The good agreement of shear and complex viscosity of Capa®6800 and Capa®6500 at 100°C implied the validity of Cox– Merz rule. Short dashed lines and symbols represent complex viscosity and capillary shear viscosity respectively.

6.2 Melt Fracture

In our capillary experiments, we found that the highest molecular weight commercial PCL exhibits melt fracture phenomena (extrudate distortions) while all the other commercial PCLs always exhibited smooth and glossy extrudates. Figure 6.6 plots the flow curve of Capa®6800 at six temperatures, namely 80, 100, 115, 130, 145 and 160°C.

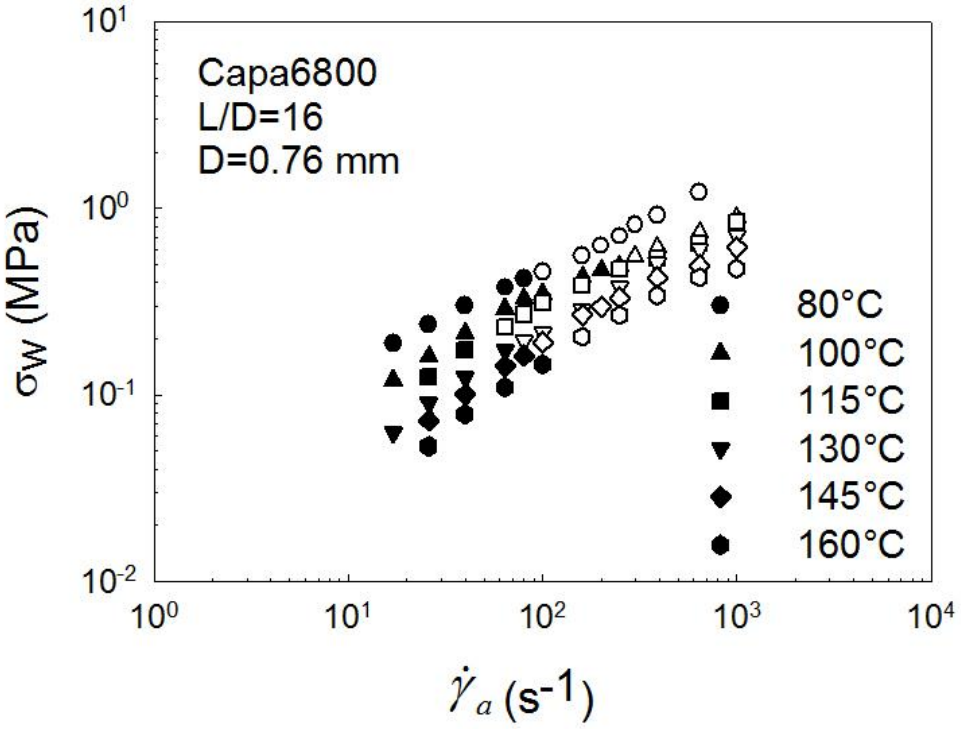

Figure 6.6 The flow curves of Capa®6800 at 80°C, 100°C, 115°C, 130°C, 145°C and 160°C. Full symbols represent conditions where extrudates are free of any distortions.

At 80°C which is close to melting temperature of PCL, shear induced crystallization causes increase of shear stress and deviation from Cox–Merz rule at high shear rates. The various instabilities observed on the surface of extrudates included loss of gloss, sharkskin or surface melt fracture, stick-slip or oscillating melt fracture and finally gross melt fracture. Loss of gloss and sharkskin melt fracture appeared at critical shear stresses between 0.17 to 0.21 MPa for the extrudates at temperatures higher than 115°C. For measurements at 100°C, sharkskin phenomena were surprisingly obtained at much higher critical stress values of greater than 0.48 MPa. At the lowest temperature of 80°C the critical shear stress for the onset of instabilities was 0.41 to 0.45 MPa which is comparable to that obtained at 100°C. It

seems that processability of this resin is better at low temperatures. Table 6.1 summarizes the critical shear stresses (σ_c) and rates for the onset of extrudate distortion using a die with the diameter of 0.76mm and the length-to-diameter ratio of 16 at the temperature range of 80 to 160°C for Capa®6800.

Table 6.1 Critical shear stress and critical apparent shear rates for the onset of melt fracture of Capa®6800 at a temperature range of 80 to 160°C for a capillary die having a diameter of 0.76mm and length-to-diameter ratio of 16.

Temperature (°C)	***Shear stress (MPa)***	***Apparent shear rate (s^{-1})***
80	0.46	100
100	0.49	250
115	0.23	64
130	0.19	80
145	0.19	100
160	0.2	160

Figure 6.7 summarizes the various types of melt fracture of the high molecular weight PCL occurred at different temperatures. The enhanced processability at 100°C is evident. The swell ratio of the extrudates was increased by increasing the shear rate and by reducing the temperature. At the apparent shear rate of 645 s^{-1}, the value of swelling varied from 1.05 at 160°C to 1.52 at 80°C. The swell values of 1.1 to 1.34 were reported for another biodegradable polymer (PLA) previously (Kanev et al. 2007).

Table 6.2 presents SEM images of extrudates of Capa®6800 extruded at 80°C, 100°C, 130°C and 160°C. All the SEM micrographs are with the same magnification (60x) and same scale (500 μm). Comparing the extrudates at various temperatures, it may be easily noted that those extruded at 130°C exhibits clearly periodic surface instabilities very pronounced even at shear rates as low as 100 s^{-1}. At higher shear rates the amplitude of distortions increases significantly as can be observed in Table 6.2. It is also clear the improved processability at the temperature of 100°C. The origin of this is not known, although similar stable processability temperature windows have been observed in the extrusion of linear polyethylenes (Pudjijanto and Denn 1994, Kolnaar and Keller 1997).

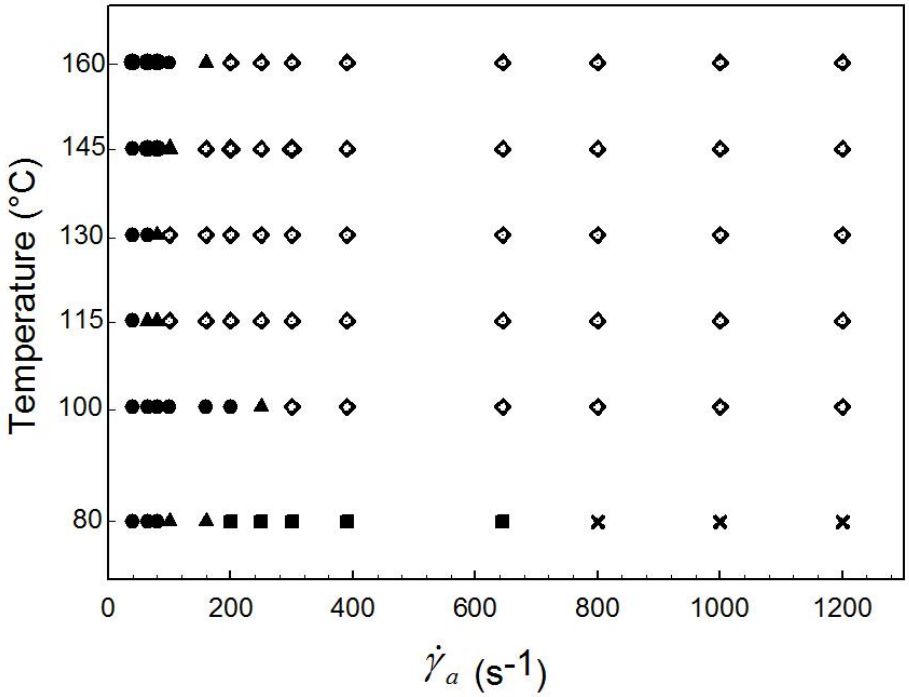

Figure 6.7 Melt fracture map of Capa®6800 at different temperatures over the range of apparent shear rates. Various types of instabilities are demonstrated by different symbols as follows: (●) smooth surface, (▲) loss of gloss (onset of sharkskin), (■)Gross melt fracture, (x) stick-slip, (◊) sharkskin.

Oscillating melt fracture or stick-slip has been observed at 80°C starting at the shear rate of 800 s^{-1}. Possibly this phenomenon occurs at all other higher temperatures at much higher shear rates not reached in the present work. In such flow, the extrudate appear to exhibit alternate smooth and distorted portions in a periodic manner as it can be seen in Figure 6.8. At the same time, the pressure drop oscillates between two extreme values independent of the apparent shear rate. Figure 6.9a, b and c depict these pressure oscillations at three different apparent shear rates from 800 to 1,200 s^{-1}. While the magnitude of these oscillations is independent of shear rate (as expected), the period decreases with increase of shear rate and decrease of the amount of polymer in the reservoir. This phenomenon has been studied in detail for other linear polymers and it is due to the combined effect of compressibility and a transition from a no-slip or weak slip to a massive or strong slip and vice versa (Hatzikiriakos and Dealy 1992b).

Table 6.2 Scanning electron microscopy micrographs of Capa®6800 extrudates at various temperatures ranging from 80°C to 160°C. The extrudates were produced by using a capillary die having a diameter D = 0.76 mm and an L/D = 16.

80°C			
$\dot{\gamma}_a = 100s^{-1}$	$\dot{\gamma}_a = 250s^{-1}$	$\dot{\gamma}_a = 390s^{-1}$	$\dot{\gamma}_a = 645s^{-1}$
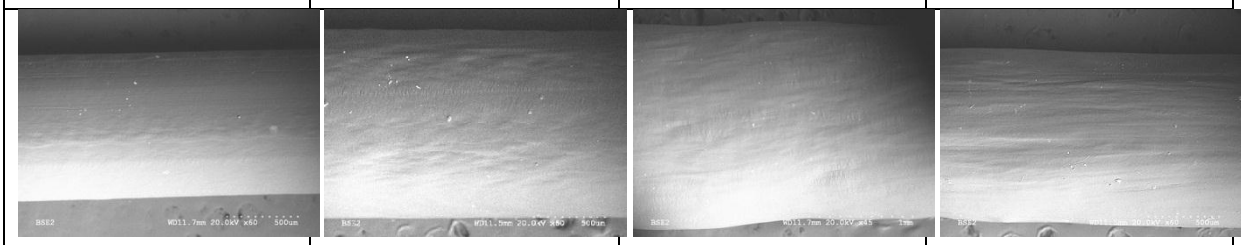			
100°C			
$\dot{\gamma}_a = 100s^{-1}$	$\dot{\gamma}_a = 250s^{-1}$	$\dot{\gamma}_a = 390s^{-1}$	$\dot{\gamma}_a = 1000s^{-1}$
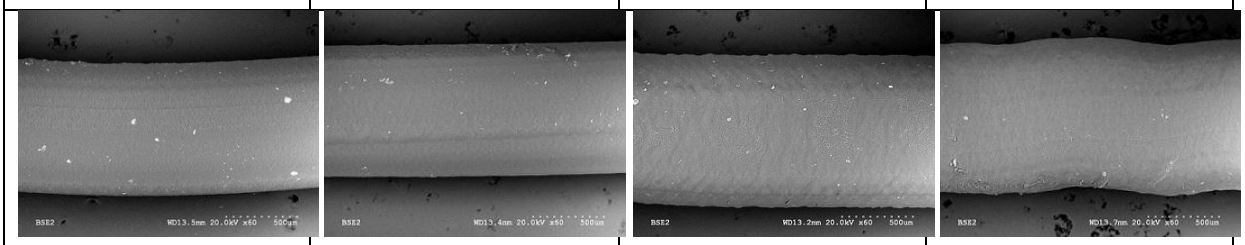			
130°C			
$\dot{\gamma}_a = 100s^{-1}$	$\dot{\gamma}_a = 160s^{-1}$	$\dot{\gamma}_a = 390s^{-1}$	$\dot{\gamma}_a = 1000s^{-1}$
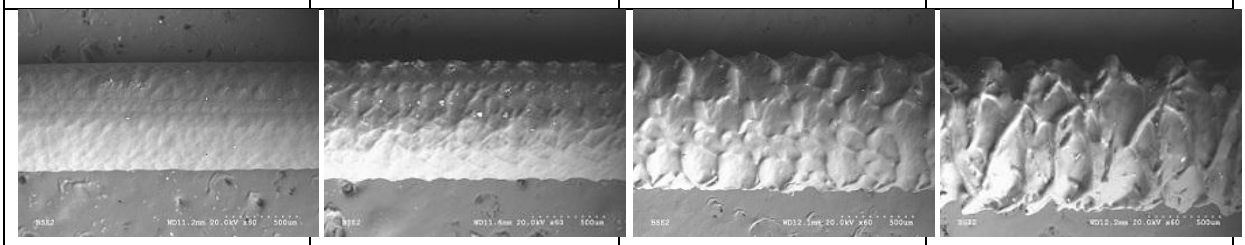			
160°C			
$\dot{\gamma}_a = 100s^{-1}$	$\dot{\gamma}_a = 250s^{-1}$	$\dot{\gamma}_a = 390s^{-1}$	$\dot{\gamma}_a = 1000s^{-1}$
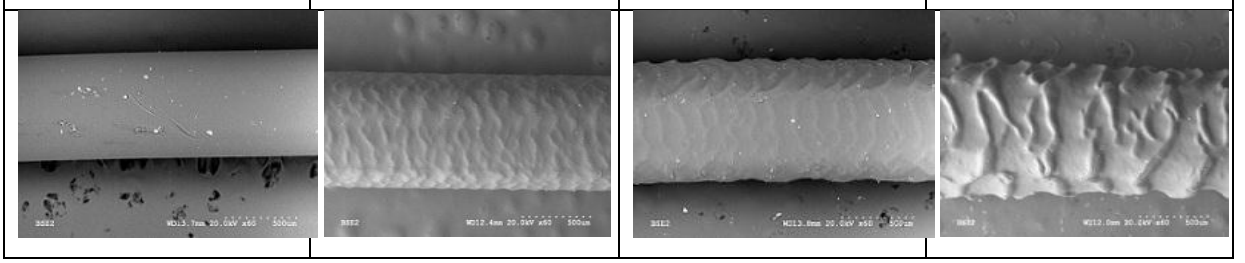			

Figure 6.8 The appearance of Capa®6800 extrudate obtained under conditions of stick-slip oscillations at 80°C. The instability occurred at the apparent shear rate of 800 s^{-1} in a capillary die having a diameter D = 0.76 mm and a length-to-diameter ratio of L/D = 16.

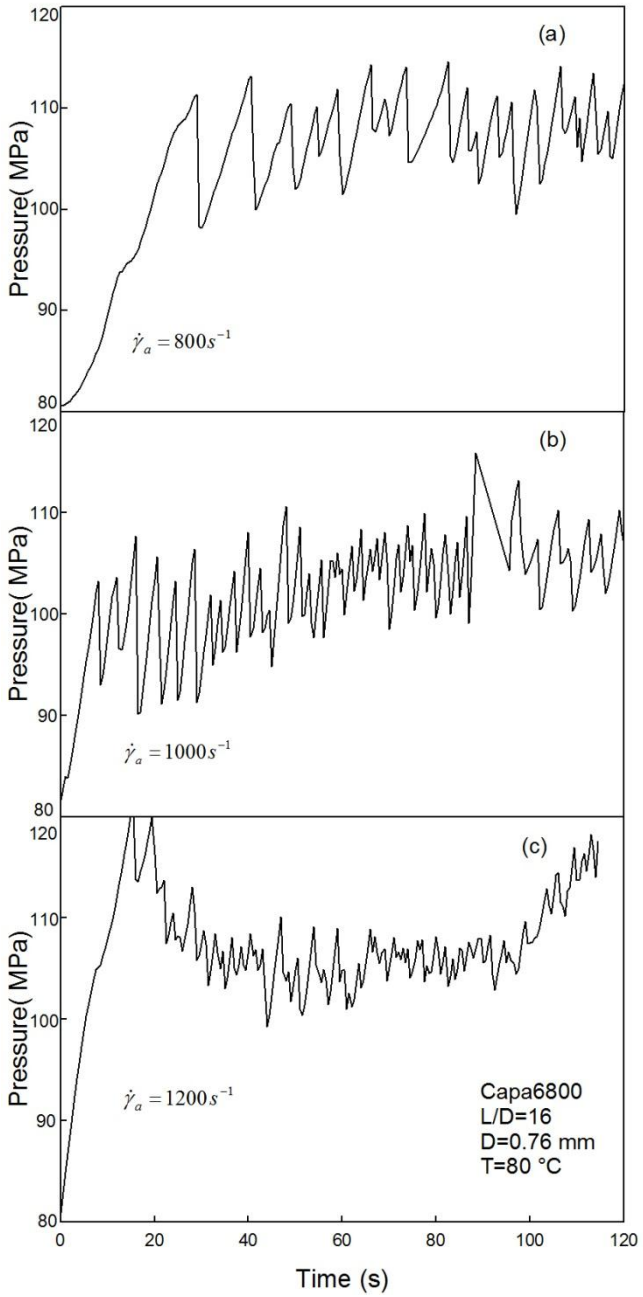

Figure 6.9 Pressure oscillations of Capa®6800 at apparent shear rates of 800, 1000 and 1200 s^{-1} resulted from a capillary die having a diameter of D=0.76 mm and a length-to diameter ratio of L/D=16.

6.3 Processing Aids

Polymer processing aids are typically used to eliminate or postpone extrusion instabilities (melt fracture phenomenon) and to improve the polymer processes from economical point of view by increasing the production rate as well as decreasing the energy cost. Processing aids have been discussed earlier in section 2.3.3. Several types of additives have been reported in literature (Hatzikiriakos et al. 1995, Achilleos et al. 2002, Amos et al. 2001, Rosenbaum et al. 1995), mostly designed for polyolefins. Immiscibility and having lower interfacial tension with the polymeric processing aid compared to the interfacial tension of the polymer and the wall, are essential parameters that makes a polymer a good candidate as polymer processing aid for the extrusion process (Rosenbaum et al. 1995). Polylactides (PLA) might be a potential option for the processing of poly(ε-caprolactone), as they are immiscible with PCLs (Wang et al. 1998, Meredith et al. 2000, Broz et al. 2003).

The effect of adding a small amount of PLA7001D on the extrusion of Capa®6800 was investigated. The extrusion of pure PCL was followed by adding a small amount of 0.5% PLA7001D. The polymers were dry mixed and loaded into the barrel of the capillary rheometer. The extrusion was performed at the temperature of 180°C (above the melting point of PLA) using a die having a diameter of 0.76 mm and length-to-diameter of 16. It is again believed that the PLA coats the wall of the die in order to act as a processing aid; consequently promotes slip and thus causes a significant drop in the extrusion pressure. Thus, an improved processability can be demonstrated. Experiments at temperatures below the melting point of PLA did not exhibit the effect presented below.

Figure 6.10 depicts the variation of the pressure during the process of wall coating in the presence of 0.5 wt% PLA7001D at $\dot{\gamma}_a = 390 s^{-1}$. First, Figure 6.10a shows the pressure transient for the capillary extrusion of pure PCL (Capa®6800). The pressure drop increases slowly and reaches a steady-state value after a certain time. Figure 6.10b depicts the pressure drop when the blend of Capa®6800+ 0.5 wt% PLA is extruded through a die. The pressure drop passes through a maximum and as the PLA gradually coats the interface of the die, due to wall slip, the extrusion pressure starts decreasing. The reduction of the apparent shear stress (or pressure) is significant in the presence of PLA (from 0.32 MPa to about 0.2 MPa) and the induction time to obtain steady-state is a few minutes (about 15 min). Monitoring the

pressure drop (Figure 6.10) shows the capability of PLA to be used as a processing aid for PCL.

Figure 6.11 shows the apparent flow curves of Capa®6800 (pure PCL) and Capa®6800 with 0.5wt% of PLA7001D obtained at 180°C. It can be clearly observed that at all shear rates, there is a significant decrease in the extrusion pressure (shear stress) in the presence of the PLA, which is mainly due to the effect of slip.

The effect of PLA on eliminating or postponing the surface instabilities of PCL extrudates at higher shear rates is displayed in Table 6.3. The PCL extrudates obtained with the help of a small amount of PLA appear relatively smooth even at high shear rate of $645s^{-1}$. It should be noted that at the same shear rate, pure PCL exhibits clear sharkskin defect (See Table 6.3).

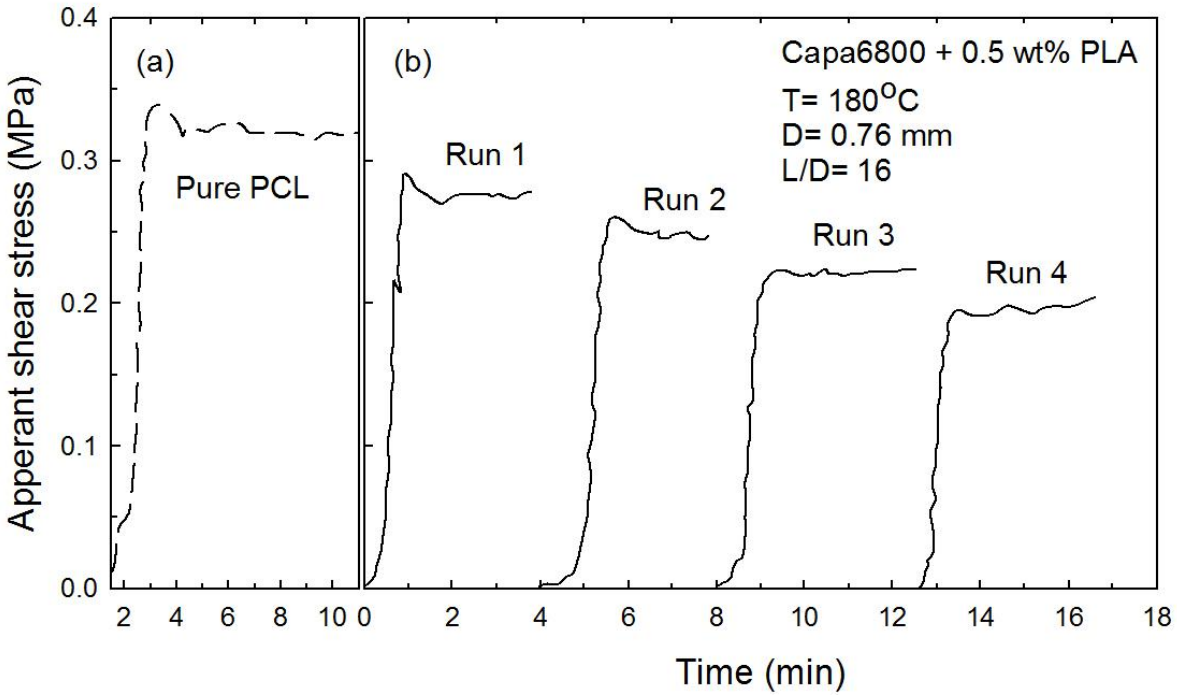

Figure 6.10 The effect of the addition of 0.5 wt % of PLA 7001D on the transient response in the capillary extrusion of PCL (Capa®6800) at 180°C and apparent shear rate of $390s^{-1}$.

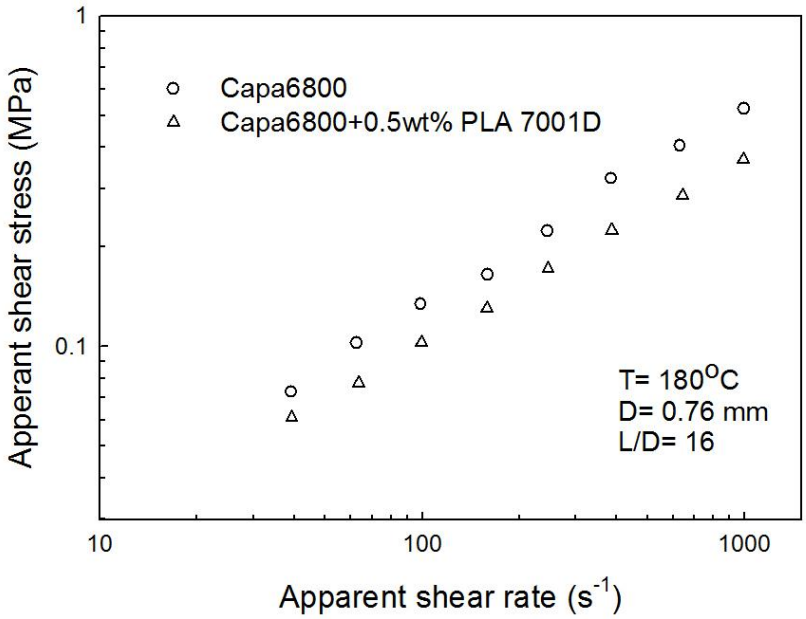

Figure 6.11 The effect of the addition of 0.5 wt % of PLA7001D on the flow curve of Capa®6800 at 180°C using a die with diameter of 0.76 mm and length-to-diameter ratio of 16.

Table 6.3 Images of Capa®6800 extrudates at different apparent shear rates extruded with and without 0.5 wt.% of a PLA7001D at 180°C.

Pure PCL (Capa®6800)		
$\dot{\gamma}_a = 390s^{-1}$	$\dot{\gamma}_a = 645s^{-1}$	$\dot{\gamma}_a = 1000s^{-1}$
	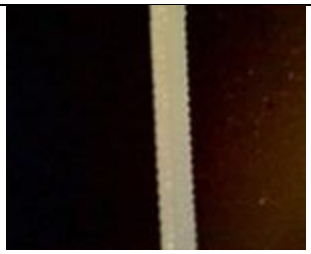	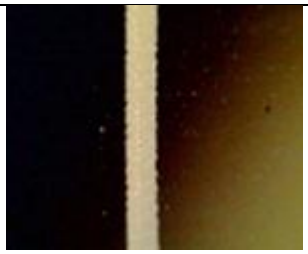
PCL (Capa®6800) +0.5 wt% PLA7001D		
$\dot{\gamma}_a = 390s^{-1}$	$\dot{\gamma}_a = 645s^{-1}$	$\dot{\gamma}_a = 1000s^{-1}$
	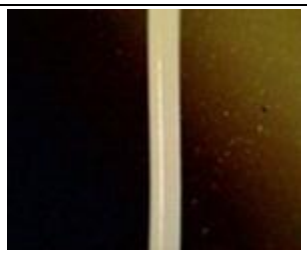	

6.4 Summary

The processing of PCLs has been studied by means of capillary rheometry. The Bagley and Rabinowitsch corrections have been applied to the rheological data in order to determine the true pressure drop in the capillary and thus the true flow curve. Measurements have revealed that no significant slip occurred during capillary extrusion. For the high molecular weight PCL, different types of instabilities were observed. The onset of melt fracture for the high molecular weight PCL occurred at around 0.2 MPa at temperatures higher than 115°C. Below 115°C the critical shear stress for the onset of melt fracture increased to 0.49 MPa indicating good processability of PCLs at low temperature. Finally, polylactide has been examined as a processing aid to eliminate the melt fracture. It was discovered that the addition of 0.5 wt% PLA was effective in eliminating and delaying the onset of melt fracture to higher shear rates. Thus, a small amount of PLA may be used as a processing aid for the processing of PCLs when they are extruded at temperatures higher than their melting point.

7 Poly(ε-caprolactone) and Polylactide Blends: Phase separation

The viscoelastic properties and the processability of poly(ε-caprolactone) polymers have been discussed in previous chapters. It was found that polylactide has the high potential to be employed as a processing aid for PCL. In this chapter, the thermodynamic and phase separation of the blends of PCL/PLA is studied by using a rheological approach. More specifically the rheological properties of the PCL/PLA system are measured in the transitional region and studying the influence of shear flow on phase transition. In addition, the effect of heating rate on the phase boundary is studied which has been proven extremely important for accurate determination of the phase diagrams (Zou et al. 2012). Moreover, the effect of molecular characteristics on the phase diagram of this system is investigated by using three PLAs with different molecular characteristics blended with the same PCL polymer.

7.1 Thermal Characterization

In order to gain better understanding of the differences between the PCL Capa®6800 and three PLAs listed in Tables 4.1 and 4.3, the thermal characteristics of these homopolymers were determined by differential scanning calorimetry (DSC). Figure 7.1 depicts the endothermic heat flows of the second heating scan corresponding to the melting characteristics of the homopolymers and their blends. As can be clearly observed from the thermograms, PLA 3051 D and PLA2002 D do not show crystallization peaks and pronounced melting peak in the second heating scan. Although in the first heating scan the endothermic peaks visibly exist, however, the rate of recrystallization of the melted structure is too slow. Simply, the crystalline structure is not developed in the second heating scan. However, PLA 3251 D clearly shows a large melting peak at 165.1°C and highly crystalline structure according to the calorimetry analysis.

Furthermore, the differential scanning calorimetry has been employed in other studies to determine the phase separation temperatures of the blends (Gharachorlou and Goharpey 2008). In this method, abrupt changes in the heat capacity are attributed to the phase separation region. For the PCL/PLA blend system, above 60 wt% of PLA, the heat capacity change occurred at about 93±2°C. Based on the insensitivity of the heat capacity change to composition and temperature, it can be concluded that DSC is not the best method to

determine the phase separation temperature for PCL/PLA. The occurrence of phase separation above the melting point of PCL might be the reason for this observation.

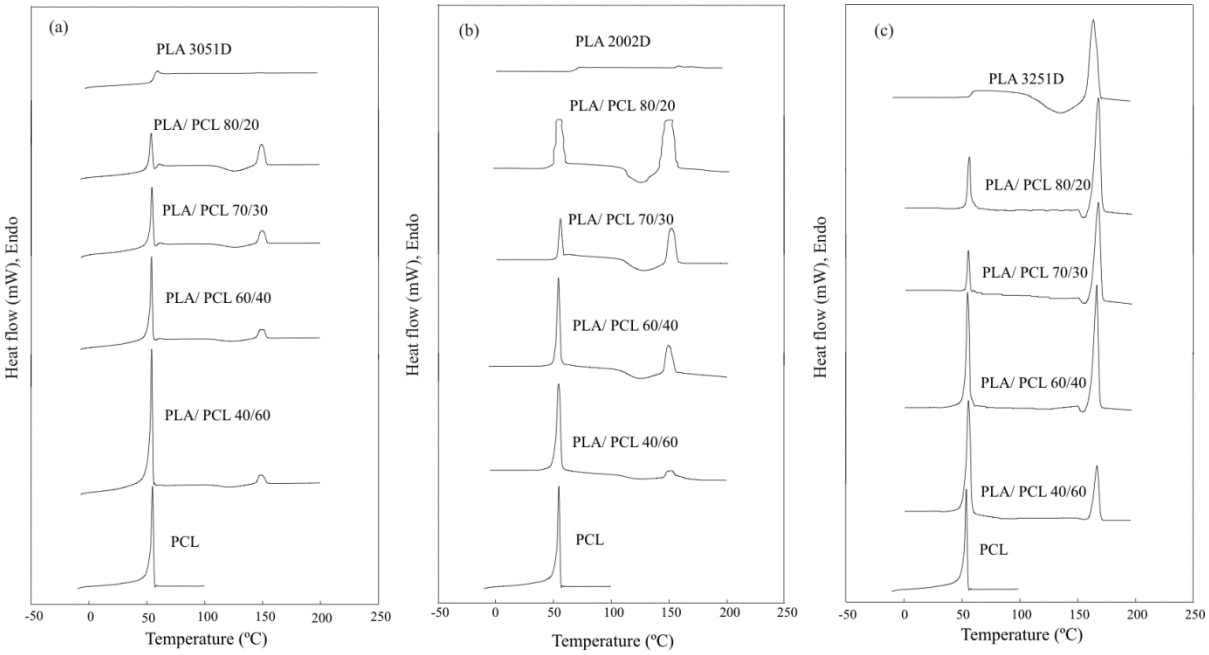

Figure 7.1 DSC thermographs of the blends (a) PLA 3051D and PCL Capa®6800 (b) PLA 2002D and PCL Capa®6800 and (c) PLA 3251D and PCL Capa®6800.

7.2 Binodal Decomposition

The rheological response in the transitional area of bi-component systems has been employed before in many reports to study their thermodynamics and to obtain the critical solution temperature of various blend systems (Vlassopoulos et al. 1997, Ajji and Choplin 1991a, Ajji and Choplin 1991b, Kapnistos et al. 1996, Chopra et al. 1998, Zhang et al. 2001).

The isochronal temperature ramp is generally an effective measurement of binodal temperatures. It has been observed that by moving away from the glass transition temperature and getting close to the phase separation temperature, known as metastable region, increasing the mobility of the chains along with the temperature increase, results in decreasing the dynamic moduli. In this region, viscoelastic modulus is mainly governed by the polymer bulk and entanglements (Zhang et al. 2009). By reaching the metastable region, there is an increase in dynamic moduli or slope variation of dynamic moduli due to the elasticity induced by the concentration fluctuations and the formation of domains enriched of more elastic component (Kapnistos et al. 1996).

As mentioned earlier, a temperature sweep test at a constant frequency has been performed to identify the phase separation temperature (binodal). Figure 7.2 demonstrates the typical evolution of elastic moduli (*G'*) in a temperature range of 70-130°C. The elastic modulus, *G'*, decreases with increasing temperature in the homogenous region due to the mobility of the polymer entanglements. There is a drastic variation in the elastic modulus in the vicinity of critical region as a result of concentration fluctuations, which overcomes the Brownian motion of the chains and induces extra stress (Kapnistos et al. 1996, Zhang et al. 2008). However, the competition between interface and concentration fluctuations as the main reason of increased elasticity in the phase transition regime is still a debatable area (Bousmina et al. 2002). Madbouly and Ougizawa (2004) reported the large change in the elastic moduli for polystyrene (PS)/poly vinyl methacrylate (PVME) blends and considered it as a result of large difference in the glass transition temperature of the components. The slope change or the inflection point of dynamic moduli indicates the binodal temperature (Chopra et al. 1998). Also, the values of *G'* increases with higher content of PLA.

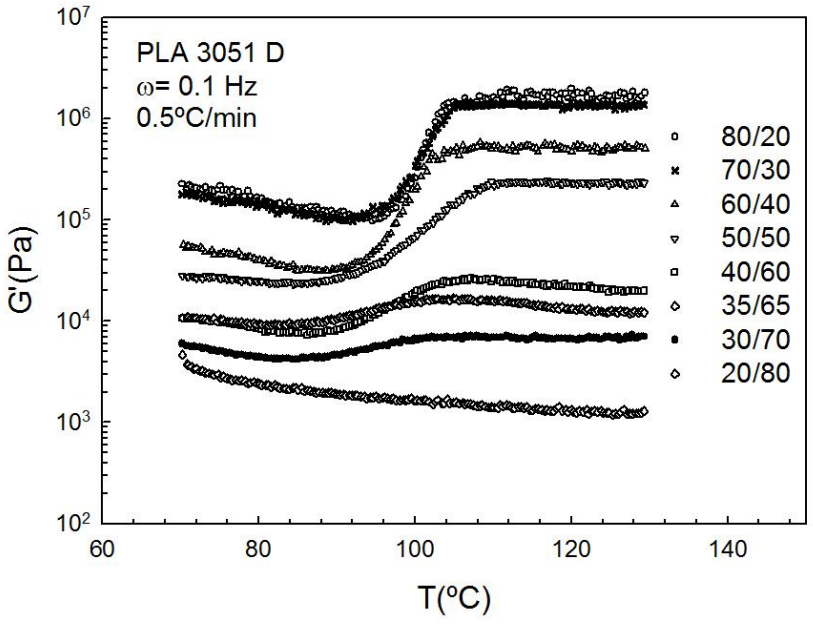

Figure 7.2 The temperature evolution of elastic modulus (*G'*) under small amplitude oscillatory shear at the fixed frequency of 0.1 Hz (0.0628 rad/s) and heating rate of 0.5°C/min for different compositions of the PLA3051 D/PCL blends.

The storage (*G'*) and loss (*G"*) moduli of PLA 3051D/PCL (60/40) as a representative system is reported at different temperatures in Figure 7.3. Failure of time-temperature superposition at low frequencies in this temperature range is an indication of phase separated region.

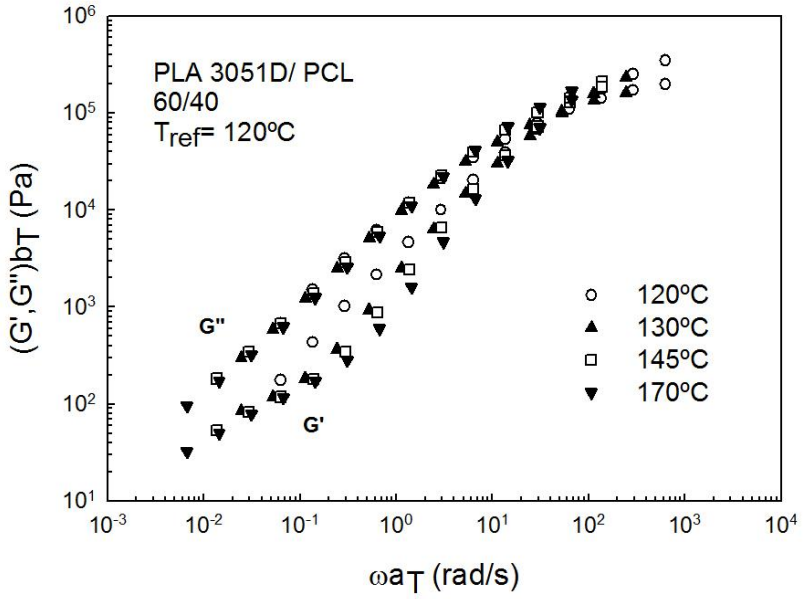

Figure 7.3 Time-temperature superposition of storage (*G'*) and loss (*G"*) modulus of PLA 3051D/ PCL (60/40) at the reference temperature of 120°C.

It is important to realize that the frequency used might significantly affect the experimental results and therefore the sensitivity of *G'* of PLA/PCL blends to the frequency was investigated in order to avoid inconsistencies. Such inconsistencies have been previously reported for PB/LPI blends (Zou et al. 2012). Figure 7.4a and 7.5a show the effect of frequency on the binodal temperature, T_b, of PLA-rich and PCL-rich blends, respectively. Figure 7.4b and 7.5b present the imaginary viscosity (η'') PLA3051 D/ PCL (60/40) and (35/65) as a sensitive tool to probe the transition temperatures. The plots are clearly consistent with Figure 7.4a and 7.5a. The temperature values, T_b, are shown on the graphs and correspond to the inflection point of *G'* or change in the slope of the elastic modulus curve (Kapnistos et al. 1996, Zou et al. 2012). Meredith and Amis (2000) previously reported the critical concentration of 36 wt% PCL for the PLA/PCL blends under static conditions. For the PLA-rich blend with 60 wt% PLA (near-critical) (Figure 7.4a), even at the highest

frequency of this study (10 Hz or 62.8 rad/s) there is a slight shift in the critical temperature. The renormalization group (RG) theory has described the shift in critical fluctuation under shear flow (Zou et al. 2012, Onuki and Kawasaki 1979). Based on this theory, at the criteria of $k_c\xi > 1$, where k_c is the wave number related to the shear rate and ξ is a semi macroscopic length correlated to the critical fluctuation, the critical fluctuation will be distorted and leads to shear induced mixing.

More details on the theory can be found in Onuki and Kawasaki (1979). For the near critical blend in this study, even the highest frequency did not reach the criteria of the RG theory to distort the critical fluctuation in order to cause shear induced mixing. Since small amplitude oscillatory shear is used the flow conditions are not far from equilibrium. For the PCL rich blend (off-critical), the considerable shift in the transition temperature was observed in the same frequency range compared to the near-critical blend (Figure 7.4). Thus, it can be inferred that the critical concentration fluctuation distortion and shear induced mixing is not the only mechanism involved here. This behavior has been described before by the effect of shear on the nucleation (Zou et al. 2012, Easwar 1992). Based on the droplet break-up and coagulation theory under shear, for the droplets not to be pulled apart, the $R_c > R^*$ criterion should be met. Note that R_c corresponds to the critical radius of nucleation related to the free energy barrier and R^* is called the Taylor break-up size related to the shear flow. The R_c value increases by approaching the binodal transition region and passes the above mentioned criterion and results in the suppression of the critical droplets in the binodal region. As a result there is a large change in the binodal critical temperature particularly at higher frequencies.

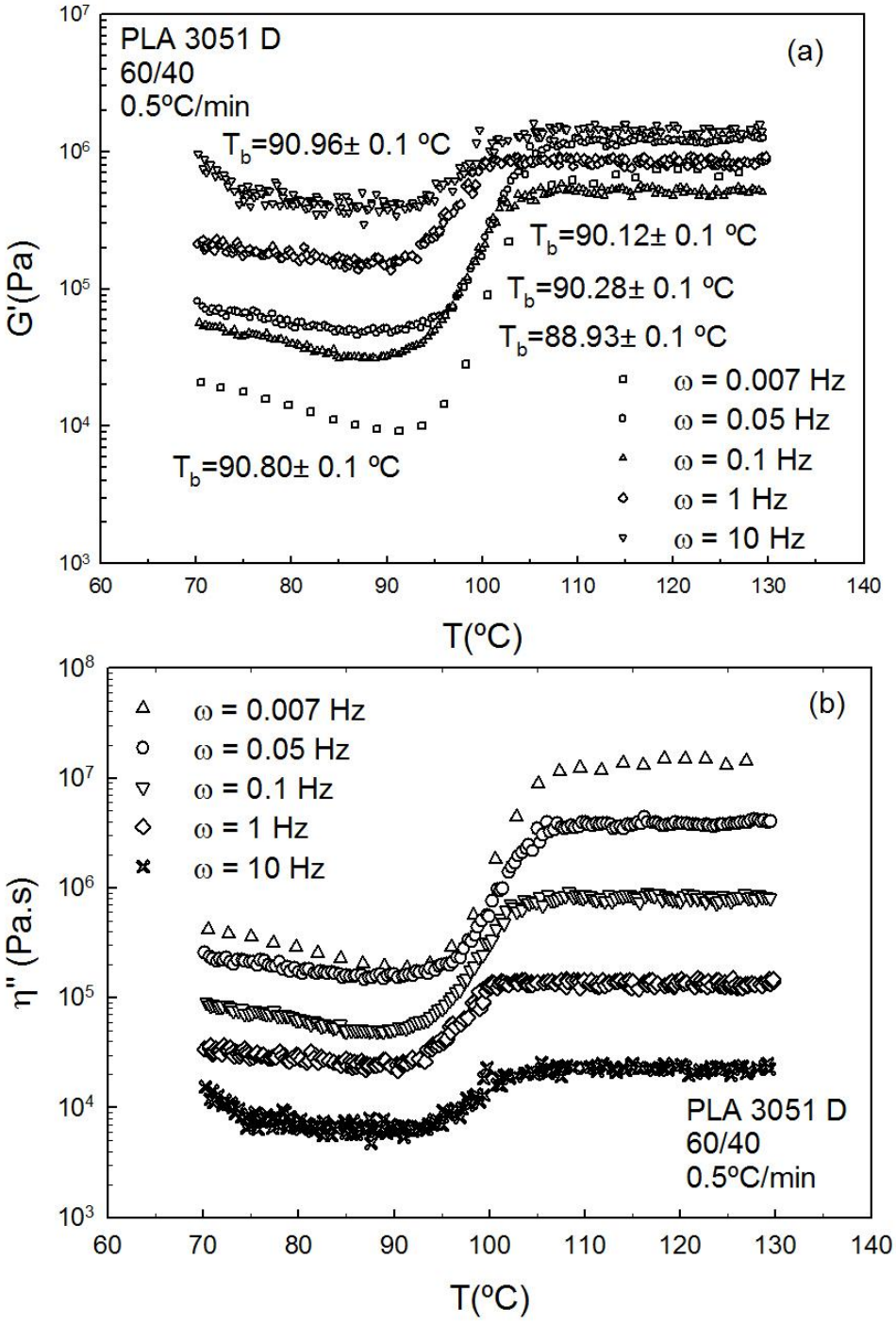

Figure 7.4 (a) Dependence of the dynamic moduli (*G'*) versus temperature on frequency used in small amplitude oscillatory shear at different frequencies from 0.007 (0.044 rad/s) to 10 Hz (62.8 rad/s) and heating rate of 0.5°C/min for the near critical (60/40) PLA3051 D/PCL blend (b) Variation of imaginary viscosity (*η"*) as a function of temperature for the (60/40) PLA3051 D/PCL blend at different frequencies.

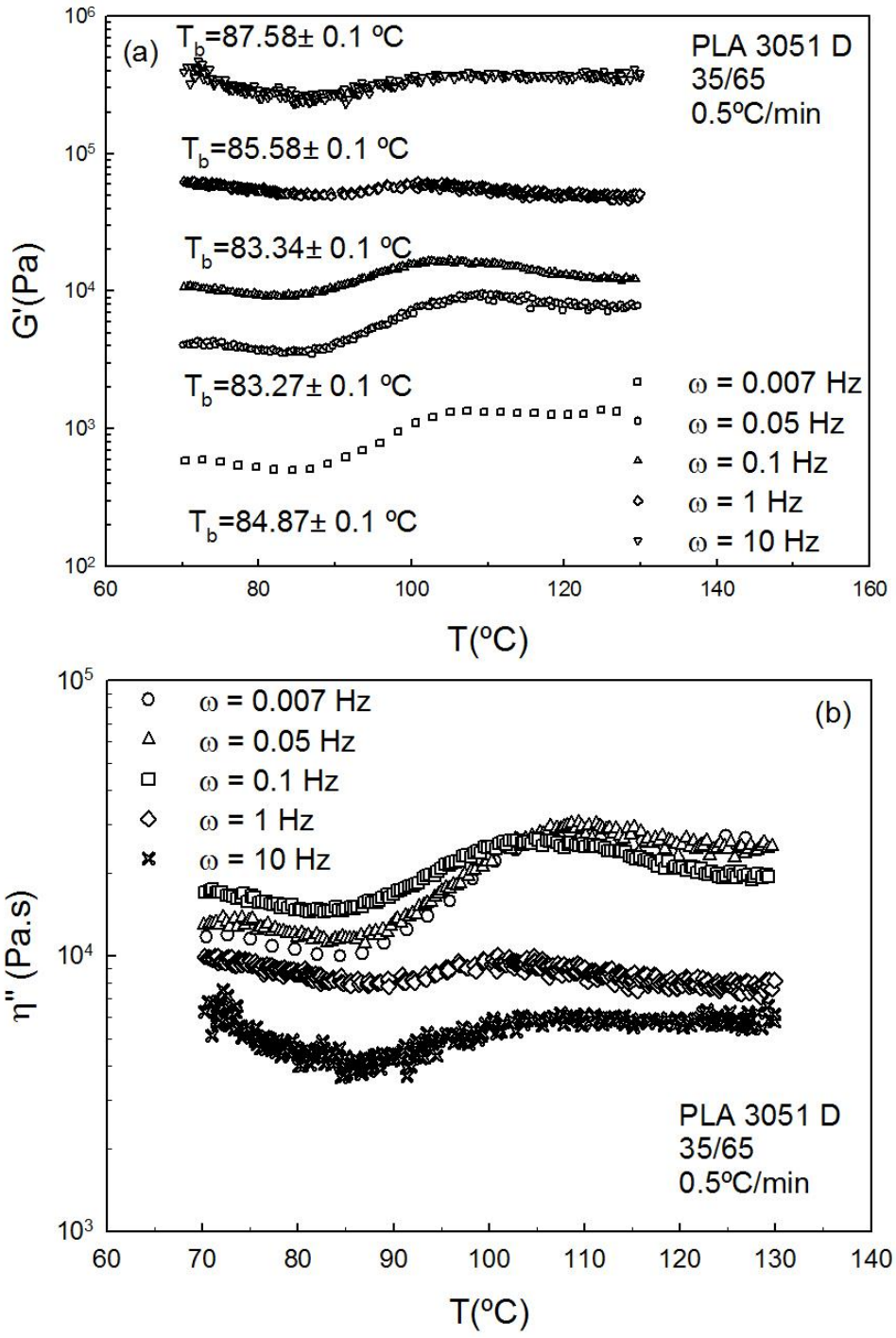

Figure 7.5 (a) Dependence of the dynamic moduli (*G'*) on the temperature under oscillatory shear at different frequencies ranging from 0.007 (0.044 rad/s) to 10 (62.8 rad/s) Hz and heating rates of 0.5°C/min for the off-critical (35/65) PLA3051 D/PCL blend (b) Variation of imaginary viscosity (*η"*) as a function of temperature for the (35/65) PLA3051 D/PCL blend at different frequencies.

Figure 7.6 summarizes the binodal separation temperatures at the frequency range of the study for the near-critical (60/40) and the off-critical (35/65) blend that shows a more significant change in the transition boundary under shear for the off-critical blend as discussed earlier.

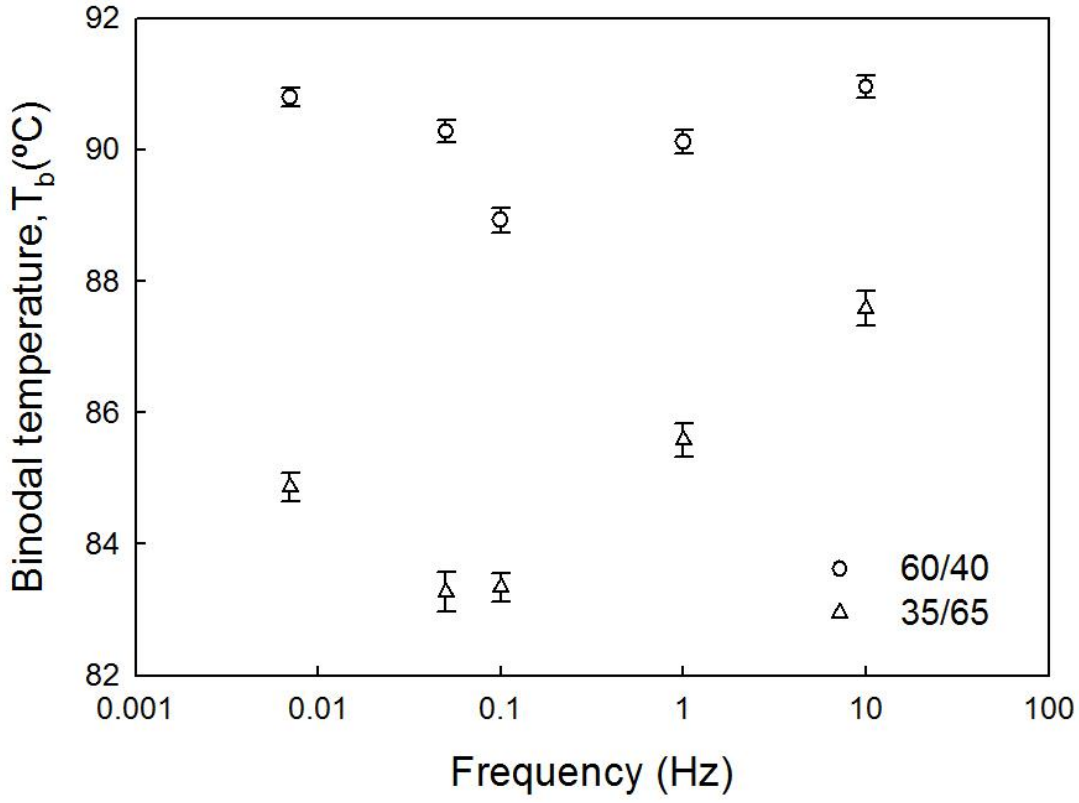

Figure 7.6 Dependence of the binodal temperature on frequencies ranging from 0.007 to 10 Hz at a constant heating rate of 0.5°C/min for the (35/65) and (60/40) PLA3051 D/PCL blends.

In the following part of this section, we demonstrate the effect of heating rate on the near critical and off-critical PLA/PCL blends. It can be clearly observed from Figure 7.7 and Figure 7.8 that the heating rate strongly affects the binodal temperature of both compositions. The lower heating rate shifts the binodal temperature, T_b, to the lower region for both near-critical and off-critical compositions. The results also show that the higher heating rates result into lower elastic modulus, which is in agreement with the previous reports on PS/PVME blends (Madbouly and Ougizawa 2004).

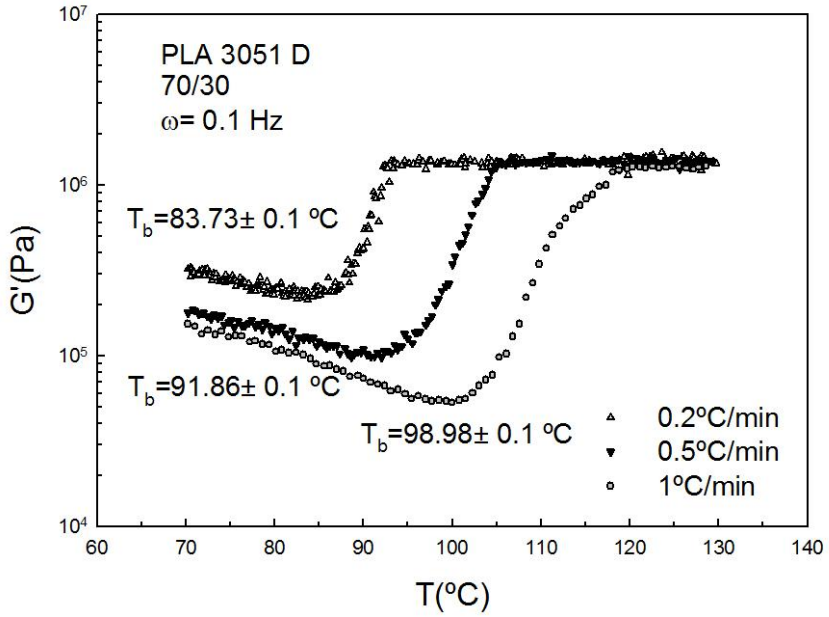

Figure 7.7 Dependence of dynamic moduli (*G'*) on temperature under oscillatory shear at different heating rates from 0.2 to 1°C/min and constant frequency of 0.1 Hz (0.628 rad/s) for the near-critical (70/30) PLA3051 D/PCL blend.

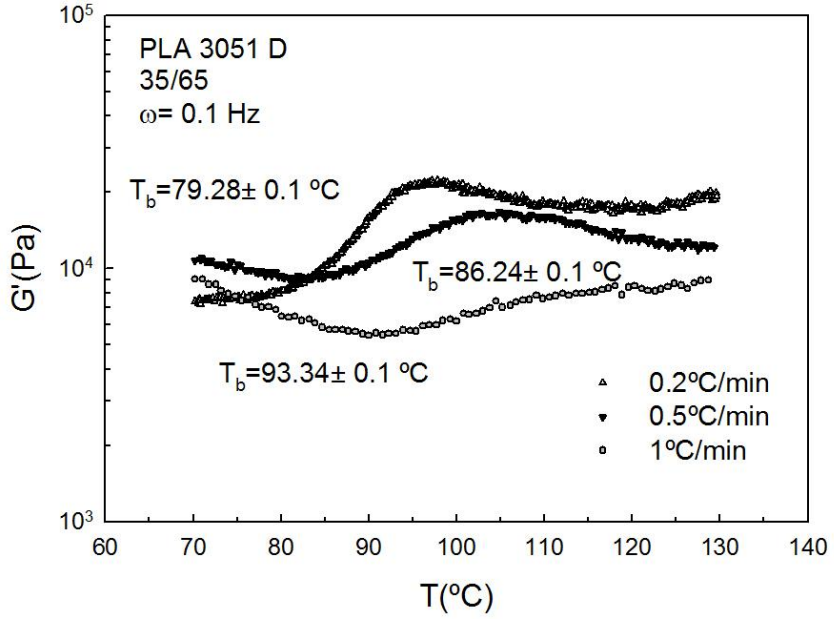

Figure 7.8 Dependence of dynamic moduli (*G'*) on the temperature under oscillatory shear at different heating rates ranging from 0.2 to 1°C/min and constant frequency of 0.1 Hz (0.628 rad/s) for the off-critical (35/65) PLA3051 D/PCL blend.

The binodal temperatures follow a linear relation with heating rate for near-critical and off-critical blends (Figure 7.9), although a nonlinear dependency has been reported before for PS/PVME blends (Madbouly and Ougizawa 2004).

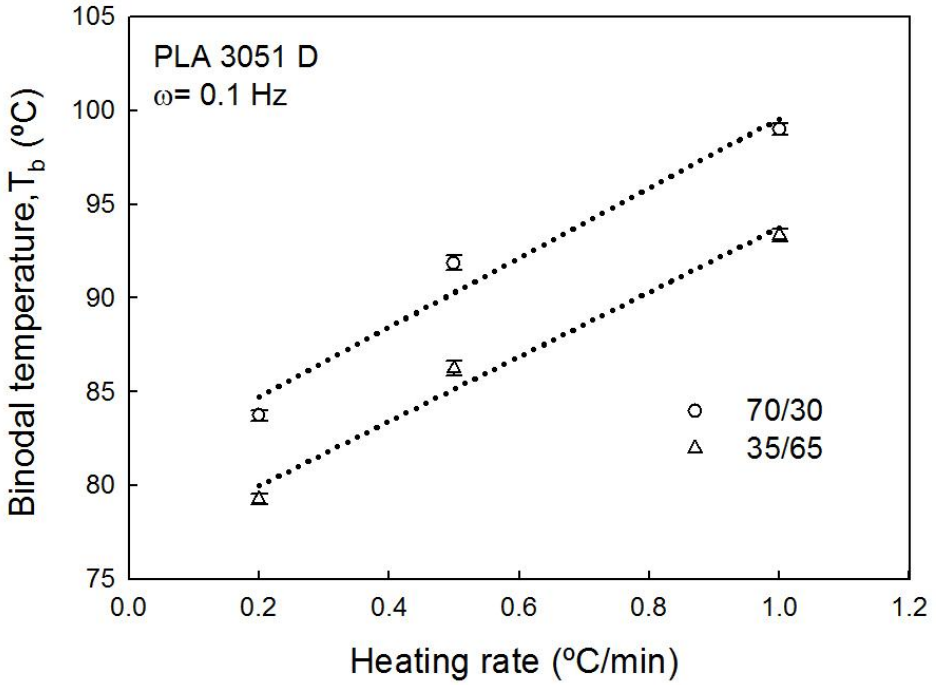

Figure 7.9 Heating rate dependency of binodal temperatures for near-critical (70/30) and off-critical (35/65) PLA3051 D/PCL blends.

Figure 7.10 shows the phase diagram consisted of binodal points for the PLA/PCL blend focusing on the effect of heating rate. The results confirmed the lower critical solution temperature (LCST) phase behavior for PLA/PCL blend which is in accordance with the previous report of Meredith and Amis (2000). As can be observed, faster heating rate can shift the critical temperature less than 10°C. However, the critical concentration region remained almost unchanged. The dotted lines are the polynomial fit of the rheologically obtained binodal temperatures.

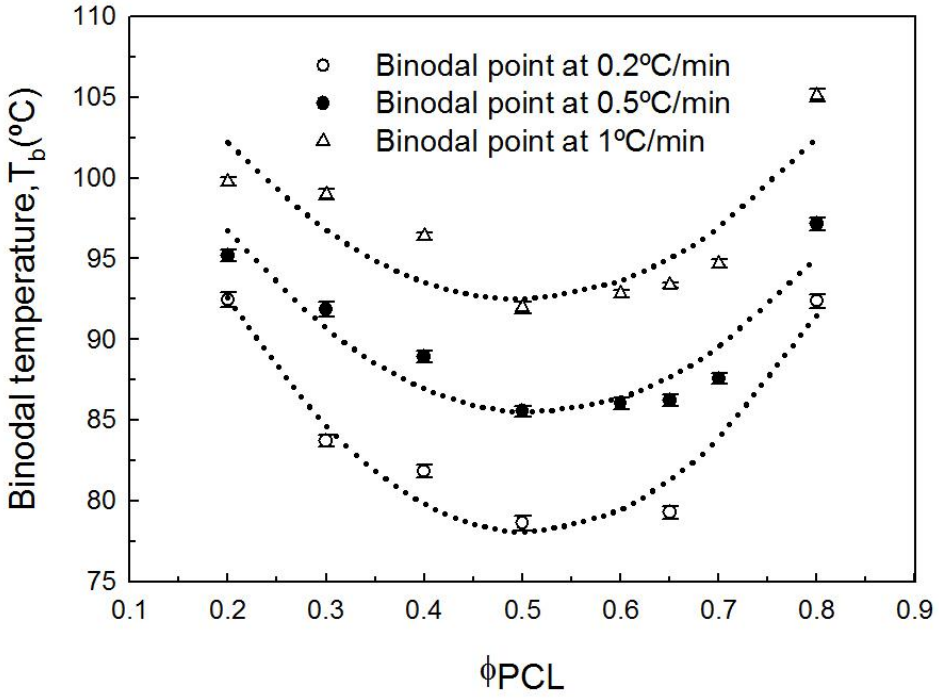

Figure 7.10 Binodal phase diagrams for the PLA3051 D/PCL blend at heating rates of 0.2, 0.5 and 1°C/min. The dotted lines are the polynomial fit connecting the experimentally determined binodal points.

7.3 Spinodal Decomposition

The spinodal decomposition temperature has been rheologically addressed by the theoretical approach of Ajji and Choplin (1991a). They have extended the Fredrickson and Larson approach for block copolymers to binary polymeric blends. Their treatment based on mean field theory, predicts the abnormal viscoelastic properties near the transition point due to the concentration fluctuations. This theory predicts the weaker contribution of concentration fluctuation on loss modulus, which is in agreement with the experimental observation. The following expression has been extracted from the abovementioned theories:

$$\frac{G'(\omega)}{\left[G''(\omega)\right]^2} = \frac{30\pi}{k_B T}\left\{\frac{a_1^2}{36\phi} + \frac{a_2^2}{36(1-\phi)}\right\}^{3/2}(\chi_s - \chi)^{-3/2} \qquad (7\text{-}1)$$

where a denotes the statistical segment length, φ is the volume fraction of one component, χ and χ_s are the Flory-Huggins interaction parameter and the interaction parameter at spinodal respectively. Assuming that the interaction parameter is described by $\chi=A+B/T$, Equation 7.1 can be rewritten in the following format:

$$\left[\frac{G''^2(\omega)}{G'(\omega)T}\right]^{2/3} = B\left(\frac{30\pi}{k_B}\right)^{-2/3}\left\{\frac{a_1^2}{36\varphi}+\frac{a_2^2}{36(1-\varphi)}\right\}^{-1}\left(\frac{1}{T_s}-\frac{1}{T}\right) \quad (7\text{-}2)$$

The spinodal temperature (T_s) can be determined by the intercept of linear relation between $[G''^2(\omega)/G'(\omega)]^{2/3}$ and $1/T$ at the $1/T$ axis. At low and high temperatures, $[G''(\omega)]^2/[TG'(\omega)]^{2/3}$ shows deviation from linearity. The reason for the nonlinearity is because the theory has been originally proposed for the one phase region close to the critical point. The spinodal determination in this theory is based on the assumption that both near-critical and off-critical compositions follow the critical fluctuation in the same way (Zhang et al. 2009). Since the linear range is determined qualitatively in this method, the error of ±2°C is repeatedly reported in this approach (Kapnistos et al. 1996, Zhang et al. 2009). Figure 7.11 displays typical results of $[G''(\omega)]^2/[TG'(\omega)]^{2/3}$ versus 1/T for the 35/65 PLA3051 D/PCL blend and the extrapolated spinodal temperatures of 103.5, 106.9 and 112.5°C for the heating rates of 0.2, 0.5 and 1°C/min, respectively. For the off-critical blends, a higher heating rate shifts the spinodal temperature to a higher value. The same relation for all the blends above 40 wt% PCL was found. This is the same pattern as that reported for the PB/LPI blend system at relatively low frequencies (Zhang et al. 2008).

At another composition ratio of 60/40 (near-critical) PLA3051D/PCL blend, a different pattern was obtained compared to that of the off-critical blends (Figure 7.12). In this composition ratio, the spinodal temperature of 100.9 °C was about the same independent of both heating rate. The independency of spinodal decomposition to the heating rate for the near–critical blend can be attributed to the fact that the critical fluctuation is the major contribution to the elastic modulus near the critical region, so heating rate has no significant effect on spinodal temperature (Zou et al. 2012). On the other hand, as discussed earlier, the off-critical blend is highly influenced by the simultaneous effect of nucleation and critical

concentration fluctuation in the phase separation area. As a result, the spinodal decomposition temperature is altered largely by the level of heating rate (Figure 7.11).

The spinodal points calculated from the Ajji-Choplin theoretical approach from two heating rates are plotted in Figure 7.13. The effect of heating rate on the spinodal decomposition at least at this range of heating rates is less pronounced compared to the binodal separation and therefore experiments were not performed at the smaller heating rate of 0.2°C/min. In addition, in the near-critical region due to the minimal role of nucleation phase separation, the spinodal lines are almost overlapped at two heating rates.

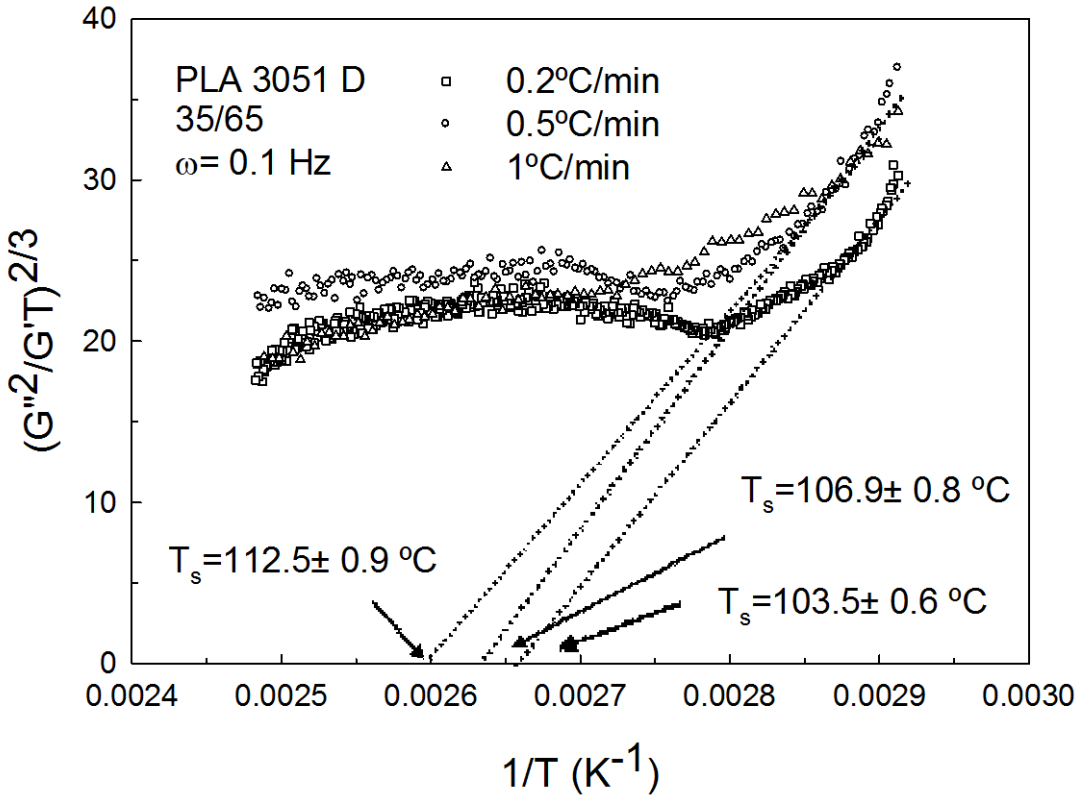

Figure 7.11 Plot of $(G''^2/G'T)^{2/3}$ versus $1/T$ for the off-critical (35/65) PLA3051 D/PCL blend at the fixed frequency of 0.1 Hz (0.628 rad/s) and different heating rates of 0.2, 0.5 and 1°C/min. The dashed lines display the extrapolation of the linear region to determine the temperature for the spinodal decomposition.

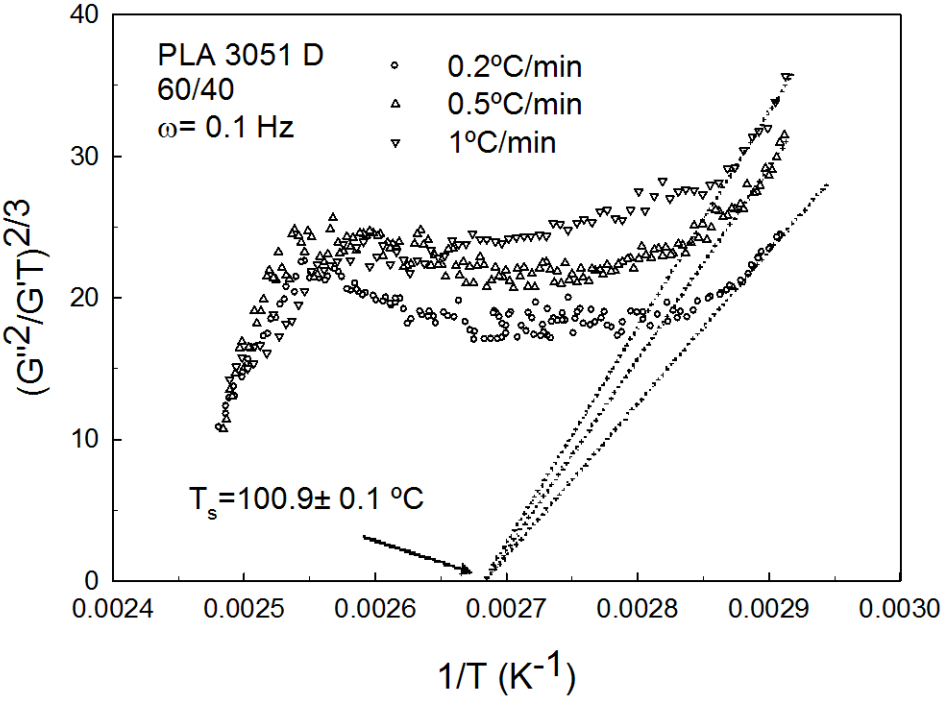

Figure 7.12 Plot of $(G''^2/ G'T)^{2/3}$ versus $1/T$ for the off-critical (60/40) PLA3051 D/PCL blend at a fixed frequency of 0.1 Hz (0.628 rad/s) and different heating rates of 0.2, 0.5 and 1°C/min. The dashed lines display the extrapolation of the linear region.

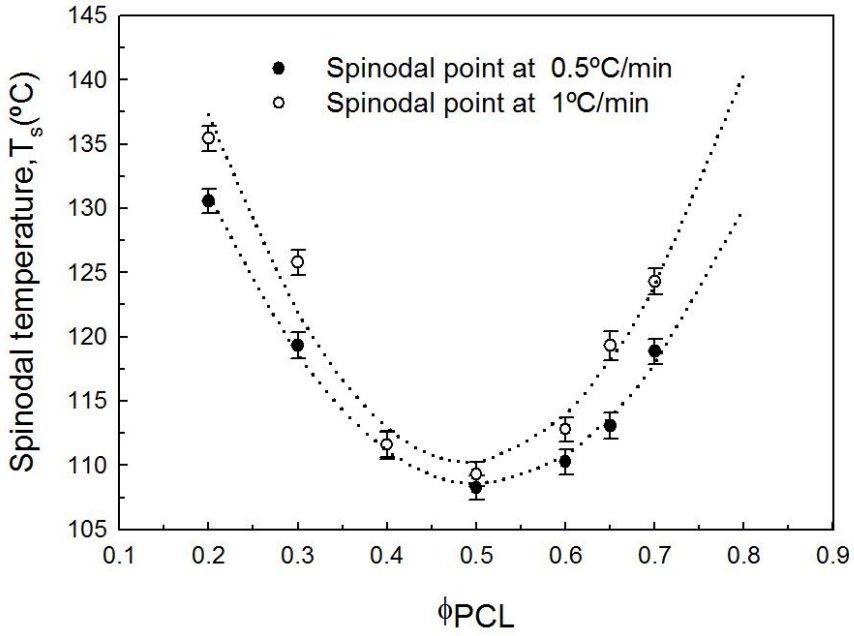

Figure 7.13 Spinodal phase diagrams of PLA3051D/PCL blends at the constant frequency of 0.1 Hz and heating rates of 0.5 and 1 °C/min.

The plots of $[G''(\omega)]^2/[TG'(\omega)]^{2/3}$ versus $1/T$ for PLA3051D/ PCL (60/40) at different frequencies are depicted in Fig.14. For the sake of clarity, three frequencies are presented in Figure 7.14. The frequency dependence of spinodal temperatures for the near-critical (60/40) and the off-critical (35/65) blend are presented in Figure 7.15.

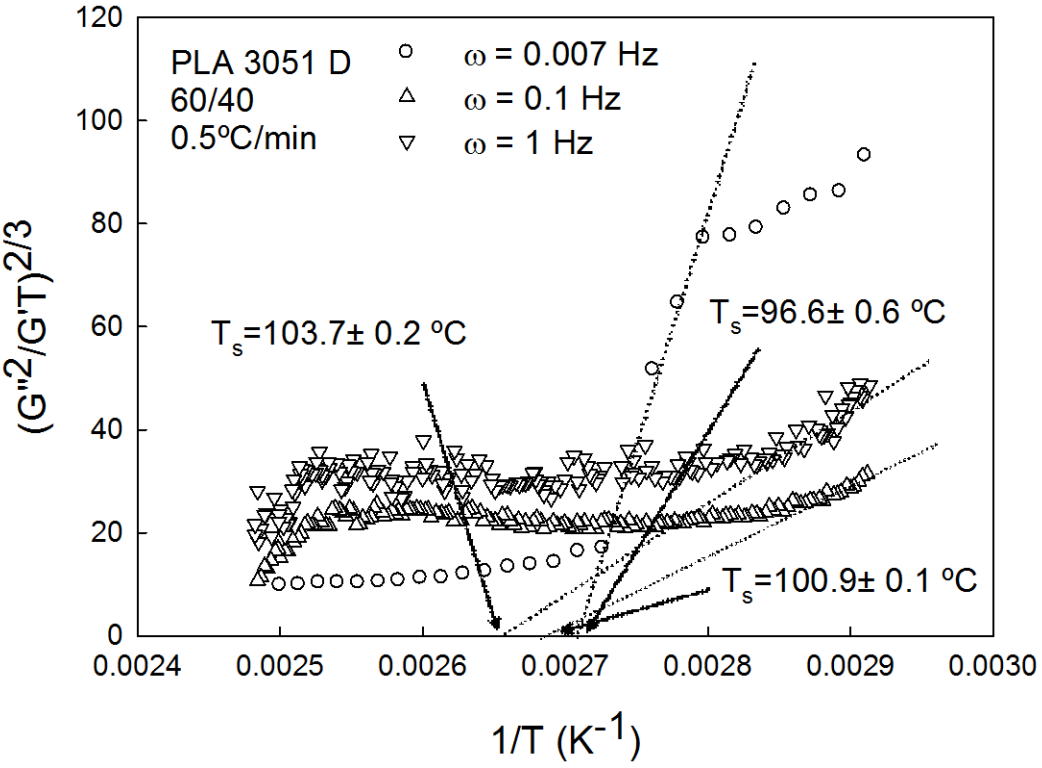

Figure 7.14 Plot of $(G''^2/ G'T)^{2/3}$ versus $1/T$ for the off-critical (60/40) PLA3051 D/PCL blend at a constant heating rate of 0.5°C/min and different frequencies. The dashed lines display the extrapolation of the linear region.

The rheologically determined phase diagram of PLA3051 D/PCL blend from the isochronal temperature ramp is illustrated in Figure 7.16. The binodal and spinodal points obtained by the two heating rates of 0.5 and 1°C/min are presented. It should be noted that below the melting point of PCL (dashed line), at high concentration of PCL, the structure is mainly single phase crystals. However, at the medium level of PCL concentration, a combination of crystals and liquid PLA exists. By increasing the temperature above the melting point of PCL, liquid and crystal mixture phase, transforms into the liquid-liquid phase separated region.

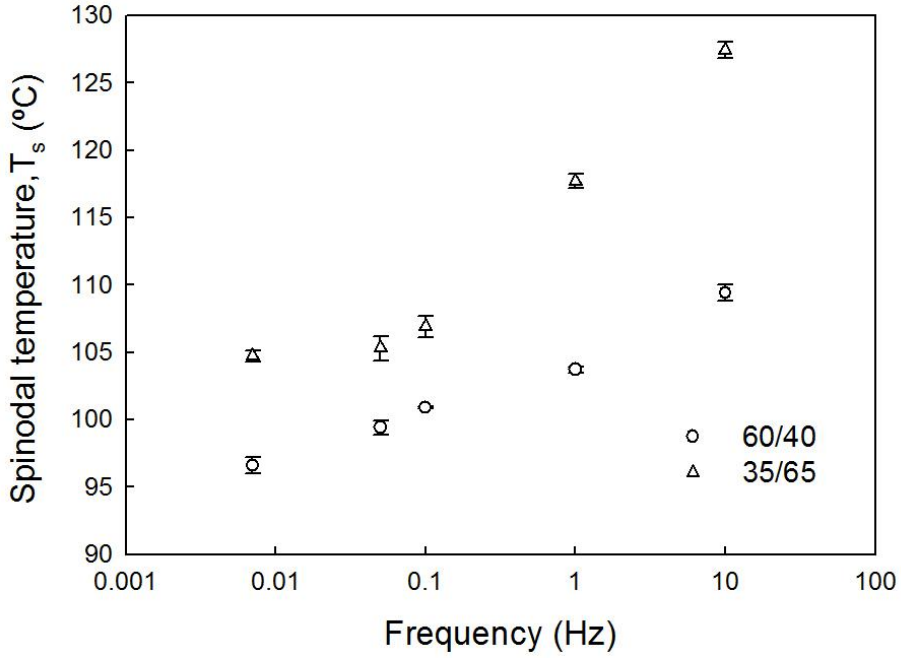

Figure 7.15 Dependence of spinodal temperature (T_s) on frequency for the (35/65) and (60/40) PLA3051 D/PCL blends.

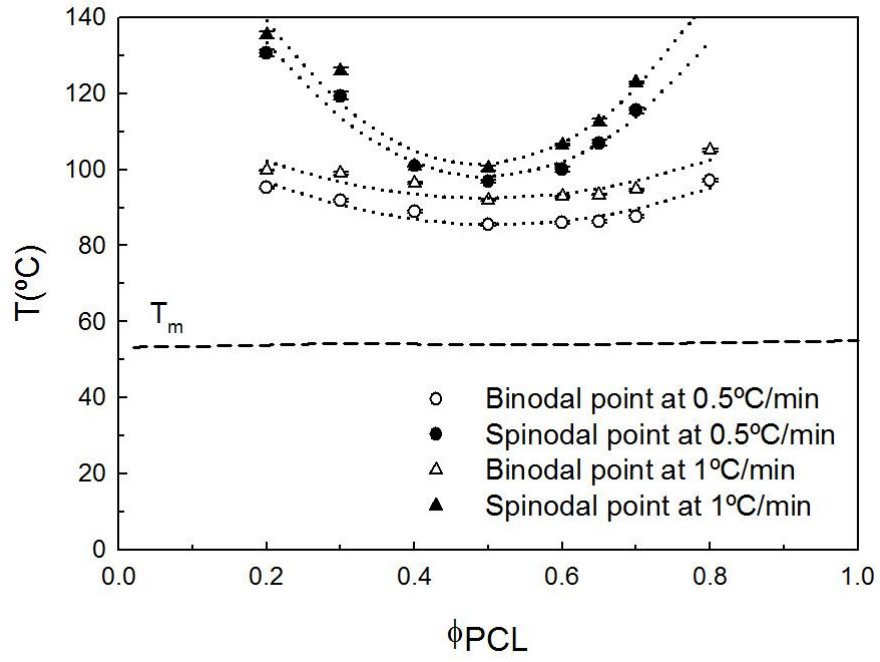

Figure 7.16 Phase diagrams of PLA3051 D/PCL blends at the constant frequency of 0.1 Hz (0.628 rad/s) and heating rates of 0.5 and 1 °C/min. The dotted lines are the extrapolation fit of the binodal and spinodal points of the PLA3051D/PCL blend.

7.4 Effect of Molecular Weight of Polylactide on the Phase Diagram

The effect of molecular weight of PLA on the phase diagram was also studied. Figure 7.17 depicts the binodal phase separation points of PLA/PCL blends with different molecular weights of PLA. The results indicate that the phase boundary shifts to the lower temperatures with increase of the molecular weight of PLA for the nearly amorphous PLAs (PLA 3051D and PLA 2002D). This observation is consistent with the phase separation behavior of PLA/PCL presented before (Meredith and Amis 2000, Yang et al. 1997). According to the differential scanning calorimetry (DSC) analysis, both of these PLAs have a very low degree of crystallinity as they are nearly amorphous. However, their level of crystallinity shows significant increase in the presence of PCL in the blends (Noroozi et al. 2012). In contrast to the pattern for the nearly amorphous PLAs, crystalline PLA 3251D which has the lowest molecular weight, shows the phase boundary shift to the lowest temperature level. DSC thermogram shows the high degree of crystallinity for PLA 3251D which can be the reason for the occurrence of the metastable region at lower temperature.

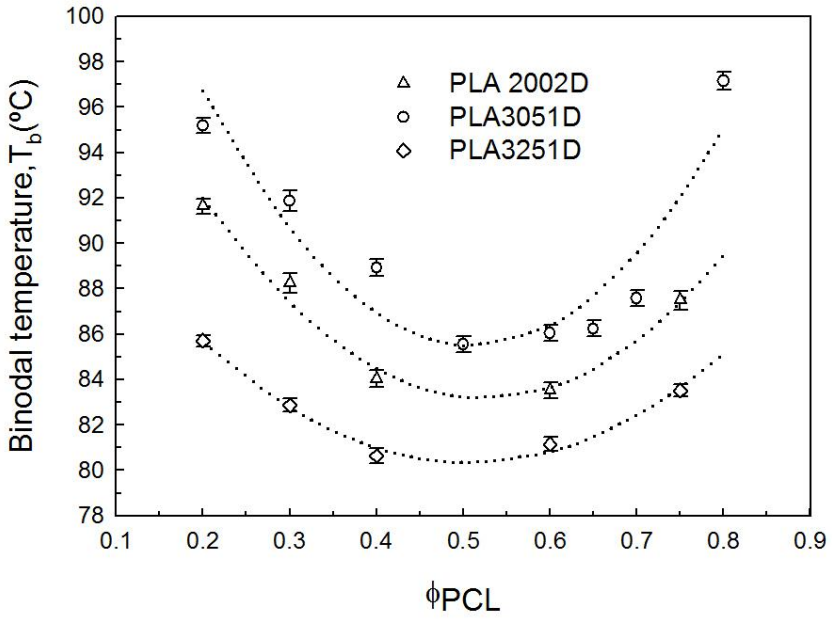

Figure 7.17 Binodal phase diagrams of PLA/PCL blends for different molecular weight PLAs at the constant frequency of 0.1 Hz (0.628 rad/s) and heating rate of 0.5°C/min. The dotted lines are the extrapolation fit of the experimentally measured binodal points.

Figure 7.17 reveals that although the phase boundary temperatures is influenced by the molecular weight of the PLA component of the blend, the critical composition shows a relatively small dependency on the molecular weight for these PLA/PCL blends.

7.5 Morphology Studies of the Poly(ε-caprolactone) and Polylactide in the Phase Separated Region

In order to gain a better understanding of the phase separation behavior, optical microscopy has been employed to follow the morphology evolution of certain blend compositions over a temperature range of interest where separation occurs. Figure 7.18 demonstrates the optical micrographs of the blend with 40 wt% of PCL after inverse quenching from homogeneous region into the binodal and spinodal region. Figure 7.18a presents the inverse quenching condition from 75°C to 95°C, which is in metastable region according to the phase diagram. Formation of nuclei is observed in this temperature which is an indication of phase separation in metastable region by nucleation. By moving into the higher temperature of 105°C, increase in the size of nuclei can be observed (Figure 7.18b). This temperature corresponds to the border of binodal to spinodal transition. By quenching more deeply into the unstable region (125°C), the interconnected and bi-continuous structure is formed (Figure 7.18c).

It should be noted that due to similarity of the refractive indices of PLA and PCL, obtaining accurate phase separation temperature based on the optical microscopy is hardly possible.

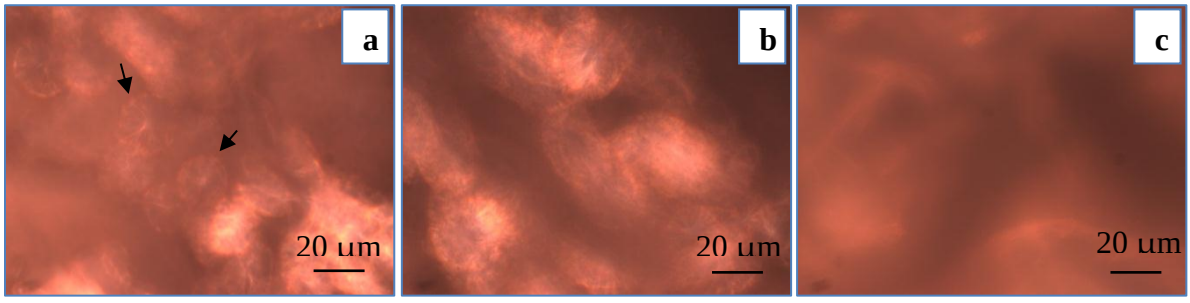

Figure 7.18 The optical micrographs of (60/40) PLA3051 D/PCL blend by inverse quenching to (a) 95°C (b) 105°C and (c) 125°C.

Figure 7.19 and 7.20 present the SEM images of the blends in the binodal and spinodal regions of the phase diagram, respectively. In order to capture the morphology in the metastable binodal region, samples were heated gradually with the heating rate of 5°C/min from 80°C (one phase) to 105°C. The temperature range was selected according to the rheologically determined phase diagram. Figure 19a, b and c displays the morphology of PLA 3051 D/PCL blends with 30, 50 and 65 wt% PCL. The dark spherical shapes correspond to the PCL phase that was dissolved in acetic acid (Figure 7.19a). At 65 wt% PCL, the spherical regions of PLA were observed (Figure 7.19c). The presence of spherical domains of PCL and PLA at different compositions is due to the nucleation and growth (NG) mechanism of phase separation in the binodal phase separation region at 105°C, which is in agreement with the presented phase diagram.

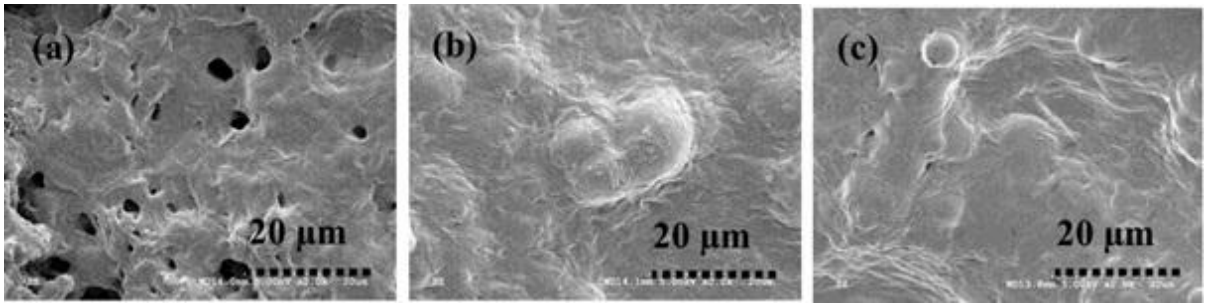

Figure 7.19 The SEM images of PLA3051 D/PCL blends: (a) 30 wt% PCL (b) 50 wt% PCL and (c) 65 wt% PCL at 105°C. Images were taken at the magnification of 2.0 K.

Figure 7.20 traces the morphology of the same composition ratios of Figure 7.19 at 130°C which is expected to be the spinodal region according to the phase diagram (Figure 7.16). Coalescence of the droplets of PCL at 130°C was clearly observed for the blend of 30wt% PCL (Figure 7.20a) towards the co-continuous morphology compare to the NG mechanism at 105°C. The same trend of larger and interconnected domains of PLA is present in Figure 7.20b and 7.20c as an indication of spinodal phase separated region.

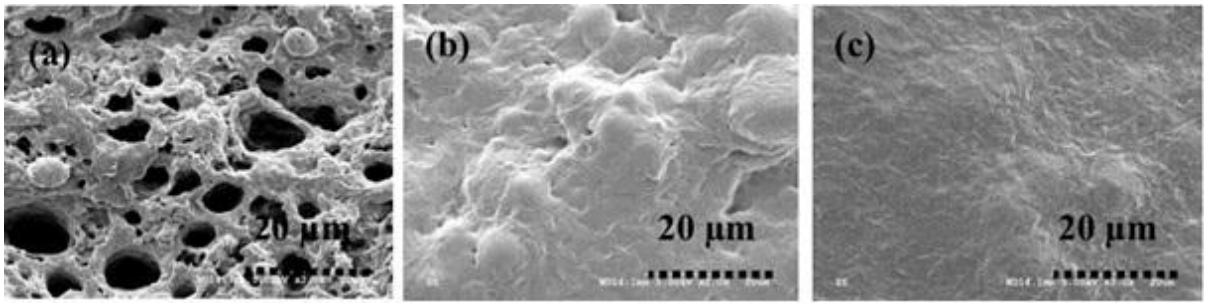

Figure 7.20 The SEM images of PLA3051 D/PCL blends: (a) 30 wt% PCL (b) 50 wt% PCL and (c) 65 wt% PCL at 130°C. Images were taken at the magnification of 2.0 K.

Figure 7.21 depicts the phase diagram of PLA3051D and PCL Capa6800 including the binodal and spinodal boundaries (Figure 7.16) along with the SEM micrographs of Figure 7.19 and 7.20.

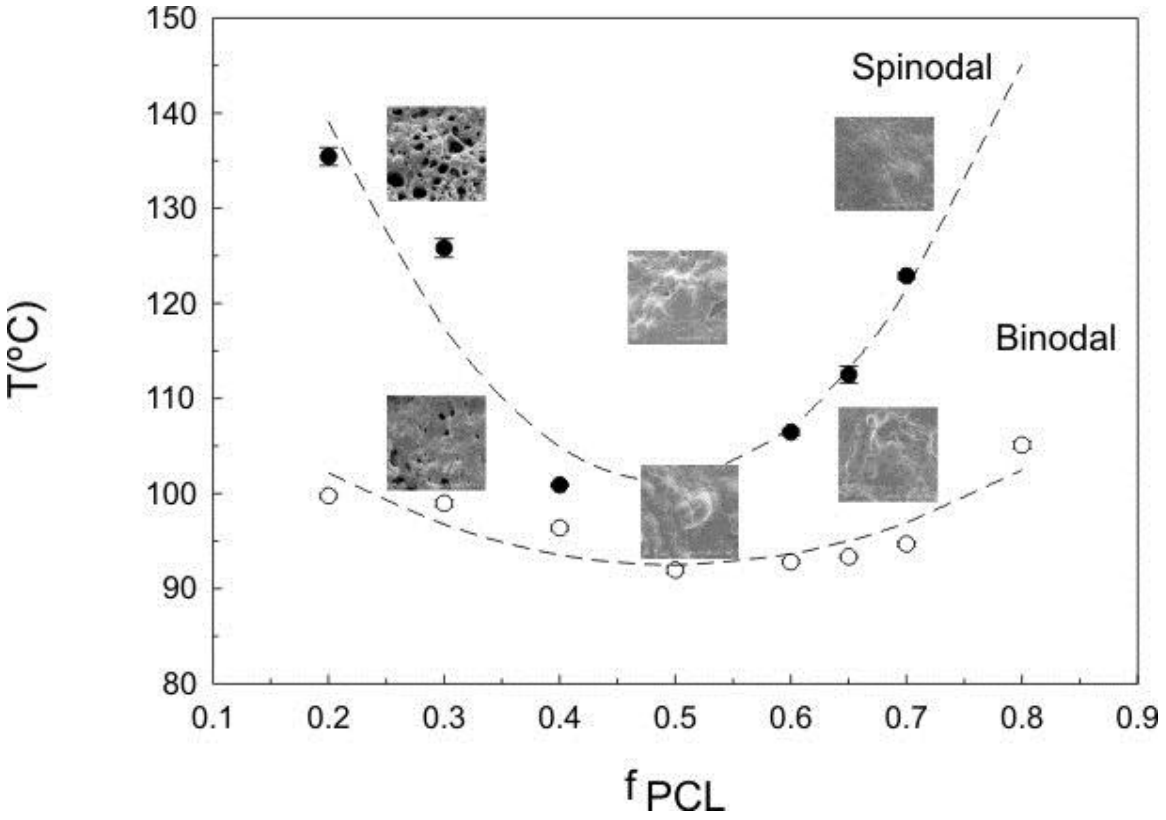

Figure 7.21 Phase diagram of PLA3051D and PCL Capa®6800.

7.6 Diblock Copolymers

The linear viscoelastic response of diblock copolymers (See Table 4.4) were measured at different temperatures from 75°C to 170°C. Figure 7.22 and 7.23 depict the master curves of linear viscoelastic moduli of diblock copolymers with different block length ratios. It can be clearly observed that the time-temperature superposition fails and a master curve could not be produced for PLA60-*b*-PCL40 (Figure 7.22) whereas for the case of PLA25-*b*-PCL75 the time temperature is applicable with the exception of the highest temperature of 170°C. This failure for temperatures beyond a certain level is indicative of the order-disorder transition temperature. The sensitivity of rheological response to the order-disorder transition temperature is more pronounced for the storage modulus (*G'*). At high frequencies, the storage (*G'*) and loss modulus (*G"*) are independent of temperature for both ordered and disordered phases. However, at low frequencies, the rheological response depends on temperature and this is where the failure is more pronounced. To determine the order-disorder temperature, the horizontal shift factors determined from the time-temperature superposition are shown in Figure 7.24. For the case of PLA60-*b*-PCL40 the activation energy (E_a) exhibits two characteristic slopes which correspond to the order and disordered regimes. The point of interception corresponds to a *T* of about 110°C which agrees with the phase separation temperature of corresponding blends at the 60/40 composition (see Figure 7.12). For the diblocks PLA25-*b*-PCL75 and PLA20-*b*-PCL80 there is a single slope showing ordered domain over the whole temperature range. For such composition the order-disorder transition is expected to occur at temperatures in the range of over 130-140°C (see Figure 7.16) and this is the reason we see the failure in Figure 7.23b to occur at 145 and 170°C. Therefore the transition temperatures are in agreement with the phase separation behavior of the PCL/PLA blends.

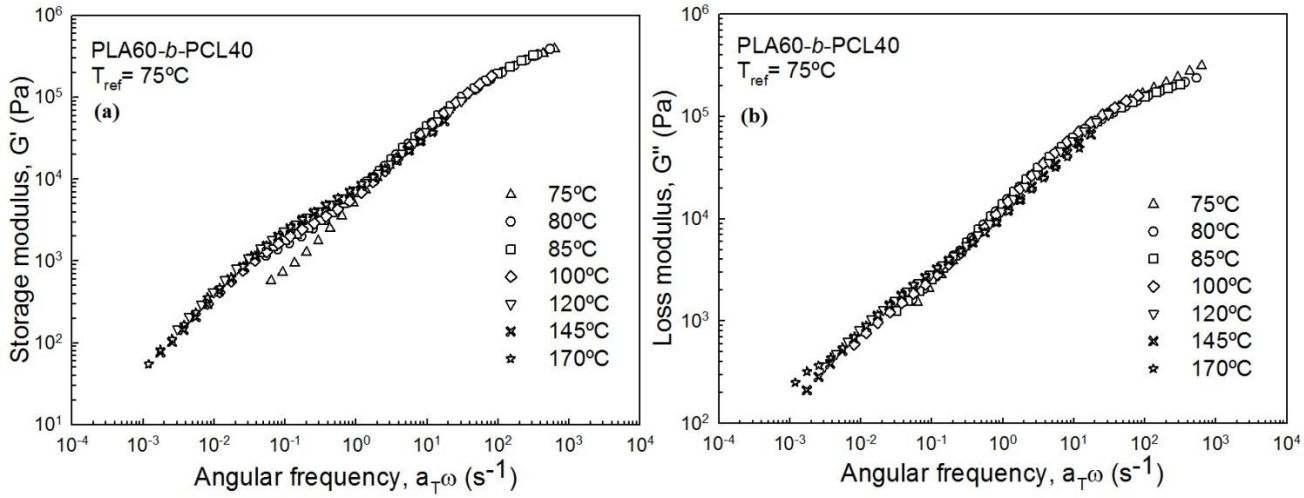

Figure 7.22 Master curve of (a) storage modulus (*G'*) and (b) loss modulus (*G"*) of PLA60-*b*-PCL40 at the reference temperature of 75°C.

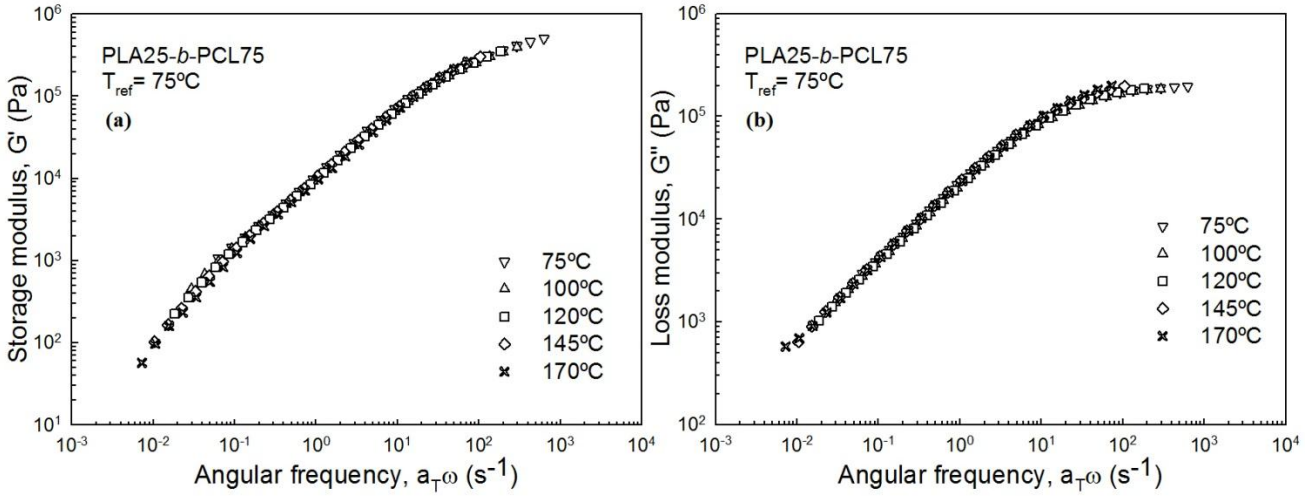

Figure 7.23 Master curve of (a) storage modulus (*G'*) and (b) loss modulus (*G"*) of PLA25-*b*-PCL75 at the reference temperature of 75°C.

The horizontal shift factors determined from the time-temperature superposition are shown in Figure 7.24. The values of activation energy (E_a) for PLA60-*b*-PCL40, PLA25-*b*-PCL75 and PLA20-*b*-PCL80 are 56.98 kJ/mol, 29.34 kJ/mol and 28.56 kJ/mol, respectively.

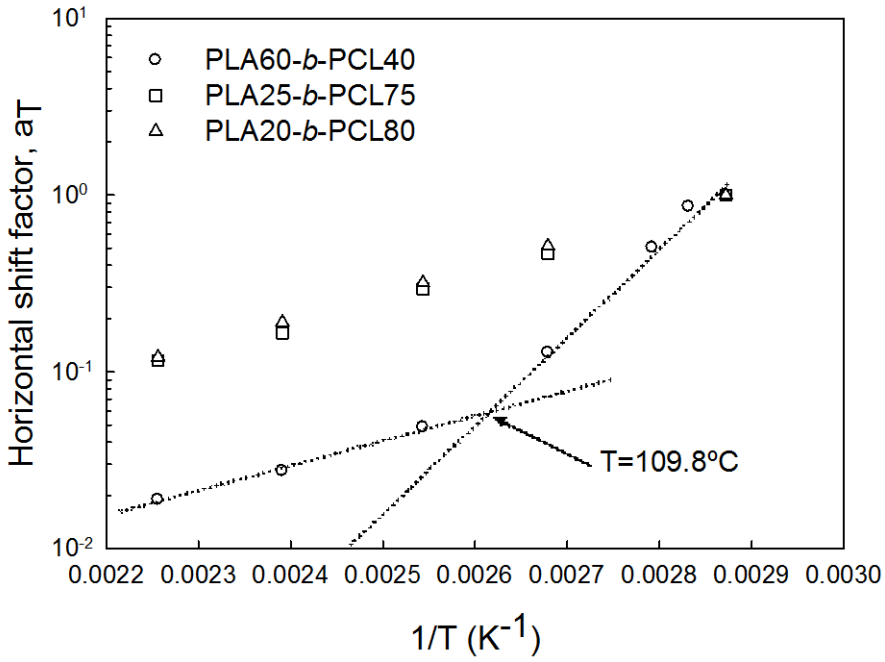

Figure 7.24 The horizontal shift factors, a_T diblock copolymers at the reference temperature of 75°C.

7.7 Summary

The phase separation of PCLPLA blends have been investigated by rheological techniques, specifically isochronal temperature sweep. The effects of frequency in small amplitude oscillatory shear and heating rate on the phase separation in the near-critical and off-critical region have been addressed. Frequency has shown a minor effect on the binodal region of the near-critical blend. On the other hand, the binodal temperatures elevated at higher frequencies for the off-critical blend. The effect of heating rate on the binodal region has found to be significant by shifting it to the higher temperatures for both near-critical and off-critical region. The Ajji-Choplin approach also employed to study the spinodal decomposition. Increasing the heating rate shows a more significant effect on the spinodal decomposition temperature of the off-critical compositions and almost no effect on the near-critical blends. In addition, it was found that increase of the molecular weight of amorphous PLA shifted the phase diagram to lower temperatures. Spherical droplets and interconnected areas have been observed in scanning electron microscopy in binodal and spinodal regions, respectively.

8 Thermorheological Properties of Poly(ε-caprolactone) and Polylactide Blends

The previous chapter discussed the phase separation behavior of PLA and PCL blends. This chapter studies PLA/PCL blends using a single PCL polymer (Capa®6800 listed in Table 4.1) and three PLAs (PLA 2002D, PLA 3051D and PLA 3251D listed in Table 4.3) of different molecular weights emphasizing: The effect of addition of PLA and/or PCL on the crystallinity of the other added component; the use of dynamic rheological measurements to study the viscoelastic properties of these blends in the phase separated region; the use and usefulness of a number of emulsion models to predict the viscoelastic response of the blends; the effect of molecular weight of the components and viscosity ratio on the applicability of these emulsion models; and finally morphological studies as a function of the blend composition.

8.1 Thermal Characteristics of the Blends

The thermal characteristics of the blends of PLA 3051D and PCL Capa®6800 are monitored by Differential Scanning Calorimetry (DSC) both in cooling and heating modes. The crystallization, T_c, and melting, T_m, temperatures are determined as well as the corresponding heats of crystallization and fusion, ΔH_c and ΔH_m , respectively. The results are listed in Table 8.1. The second endothermic and exothermic peaks are depicted in Figure 8.1a and b, respectively.

Table 8.1 Thermal analysis of the blends of PLA 3051D and PCL with different compositions.

PLA/PCL	T_c (°C)		ΔH_c (J/g)		T_m (°C)		ΔH_m (J/g)		$X_{c,PLA}$	$X_{c,PCL}$
	PLA	**PCL**	**PLA**	**PCL**	**PLA**	**PCL**	**PLA**	**PCL**		
100/0	-	-	-	-	-	-	-	-	-	-
80/20	126.4	24	7.78	10.06	149.2	53.8	10.79	7.7	24.95	27.64
70/30	127.7	29.1	6.32	9.65	149.6	54.4	5.49	11.81	18.14	28.26
60/40	126.4	28.1	3.87	19.35	149.4	54.1	4.18	15.81	14.42	28.37
40/60	122.9	27.6	4.09	29.26	148.5	53.9	3.46	25.41	20.29	30.4
0/100	-	26.1	-	51.3	-	55	-	39	-	27.99

The glass transition temperature (T_g) of PLA3051 is 60.6°C, which is very close to the melting temperature of PCL (55°C). As a result, it might interfere in tracing the miscibility of

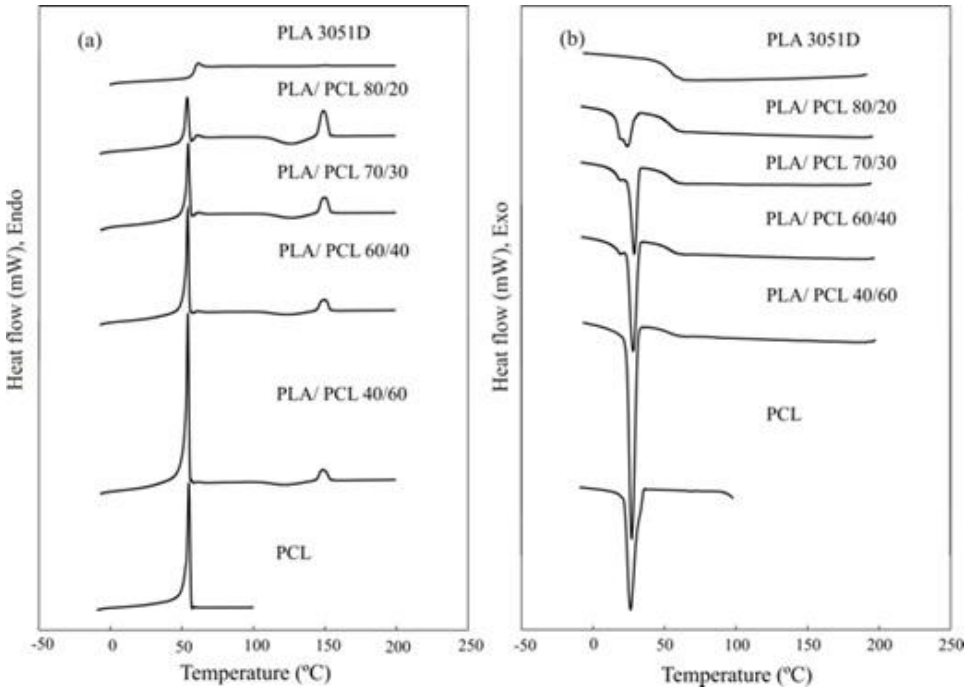

Figure 8.1 DSC thermographs of the blends of PLA 3051D and PCL Capa®6800 (a) Endothermic heat flows of the second heating scan (b) Exothermic heat flows of the cooling scan.

these polymers. No significant change in the melting temperatures of PCL and PLA3051 in the blends was detected compared to that of pure PCL and PLA3051 (see Table 8.1). Addition of PCL to PLA3051 reveals an endothermic peak slightly below 55°C, which is possibly a combination of the melting temperature of PCL and glass transition of PLA3051 (see Table 8.1). The blend of 20% PCL shows a pronounced melting peak for PLA3051 and a large increase in the heat of fusion as a result of the increased amount of PLA3051 crystals. Two separate melting peaks were observed for PLA and PCL at about 149°C and 54°C respectively. This shows that the system is immiscible, an observation which was previously reported for this system by Dell'Erba et al. (2001).

The influence of the addition of PCL on the crystallization of PLA3051 and crystallinity of PCL were confirmed by the following equations (Sarazin et al. 2008, Tsuji and Horikawa 2007):

$$X_{c,PLA} = \frac{(\Delta H_{m,PLA} + \Delta H_{c,PLA})}{\Delta H_{0,PLA} w_{PLA})} \times 100 \quad (8\text{-}1)$$

$$X_{c,PCL} = \left(\frac{\Delta H_{m,PCL}}{\Delta H_{0,PCL} w_{PCL}} \right) \times 100 \tag{8-2}$$

where $\Delta H_{m,PLA}$ and $\Delta H_{c,PLA}$ are the enthalpies of melting and crystallization of PLA3051 in the blends respectively, $\Delta H_{0,PLA}$ is the enthalpy of fusion of 100% crystalline PLA3051 assumed to be 93 J/g (Fisher et al. 1973), $\Delta H_{m,PCL}$ is the enthalpy of fusion of PCL in the blend and $\Delta H_{0,PCL}$ is the heat of fusion of fully crystalline PCL, which has been reported to be 139.3 J/g (Crescenzi et al. 1972). The crystallinity values are listed in Table 8.1 for the PLA3051D/PCL blend system. The results indicate that the crystallinity of PCL in the blends is quite similar to that of pure PCL. On the other hand, the PLA level of crystallinity increases in the presence of PCL, which might be attributed to the influence of the interface of this immiscible system, acting as a nucleation agent (Yang et al. 1997).

8.2 Viscoelastic Behavior of the Poly(ε-caprolactone) and Polylactide Blends

The linear viscoelastic properties of the blends of PCL with different molecular weight of PLAs were determined at 170°C. As discussed earlier in chapter 7, at this temperature, the blends are in the phase separated region. Rheological measurements were performed as an illustrative way to study the miscibility and phase inversion in this system. The measurements were performed for several composition ratios. Figure 8.2 shows the storage modulus (G'), loss modulus (G'') and complex viscosity (η^*) of the blend of PLA 3051D and PCL at only a few concentrations for the sake of clarity. The viscosity ratio of PCL and PLA3051D (η_{PLA}/η_{PCL}) is varied between 0.86 and 0.74 over the whole range of frequencies. At high frequencies, the elastic modulus of all blends reaches almost the same values. In contrast, at the low frequency region (ω<1) the elastic modulus of the blends significantly deviates from the characteristic slope of 2, which indicates terminal relaxation zone. The enhancement in the elastic modulus (significant in the present case) has been reported several times for different incompatible/immiscible binary polymer blends (Gramespacher and Meissner 1992, Wu et al. 2008, Scholz et al. 1989, Steinmann et al. 2002). The behavior is

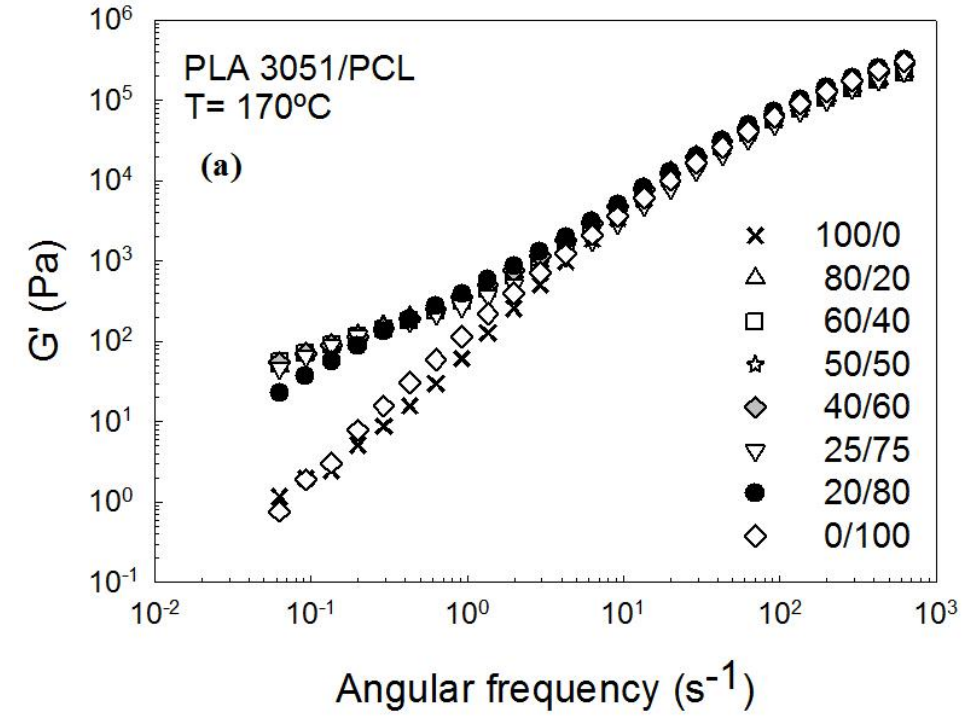
PLA 3051/PCL
T= 170ºC
(a)
100/0
80/20
60/40
50/50
40/60
25/75
20/80
0/100
G' (Pa)
Angular frequency (s-1)

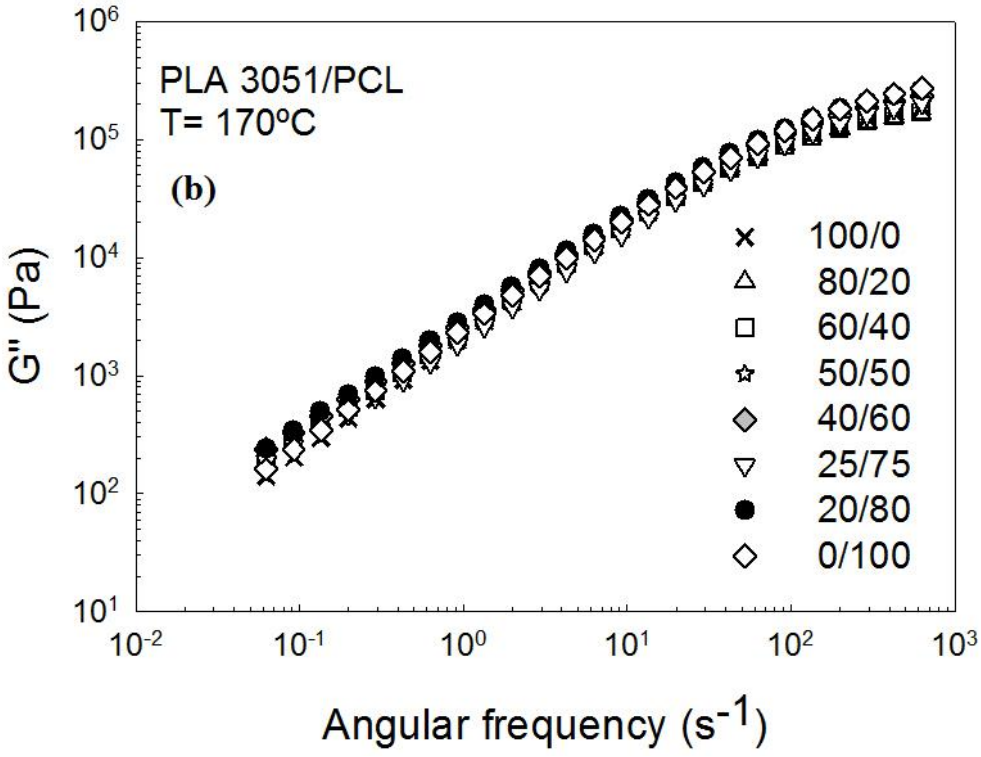
PLA 3051/PCL
T= 170ºC
(b)
100/0
80/20
60/40
50/50
40/60
25/75
20/80
0/100
G'' (Pa)
Angular frequency (s-1)

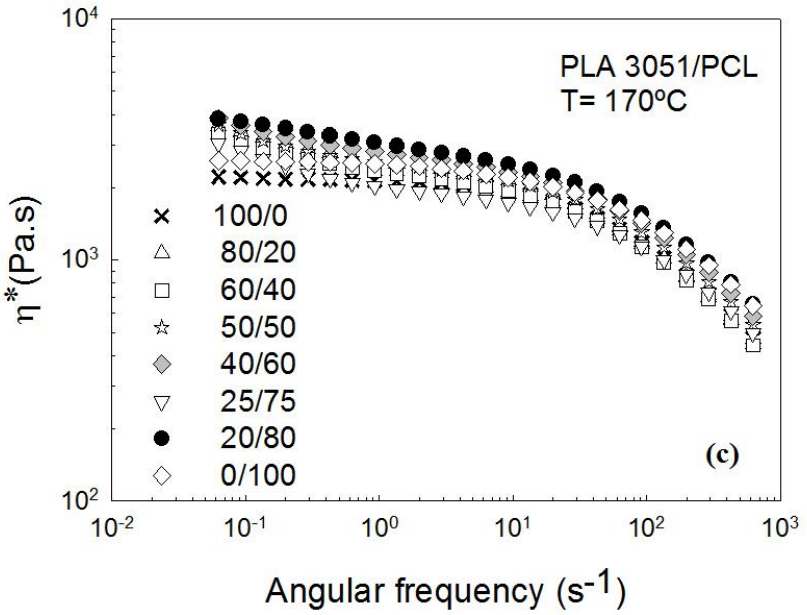

Figure 8.2 (a) Storage modulus (*G'*), (b) loss modulus (*G"*) and (c) complex viscosity (η^*) of PLA 3051D/PCL blends with different compositions measured at 170°C.

attributed to the shape relaxation of the dispersed domain at low frequencies under shear, mainly due to the presence of the interface. In immiscible and incompatible systems such as the one of the present study, the interfacial energy affects the viscoelastic behavior significantly. Under shear deformation at low frequencies, the contribution of interfacial energy to elastic modulus increases, leading to the enhancement of the elastic modulus of the blends compared to those of the pure components.

To obtain a better understanding of immiscibility utilizing a rheological approach, the Cole-Cole and the Han plots (Chopra et al. 2002) are shown here in Figure 8.3 and Figure 8.4 respectively. The presence of a tail or peak in the Cole-Cole plots of the blends show different relaxation processes compare to pure polymers which is indicative of phase separation in this system (Dumoulin et al. 1991, Carreau et al. 1994). The phase separated system includes two frequency regions related to the different relaxation processes. The relaxation behavior at low frequencies corresponds to the deformation of the dispersed phase. However, the second relaxation region at higher frequency relates to the phase relaxation (Domoulin et al. 1991, Utracki 1991). In addition, deviation from the *G'-G"* power-law relationship of the pure PLA and PCL components in the Han plot (Figure 8.4) indicates the

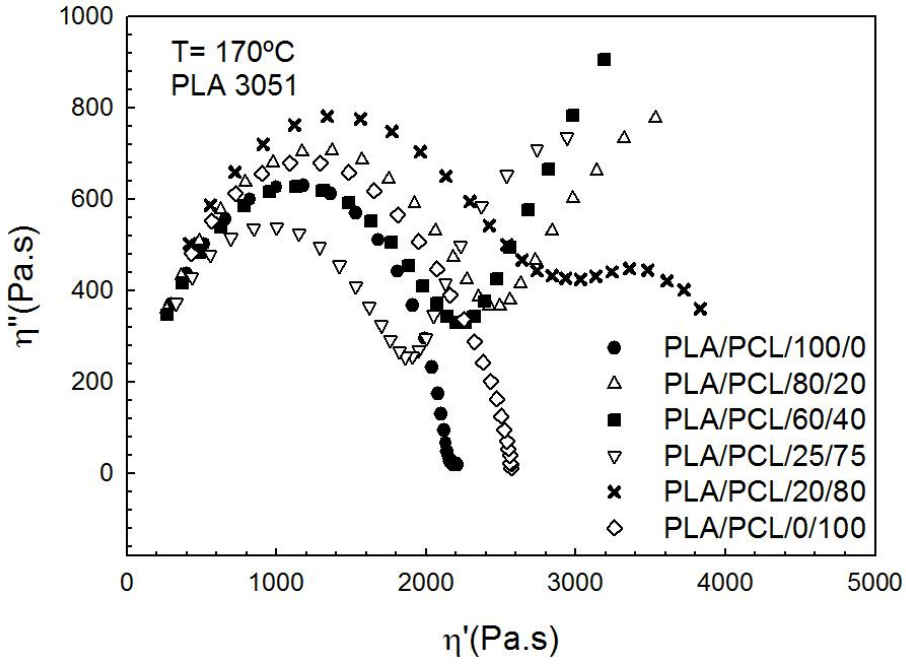

Figure 8.3 Cole-Cole plot of PLA3051D/PCL at various blending ratios at 170°C.

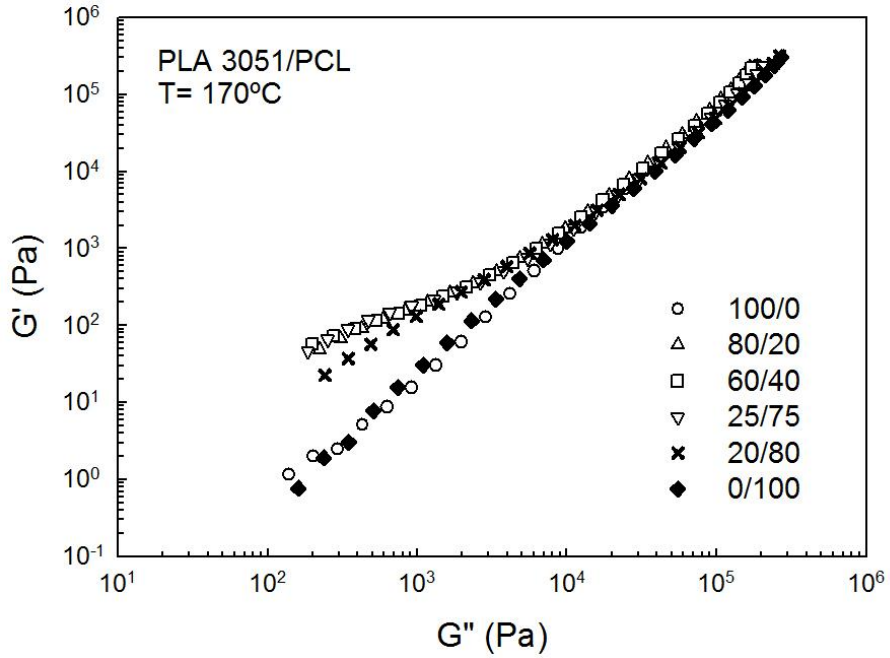

Figure 8.4 Han plot of PLA3051D/PCL at various blending ratios at 170°C.

immiscibility of the blends (Chopra et al. 2002, Ajji et al. 1988). In other words, the type of deviation obtained in Figure 8.4 shows the *G'* enhancement as discussed in the context of Figure 8.2a.

The effect of molecular weight of PLA on the immiscibility of the PCL/PLA system was investigated by using the two other PLAs which have different viscosity ratios with the PLA examined so far. For the highest molecular weight PLA (2002D), the viscosity ratio (η_{PLA}/η_{PCL}) varies from 2.3 at low frequency to 1.11 at high frequency. On the other hand, the low molecular weight PLA (3251) has relatively lower viscosity ratio from 0.2 to 0.31 in the same frequency range. Figure 8.5 and Figure 8.6 depict the elastic modulus (*G'*) and loss modulus (*G"*) of PLA2002D/PCL and PLA3251D blends.

In the high molecular weight PLA (2002D) system, the storage and loss modulus decreases with increasing the PCL content as PCL is the less viscous component. In contrast, for low molecular weight PLA (3251D) system, it is noticeable that the *G'* and *G"* of the blends increase with increase of PCL phase as demonstrated in Figure 8.6a and Figure 8.6b. The Cole-Cole plots of the blends with high and low molecular weight of PLA are illustrated in Figure 8.7a and Figure 8.7b. The appearance of the second peak is an indication of phase transition as discussed above (Ajji et al. 1988, Ferry 1980). The shoulder in the elastic modulus and the shape of Cole-Cole plot of the blends signifies immiscibility of the system.

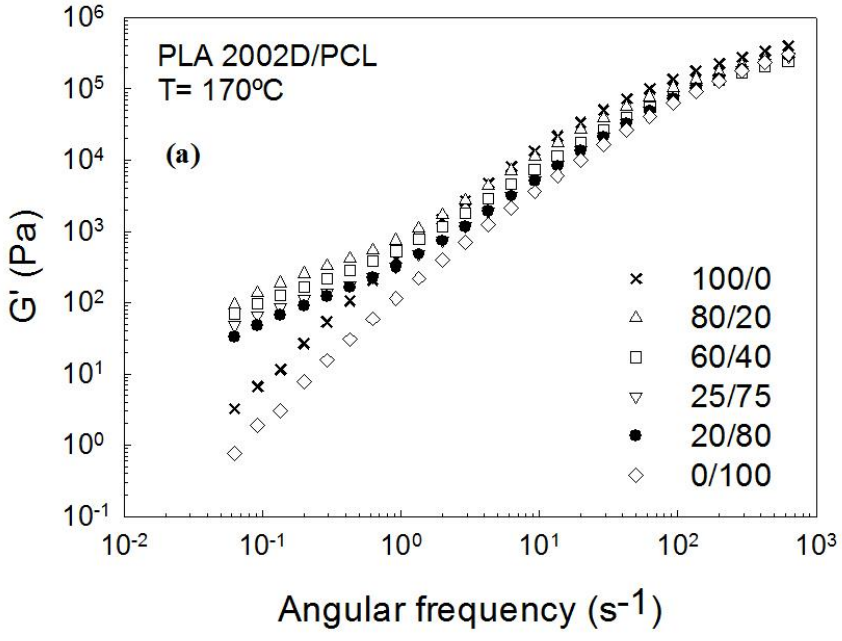

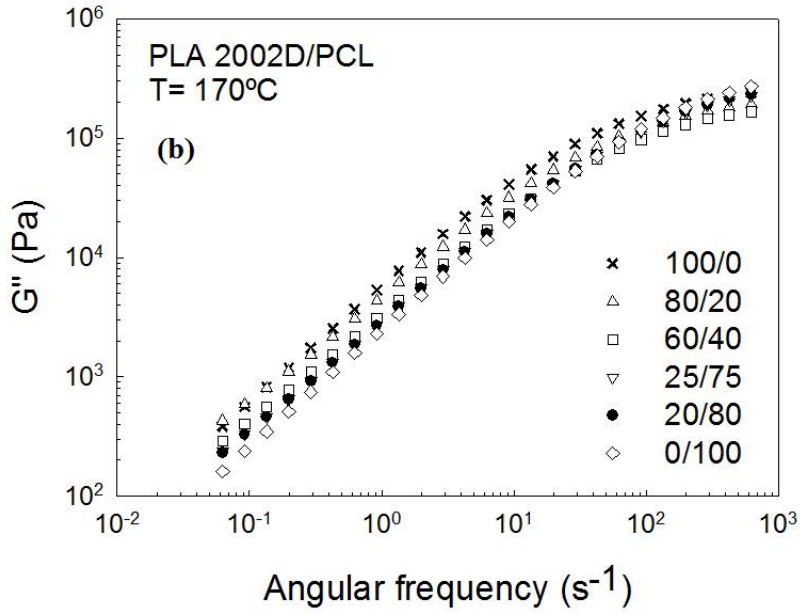

Figure 8.5 (a) The storage (*G'*) modulus and (b) the loss modulus (*G"*) of the PLA 2002D/PCL blend system with different compositions at 170°C.

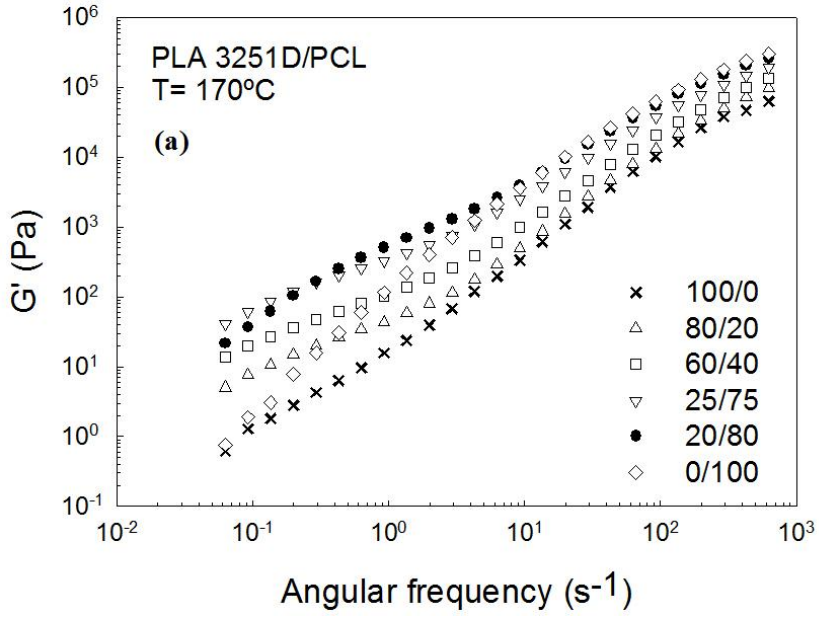

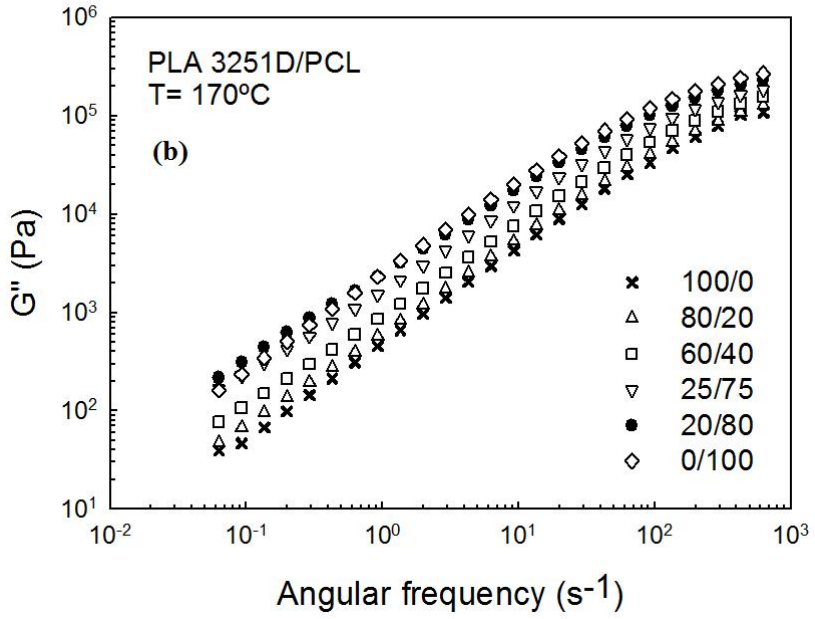

Figure 8.6 (a) The storage (*G'*) modulus and (b) the loss modulus (*G"*) of PLA 3251D/PCL blend system with different compositions at 170°C.

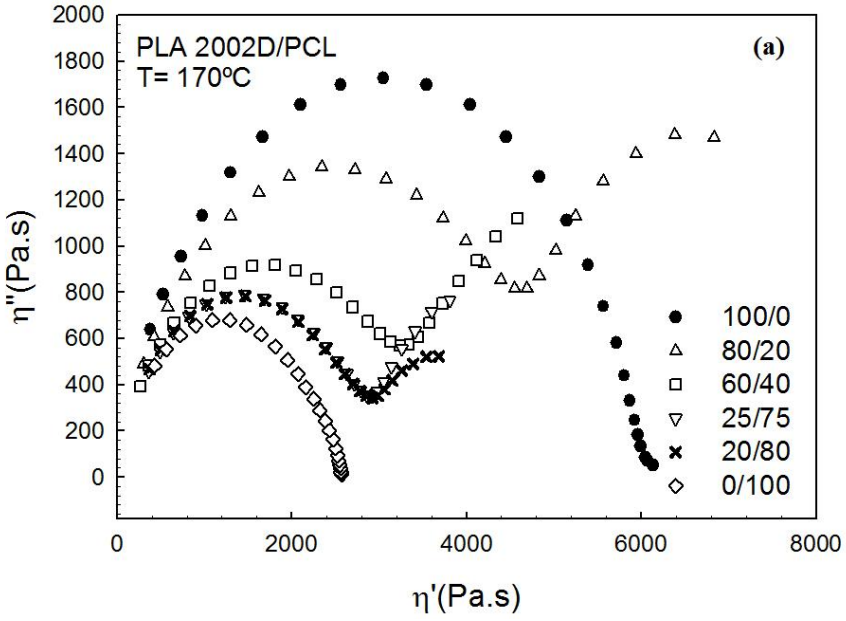

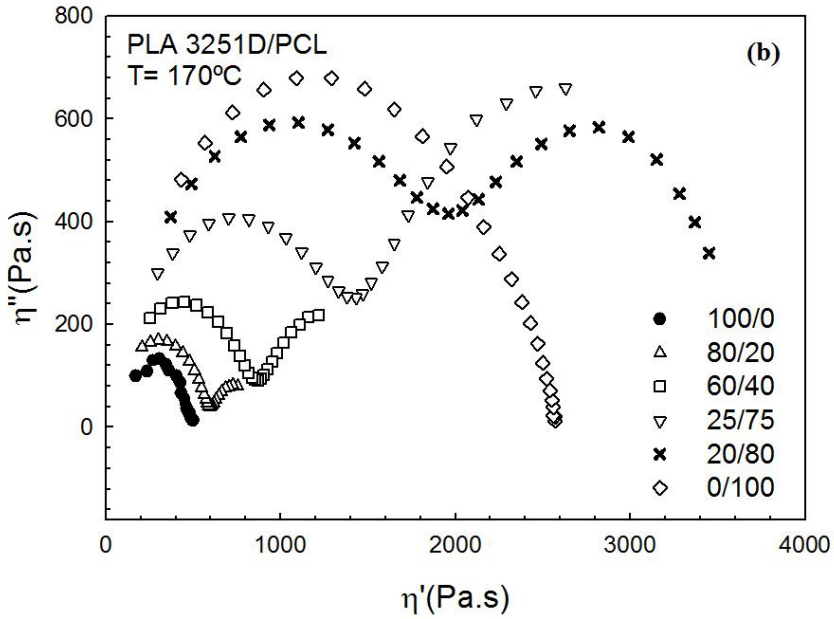

Figure 8.7 Cole-Cole plot of (a) PLA 2002D/PCL and (b) PLA3251D/PCL at various blending ratios at 170°C.

The continuous relaxation spectra, *H(λ)* provides complementary information on miscibility and relaxation behavior of these systems. *H(λ)* was calculated numerically by fitting measured storage *(G')* and loss *(G")* modulus according to the following equations (Utracki 1991):

$$G'(\omega) = \int_{-\infty}^{+\infty} H(\lambda) \frac{\omega^2 \lambda^2}{1+\omega^2 \lambda^2} d \ln \lambda \tag{8-3}$$

$$G''(\omega) = \int_{-\infty}^{+\infty} H(\lambda) \frac{\omega \lambda}{1+\omega^2 \lambda^2} d \ln \lambda \tag{8-4}$$

Figure 8.8 presents the weighted relaxation spectra *(λH(λ))* of blends of different molecular weight of PLA at various composition ratios. The pure PLAs and PCL shows single peaks of relaxation except for the low molecular weight PLA that the terminal region could not be reached due to torque limitation of the rheometer. The single peak represents the

unique characteristic relaxation time. The relaxation time of PLA in the high molecular weight PLA system is almost one order of magnitude larger than PCL.

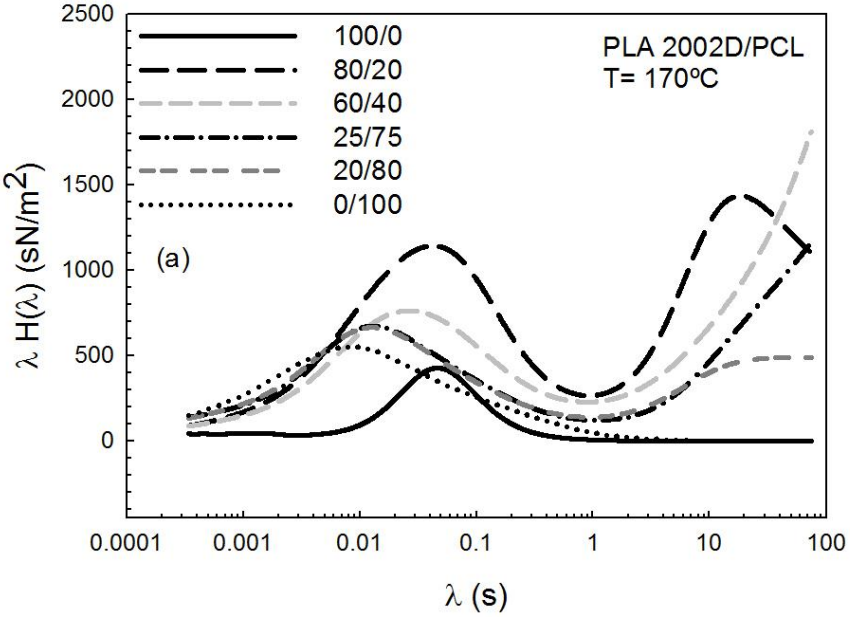

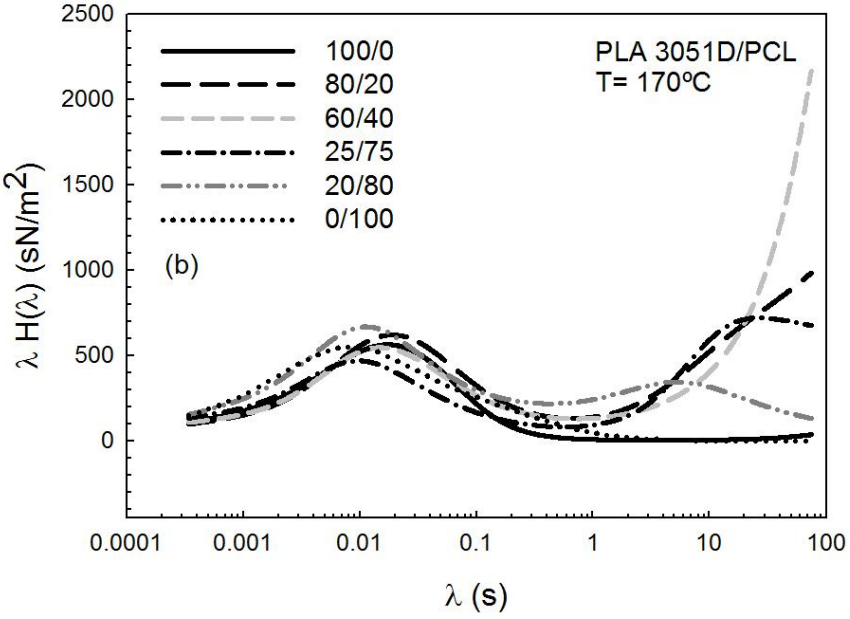

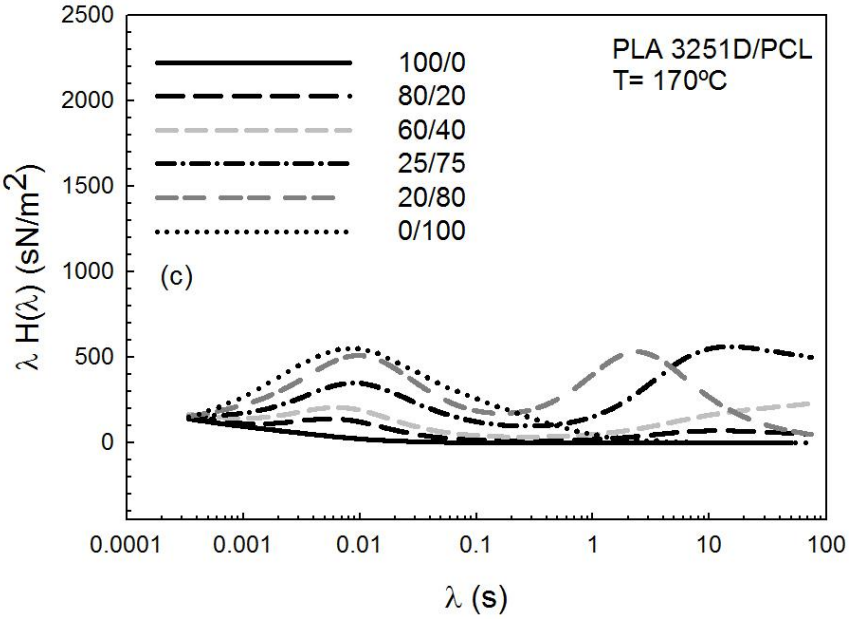

Figure 8.8 Weighted relaxation spectra of (a) PLA 2002D/PCL, (b) PLA3051D/PCL and (c) PLA 3251D/PCL at various blending ratios at 170°C.

For the blends, the onset of the second peak is obvious. For compositions of PLA3051D/PCL and PLA3251D/PCL, higher than 75 wt% in PCL, the second relaxation peak clearly occurs, which is a sign of immiscibility. Figure 8.8c also shows that the second relaxation peak is captured at higher PCL contents.

Figure 8.9 depicts the viscosity and elastic modulus dependence on PCL content of the blends with various molecular weights of PLAs as a rheological criterion of immiscibility and phase inversion. All the values are collected at the low frequency region. For different molecular weights of PLA and at all compositions of the blends, the viscosity and elastic modulus positively deviate from the linear log-additivity rule. This type of behavior has been reported for many binary polymer blends in literature (Ajji et al. 1988, Choi and Schowalter 1975). This positive deviation behavior (PDB) is a sign of high interaction between the two phases in an immiscible blend. For the PLA3251D/ PCL blends a negative/positive deviation is observed. The maxima in Figure 8.9 for the viscosity and the elastic modulus correspond to the phase inversion composition which is also in agreement with the occurrence of the second peak in the Cole-Cole plots (Figure 8.3 and 8.7).

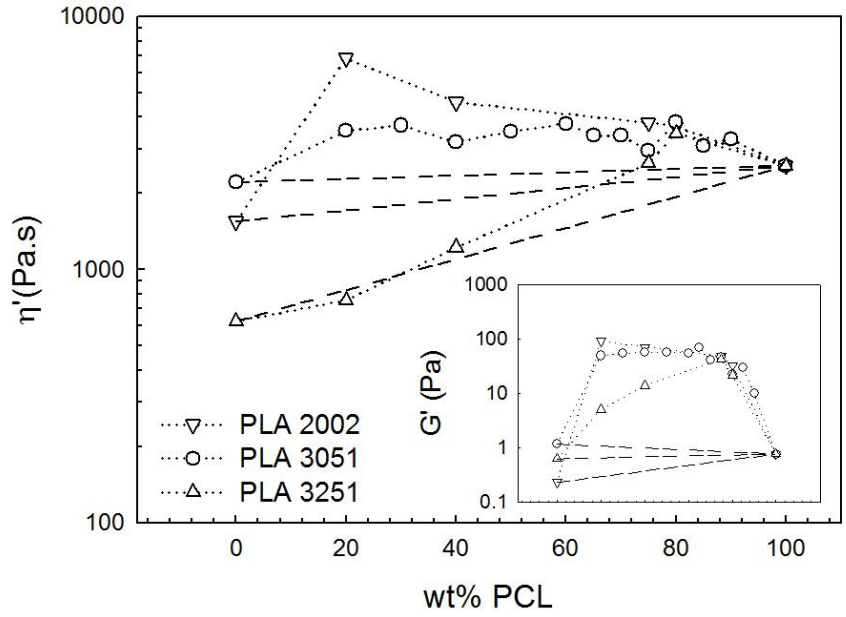

Figure 8.9 Real viscosity and elastic modulus corresponding to different blend ratios. Dashed lines represent the linear log-additivity rule; Dotted lines represent a connecting line between the experimental data.

8.3 Morphological Studies

SEM micrographs of the fractured surfaces of blends of PLA3051 D and PCL are reported in Figure 8.10. Images in Figure 8.10a-c correspond to blends with compositions of 20, 30 and 40 wt% of PCL respectively. They essentially show homogeneously dispersed droplets of nearly spherical PCL as the dispersed phase. However, by increasing the PCL content, the size of the droplets increases due to coalescence (Dell'Erba et al. 2001). The distinct interface between the two phases is evidence of high immiscibility of this system. By increasing the PCL content above 50 wt% the morphology starts changing into a co-continuous structure (Figure 8.10d-g). The variation in morphology is due to the significant increase in the coalescence of PCL droplets (Wu et al. 2008). Droplet breakup and coalescence are the competing mechanisms that determine the morphology of this system similar to other immiscible blends. There is a percolation threshold at which the coalescence is the dominant process that is affected by interfacial tension and viscoelastic behavior of the phases (Paul and Barlow 1980). Finally, at a high concentration of PCL, the dispersed phase is now PLA3051D and the droplet morphology is evident again in Figure 8.10h-j.

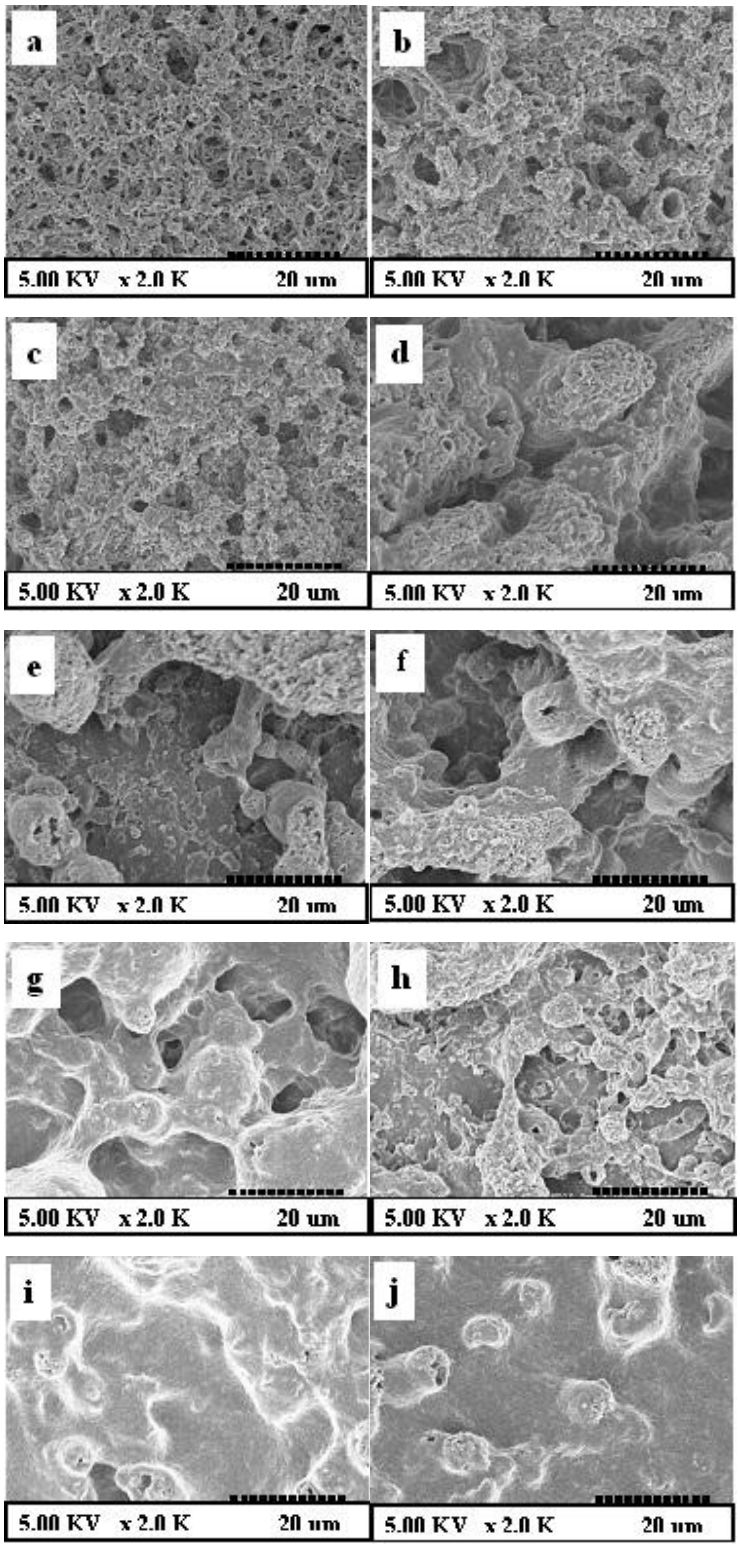

Figure 8.10 SEM images of blends of PLA 3051D/PCL with different compositions (a) 80/20 (b) 70/30 (c) 60/40 (d) 50/50 (e) 40/60 (f) 35/65 (g) 30/60 (h) 25/75 (i) 20/80 (j) 15/85.

Similar morphologies were obtained for the other blend systems investigated, namely PLA2002/PCL and PLA3251D/PCL. The morphology of the blends with 20 wt% of PCL and 80wt%PLA 2002D and PLA 3251D are shown in Figure 8.11a and Figure 8.11b respectively. Images demonstrate a good level of distribution of the dispersed phase (PCL) in PLA matrix for both molecular weight of PLA. These Figures are to be compared with Figure 8.10a. It appears that the morphologies of all these blends appear to be quite similar independent of the molecular weight of PLA.

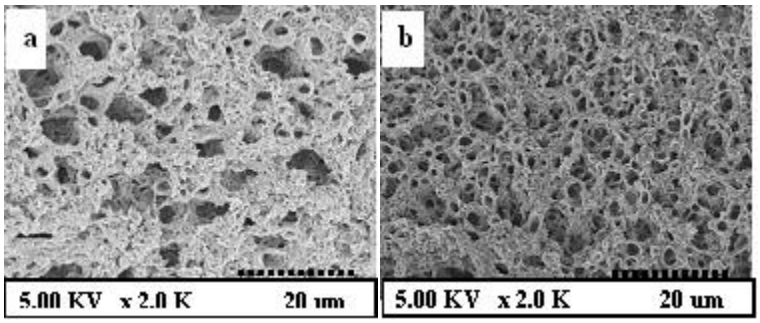

Figure 8.11 SEM images of the blends of (a) PLA 2002D/PCL and (b) PLA 3251D/ PCL at the composition ratio of PLA/PCL 80/20.

8.4 Modeling of the Viscoelastic Behavior of the Poly(ε-caprolactone) and Polylactide Blends

To predict the viscoelastic behavior of the blends from the corresponding properties of the pure components, two different emulsion models have been employed in the present study. These models are based on the assumptions made for the case of Newtonian emulsions considering the linear viscoelastic properties of the phases and the contribution of the interfacial tension effect to the stress tensor. These models are also used to determine the interfacial tension in immiscible polymer blends as a means of a fitting parameter, which can be subsequently compared with experimental values. In immiscible systems, coalescence and breakup of the disperse phase is a collaboration of interfacial tension and viscoelastic properties of the blends (Broz et al. 2003). As discussed before, these binary blend systems have higher elastic modulus *(G')* in the low frequency region due to the so-called shape relaxation of the dispersed phase (Scholz et al. 1989) resulting from the interfacial behavior. The viscoelastic properties of these multiphase polymer systems have been described by a

number of emulsion models considering the contribution of interfacial tension and viscoelastic parameters of their pure components. Gramespacher and Meissner (Gramespacher and Meissner 1992) have used the simplified theory for mixtures of Newtonian liquids (Wu et al. 1971) that introduced by Scholz et al. (1989):

$$G'_{blend} = \varphi G'_{disperse} + (1-\varphi)G'_{matrix} + \frac{\eta}{\tau_1}(1-\frac{\tau_2}{\tau_1})\frac{\omega^2\tau_1^2}{1+\omega^2\tau_1^2} \tag{8-5}$$

$$G''_{blend} = \varphi G''_{disperse} + (1-\varphi)G''_{matrix} + \frac{\eta}{\tau_1}(1-\frac{\tau_2}{\tau_1})\frac{\omega\tau_1}{1+\omega^2\tau_1^2} \tag{8-6}$$

The parameters of Equations 8.5 and 8.6 are as follows:

$$\eta = \eta_{matrix}\left[1+\varphi\frac{(5K+2)}{2(K+1)}+\varphi^2\frac{5(5K+2)^2}{8(K+1)^2}\right] \tag{8-7}$$

$$\tau_1 = \tau_0\left[1+\varphi\frac{5(19K+16)}{4(K+1)(2K+3)}\right] \tag{8-8}$$

$$\tau_2 = \tau_0\left[1+\varphi\frac{3(19K+16)}{4(K+1)(2K+3)}\right] \tag{8-9}$$

$$\tau_0 = \frac{\eta_{matrix}R}{\sigma}\frac{(19K+16)(2K+3)}{40(K+1)} \tag{8-10}$$

$$K = \frac{\eta_{disperse}}{\eta_{matrix}} \tag{8-11}$$

where φ is the volume fraction of disperse phase, R is the radius of droplets of disperse phase and σ is the interfacial tension and η_{matrix} and $\eta_{disperse}$ are the zero-shear viscosities of the pure components of the blend.

The modified Palierne model (Graebling et al. 1993) can also be used to describe the complex modulus of the blend by assuming that the local shear and variation of interfacial area has no effect on the interfacial tension between phases. The complex modulus can be calculated by the following expressions:

$$G^*_{blend}(\omega) = G^*_{matrix}(\omega)\frac{1+3\sum_i \varphi H_i(\omega)}{1-2\sum_i \varphi H_i(\omega)} \tag{8-12}$$

where φ is the volume fraction of the disperse phase and $H_i(\omega)$ is as follows:

$$H_i(\omega) = \left\{\begin{array}{l} 4(\sigma/R_i)\left[2G^*_{matrix}(\omega)+5G^*_{disperse}(\omega)\right]+ \\ \left[G^*_{disperse}(\omega)-G^*_{matrix}(\omega)\right]\left[16G^*_{matrix}(\omega)+19G^*_{disperse}(\omega)\right] \end{array}\right\} / \left\{\begin{array}{l} 40(\sigma/R_i)\left[G^*_{matrix}(\omega)+G^*_{disperse}(\omega)\right]+ \\ \left[2G^*_{disperse}(\omega)+3G^*_{matrix}(\omega)\right]\left[16G^*_{matrix}(\omega)+19G^*_{disperse}(\omega)\right] \end{array}\right\} \tag{8-13}$$

In all the above mentioned models, R is the radius of the dispersed phase, which is determined from scanning electron microscopy (SEM). This can be either an average radius for droplet morphology or a characteristic length of the domains in the co-continuous morphologies.

The experimental number average radii (R_n) and volume average radii (R_v) were calculated by analysing the SEM images (Figure 8.10a-i) according to the following expressions:

$$R_n = \frac{\sum_i n_i R_i}{\sum_i n_i} \tag{8-14}$$

$$R_v = \frac{\sum_i n_i R_i^4}{\sum_i n_i R_i^3} \tag{8-15}$$

The values of radii of disperse phase calculated by Equation 8.14 for compositions of 80/20, 70/30, 40/60 and 15/85 are 1.2 μm, 1.3 μm, 10.1 μm and 5.8 μm respectively. By increasing the PCL content, due to the coalescence of the droplets the domain size of the disperse phase increases, and increases much more significantly after the inversion point (PCL rich compositions). Also it has been observed that in the systems with the same

composition and higher viscosity ratio, the domain size increases slightly (disperse domain size in PLA2002D blend with 20 wt% PCL is 1.874±0.1 μm). To evaluate the viscoelastic properties of the blends by the emulsion models, the PCL/PLA interfacial tension was considered as a variable adjustable parameter, which was calculated by fitting the experimental linear viscoelastic values to the models and minimizing the relative error. Interfacial tension between PLA and PCL obtained from the fitting procedure varied from 1.18 to 4.57 mN/m at various composition ratios and molecular weights.

The PCL/PLA interfacial tension between the two polymers can also be calculated by an equation derived from the following equation in terms of the surface tensions of pure solid polymers and the polar and dispersion contributions/interactions (Wu 1971).

$$\gamma_{12} = \gamma_1 + \gamma_2 - \frac{4\gamma_1^d \gamma_2^d}{\gamma_1^d + \gamma_2^d} - \frac{4\gamma_1^p \gamma_2^p}{\gamma_1^p + \gamma_2^p} \tag{8-16}$$

In this equation, γ is the surface tension of the polymer, γ^d and γ^p are dispersive and nondispersive (polar) force contributions to the surface tensions, respectively. The values of these parameters for PLA and PCL were obtained from previous studies and they are summarized in Table 8.2 (Schwach and Averous 2004).

Table 8.2 Energy parameters and surface tensions of PLA and PCL.

	γ (mN/m)	γ_p (mN/m)	γ_d (mN/m)
PLA	49±2	11±2	37±2
PCL	52±2	11±2	41±2

The calculated value of the interfacial tension between PLA and PCL according to Equation 8.15 is 1.206 mN/m, which is in the range of the calculated/fitted values by the models. The dependence of interfacial tension on molecular weight has been previously studied for other binary polymer systems. It is reported that interfacial tension increases with molecular weight and reaches a steady value for molecular weights above the entanglement

(Kamal et al. 1994, Anastasiadis et al. 1988). The PLAs of the present blends are all above the entanglement molecular weight, which is 3959 g/mol at 140°C (Dorgan et al. 2005).

Figures 8.12a-d examine the capability of the emulsion models to predict the viscoelastic parameters of the blends from the corresponding properties of the pure components, considering the interfacial tension as a known parameter equal to 1.206 mN/m from Equation 8.15. The different compositions of the blends examined are those whose morphologies were presented before. Model predictions in Figures 8.12a-d shows that at high PCL content (Figure 8.12c) which corresponds to co-continuous morphology, the emulsion models are not successful in the low frequency region, where the *G'* enhancement is obtained, perhaps due to the uncertainty of obtaining a good estimate of the domain size. This behavior has been previously reported for other binary systems (Lacroix et al. 1997). It appears that the emulsion models and in particular the Gramespacher-Meissner (G-M) model performs better for compositions well before the inversion point.

Figure 8.13 depicts the emulsion models' capabilities in predicting the viscoelastic properties of the blends with PCL of different molecular weight systems at the 80/20 composition (morphologies presented in Figure 8.11). In general the Gramespacher-Meissner (G-M) model performs better than the modified Palierne model as also shown in Figure 8.12a and 8.12b.

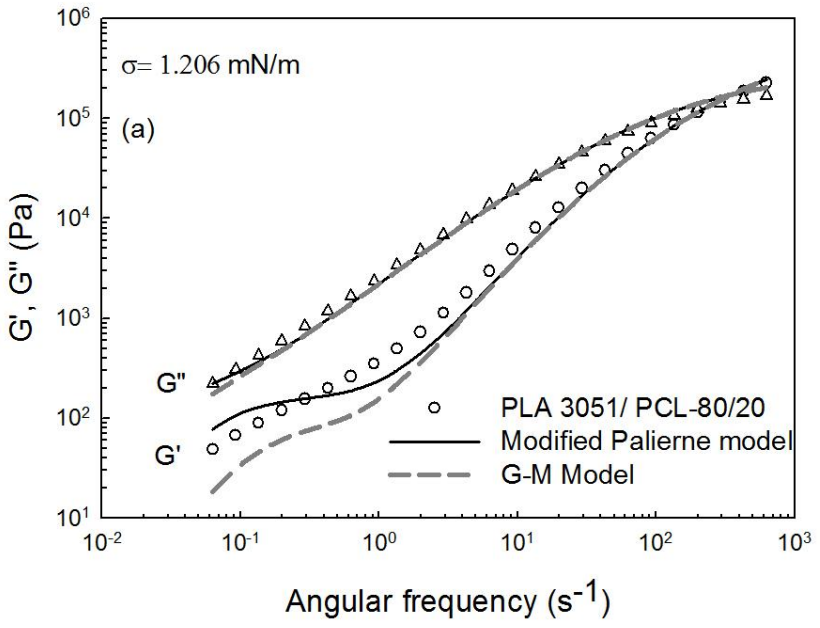

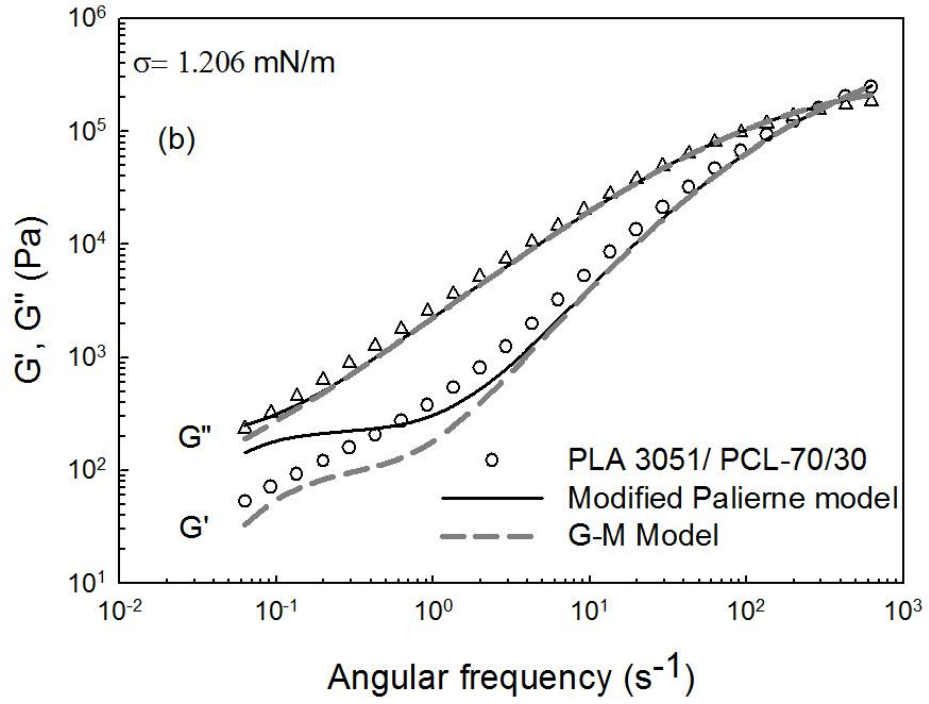
σ= 1.206 mN/m
(b)
G', G" (Pa)
G"
G'
PLA 3051/ PCL-70/30
Modified Palierne model
G-M Model
Angular frequency (s-1)

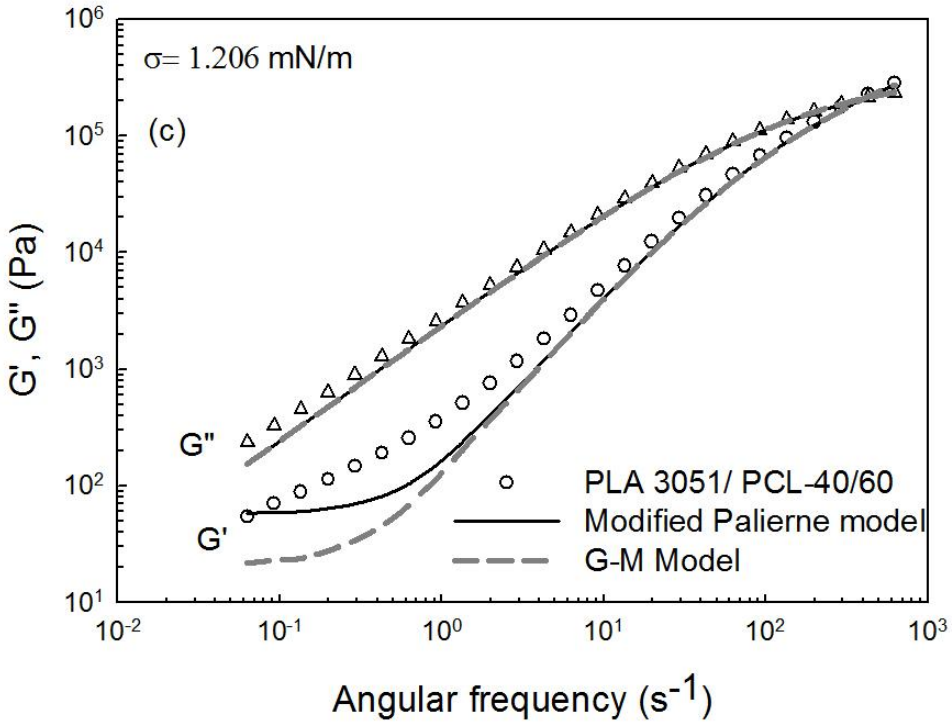
σ= 1.206 mN/m
(c)
G', G" (Pa)
G"
G'
PLA 3051/ PCL-40/60
Modified Palierne model
G-M Model
Angular frequency (s-1)

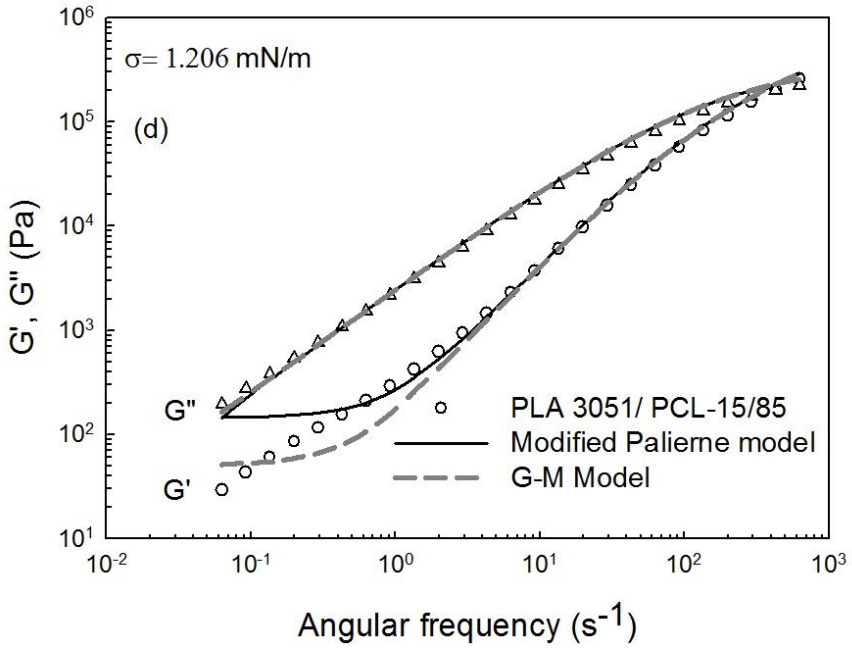

Figure 8.12 Prediction of viscoelastic properties of Blends by Modified Palierne and Gramespacher-Meissner (G-M) models using constant value of interfacial tension for PLA 3051D and PCL blends of different composition ratios at 170°C, (a)80/20 (b) 70/30 (c) 40/60 (d) 15/85.

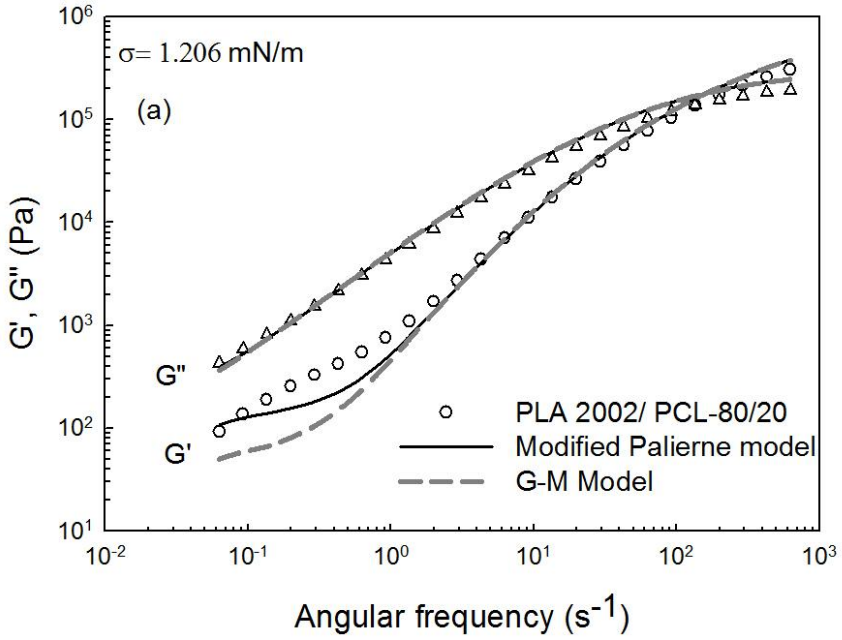

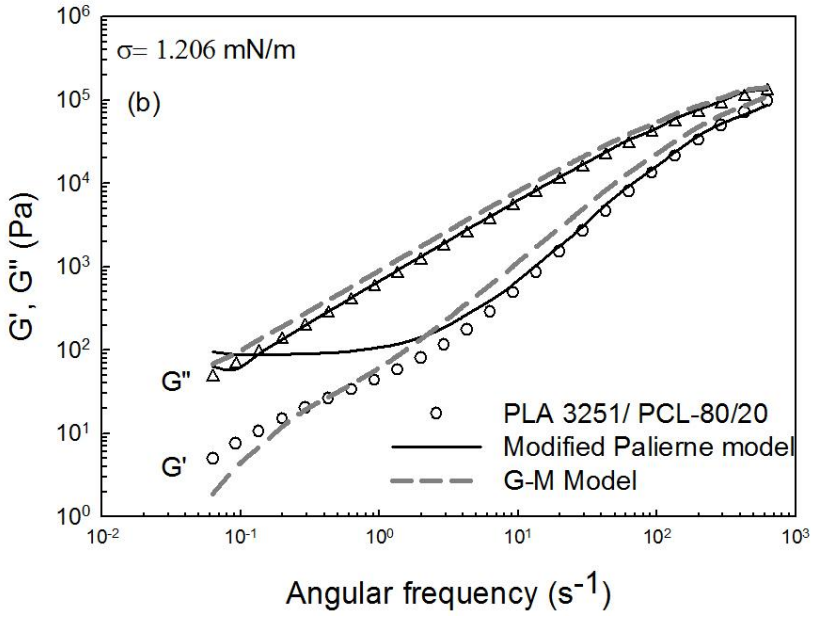

Figure 8.13 Prediction of viscoelastic properties of Blends by Modified Palierne and Gramespacher-Meissner (G-M) models using constant value of interfacial tension for (a) PLA 2002D and (b) PLA 3251D blends at 170°C.

8.5 Mechanical Properties of PLA and PCL Blends

The mechanical properties of the blends of two high molecular PLA (PLA3051D and PLA2002D listed in Table 4.3) and PCL Capa®6800 are discussed in this section. Figure 8.14 shows the evolution of tensile strength of the blends of PCL Capa®6800 and PLA3051D, PLA 2002D as a function of PLA content. Both PLAs exhibit similar enhancement effect on the tensile strength. Addition of 20wt% PLA to the PCL increases the tensile strength by 12.5% compared to the pure PCL. Up to 40wt% PLA, there is a gradual effect on tensile strength which follows by the significant increase at 60 and 80 wt% PLA. In the case of PLA 3051D, 80wt% PLA leads to up to 77% increase in tensile strength compared to neat PCL. The elastic modulus of the blends shows improvement by addition of PLA in a relatively linear trend with PLA content (Figure 8.15). Moreover, the elongation at break, exhibits significant drop by addition of as low as 20wt% PLA compared to the PCL homopolymer (Figure 8.16). The analysis of the mechanical properties data of the PLA3051D, PCL Capa®6800 and their blends are summarized in Table 8.3. The same analysis for PLA 2002D is reported in Appendix C. It should be noted that the presence of 20wt% PLA 301D, reduces

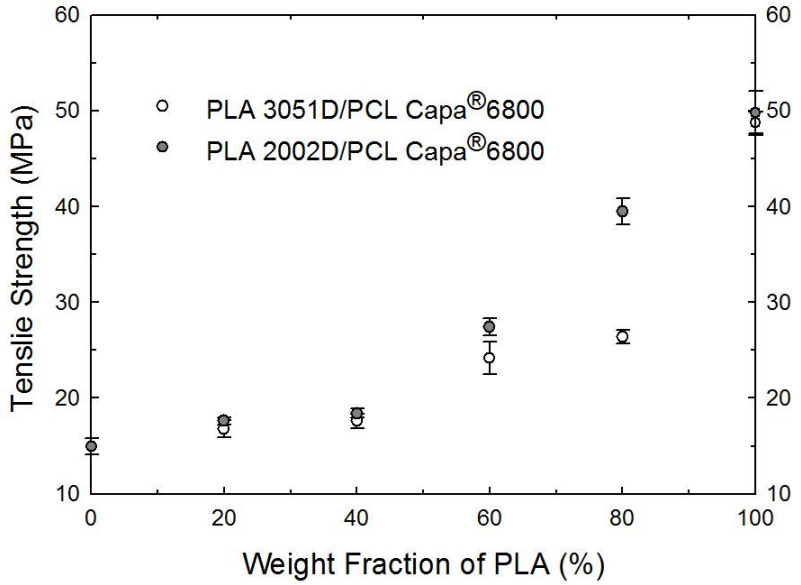

Figure 8.14 Tensile strength of PLA 3051D, PLA 2002D, PCL Capa®6800 homopolymers and their blends as a function of the weight fraction of PLA.

the elongation at break of the rubbery PCL down to 76%. The results indicate the ductility effect of PCL on the PLA homopolymer which is in agreement with previous studies (Lopez-Rodriguez et al. 2006, Broz et al. 2003).

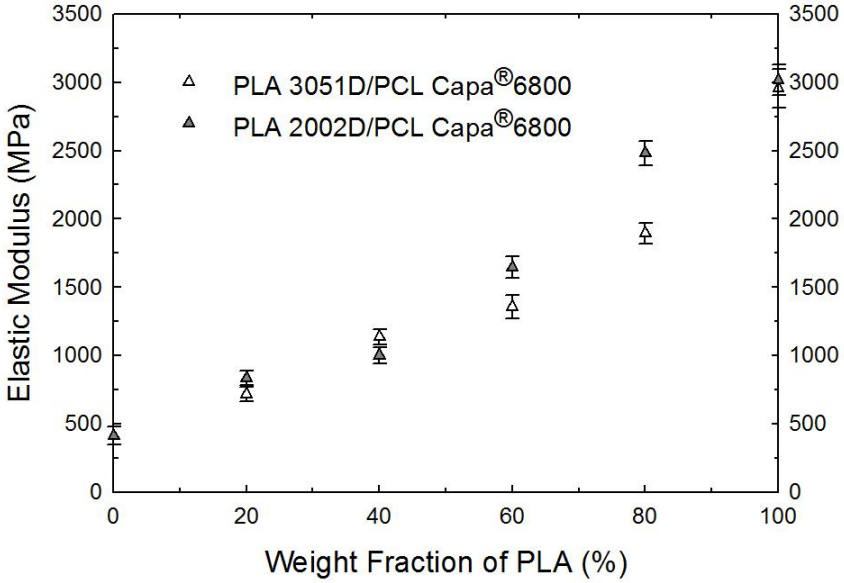

Figure 8.15 Elastic modulus of PLA 3051D, PLA 2002D, PCL Capa®6800 homopolymers and their blends as a function of the weight fraction of PLA.

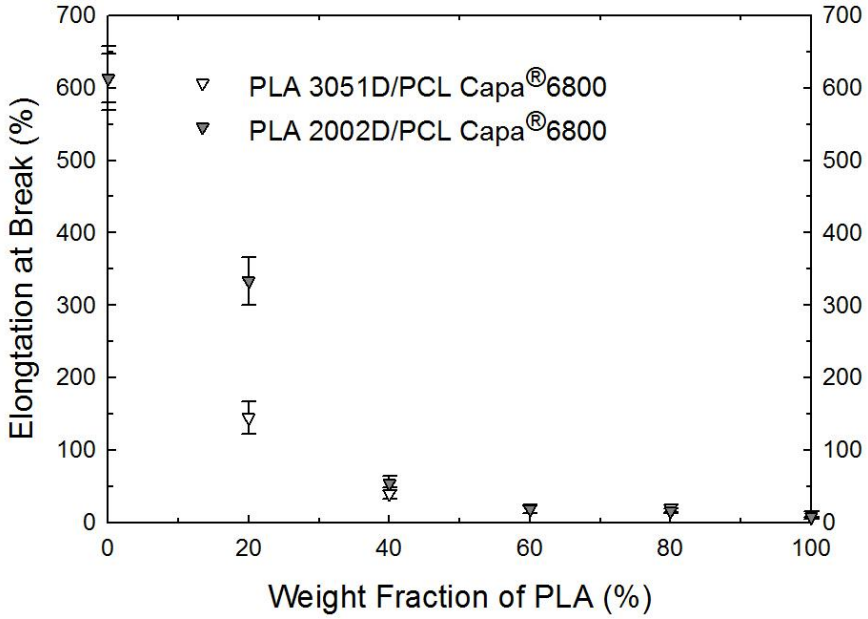

Figure 8.16 Elongation at break of PLA 3051D, PLA 2002D, PCL Capa®6800 homopolymers and their blends as a function of the weight fraction of PLA.

Table 8.3 Mechanical properties of PCL Capa®6800/ PLA3051D blends.

PLA 3051D (wt%)	*Tensile strength (MPa)*	*Elastic modulus (GPa)*	*Elongation at break (%)*
0	14.9± 0.8	0.4±0.06	613.1±33.9
20	16.8±0.9	0.7±0.05	144.5±21.9
40	17.6±0.7	1.1±0.05	39.8±7.9
60	24.2±1.7	1.4±0.08	18.5±5.3
80	26.4±0.7	1.9±0.07	19.6±5.7
100	48.8±1.2	2.9±0.14	10.1±5.6

8.6 Summary

Thermal analysis of the blends of PLA and PCL shows the improvement effect of PCL on the crystallization of an amorphous PLA up to 87%. Moreover, relatively no change in the melting peaks of PLA and PCL is an indication of immiscibility of these polymers. The

rheological behavior of the blends was studied at the phase separated region. Enhancement of elastic modulus at low frequencies is a result of the presence of the interface of the two immiscible polymers. Clear boundary between phases was observed by SEM images as well having a co-continuous morphology above 50wt% PCL. Emulsion models were found inadequate to predict the viscoelastic properties for the blends having co-continuous morphology. Finally, the mechanical properties of the PCL/PLA blends were studied, exhibiting the ductility effect of PCL on PLA polymer.

9 Conclusions, Contribution to Knowledge and Recommendations

9.1 Conclusions

The solution and melt rheological properties of PCL homopolymers (commercial and newly synthesized) having different molecular characteristics, have been investigated. First, regarding the solution rheological properties, the values of the Mark-Houwink parameters and characteristic radii agreed with values reported for the linear flexible polymers confirming the linear macrostructure of PCLs. The presence of thermal stabilizer in commercial PCLs affects the thermal stability as well as the rheological properties. From linear viscoelasticity, applicability of time–temperature superposition for all PCLs shows the simplicity of thermorheological behaviour of PCL mainly due its linear structure. The molecular weight between entanglements for PCL of approximately 3,900 g/mol was determined from the plateau modulus of 0.9 MPa that is independent of molecular weight. The scaling exponent of zero-shear viscosities with molecular weight is higher than those reported for linear nearly monodisperse well-entangled polymers. No strain hardening was observed under extensional flow at low temperature and high Hencky strain rate. Even at low temperature, the relaxation time of the chain is very small compared to the deformation time scale, which cannot lead to strain hardening behavior.

The melt fracture phenomenon of high molecular weight commercial PCL homopolymer has been examined in the capillary flow. No significant slip has been occurred during the processing of the high molecular weight PCLs. It was found that for high molecular weight PCL, all different types of flow instabilities occur, namely loss of gloss, sharkskin, stick-slip and gross melt fracture. The onset of melt fracture for high molecular weight PCL occurred at around 0.2 for temperatures above 115°C. Below 115°C the critical shear stress for the onset of melt fracture increased to 0.49 MPa and it was observed that at the temperature of 100°C, the processability surprisingly improves. The critical shear rate for the onset of melt fracture increased by increasing the temperature above 115°C, however, the critical shear stress remained constant. In terms of processing aids, addition of 0.5 wt% polylactide (PLA) was effective in eliminating and postponing the onset of melt fracture to higher shear rates and caused a significant pressure drop compared to the pure PCL.

Rheological techniques, specifically isochronal temperature sweep have been used to investigate the phase separation behaviour of the PCL/PLA blend system. The effects of

frequency in small amplitude oscillatory shear and heating rate on the phase separation have been addressed depending on the composition of the blend in the near-critical and off-critical region. In case of the near-critical blend, the frequency has been found to have a minor effect on the binodal region; this behavior is related to the main origin of viscoelastic response abnormality at the phase separation region which is the concentration fluctuation. For the off-critical blend the scenario is different due to the effect of shear on nucleation. Therefore, the binodal temperatures increased at higher frequencies. Change in the heating rate also has shown a significant effect on the binodal region by shifting it to the higher temperatures for both near-critical and off-critical region. The Ajji-Choplin approach also employed to study the spinodal decomposition. Increasing the heating rate shows a more significant effect on the spinodal decomposition temperature of the off-critical compositions and almost no effect on the near-critical blends. Overall the effect of heating rate was found to be more significant in studying the binodal decomposition. In addition, it was found that increase of the molecular weight of amorphous PLA shifted the phase diagram to lower temperatures. The optical microscopy technique has shown the crystalline structure of PCL at room temperature and liquid-liquid interconnected phase separated domains at high temperatures for the PCL-rich blends, and isotropic structure of the blend at PLA-rich compositions, which is in accordance with the rheological measurements, although not sufficient for the accurate phase separation temperature measurement. Scanning electron microscopy has demonstrated the phase separated morphology in the form of spherical domains in the binodal region and the interconnected and extended size of domains in the unstable region.

Finally, the thermal, rheological and mechanical properties of the PCL/PLA blends have been investigated using a reference PCL polymer and three PLA polymers of various molecular weights. The enthalpy of crystallization confirms the improvement that the PCL addition has on the crystallization of PLA. In particular, addition of 20% PCL increases the level of crystallinity of PLA up to 87%. On the other hand, PLA addition does not have an effect on PCL crystallinity. No significant change in the melting temperatures of PLA and PCL was observed as a result of the immiscibility of these polymers.

Rheological studies at the phase separated region revealed significant enhancement of the G’ at low frequencies in all systems, which is clearly due to the presence of interface due to immiscibility of the two components. The clear boundary between phases of this immiscible system having droplet morphology at low contents of PCL and the co-continuous structure at

above 50% of PCL have been observed by SEM. Emulsion models have predicted the viscoelastic properties of the blends in a satisfactory way for the cases of blends possessing droplet morphology, However, both models are not adequate to represent the viscoelastic properties of blends possessing co-continuous morphology or evolving morphologies. From tensile testing, addition of PCL to the PLA matrix has shown strong ductility effect, as well as the improvement in tensile strength and elastic modulus compared to the PCL in the blends.

9.2 Contributions to Knowledge

The present work has yielded the following contributions to knowledge:

1. From the linear viscoelastic measurements, for a broad range of molecular weight and nearly monodisperse polymers, the exponent of 4 relates the power-law function of molecular weight to the zero-shear viscosity. Other important rheological parameters in modeling have been resulted from this analysis.
2. Extensional rheology of PCL at low temperature and high Hencky strain rates did not show any strain hardening. This behavior can be concluded as the small relaxation time of the linear polymer compare to the deformation time scale.
3. The processability of PCL addressed in this study, revealed a processing window at low temperatures were PCLs exhibit enhance processability. Moreover, PLA is discovered as a processing aid to successfully postpone and eliminate the surface instabilities of PCL due to the immiscibility of this system.
4. This study adds new contribution to the rare available data in literature regarding the thermodynamics and phase separation behavior of PCL/PLA blend system. The findings support that dynamic conditions, shear and heating rate, largely affect the phase separation boundary. Moreover, this study proves the effect of molecular structure such as crystallinity and molecular weight on phase separation.
5. The capability of emulsion models to predict the viscoelastic properties was examined and it was found that depends on the composition ratio or morphology of the blend as well as on the viscosity ratio of the components.

9.3 Recommendations for Future Work

There are several aspects of this work that could be investigated in the future. Some suggestions and recommendations on future studies are as follows:

1. A detailed, systematic study of the effect of flow on the crystallization of PCL can be carried out. This type of study can also be related to the melt fracture phenomenon in a capillary die.
2. A systematic study of the effect of molecular weight distribution (MWD) of PCL on the melt fracture phenomenon can be performed. The synergistic effect of molecular weight and molecular weight distribution (MWD) on slip can be addressed. Furthermore, the origin of the enhance processability of of PCL at low temperature can be studied.
3. The capability of other biodegradable polymers such as poly(β-hydroxybutyrate) (PHB) that are immiscible with PCL, can be investigated as possible processing aids for PCL polymers.
4. A detailed study on the compatibilizing effect of biodegradable copolymers and nanofillers to improve the miscibility of the PCL/ PLA blend system can be performed.

Bibliography

Achilleos, E., Georgiou, G., Hatzikiriakos, S. (2002). Role of processing aids in the extrusion of molten polymers. *Journal of Vinyl & Additive Technology, 8*(1), 7-24.

Acierno, S., Di Maio, E., Iannace, S., Grizzuti, N. (2006). Structure development during crystallization of polycaprolactone. . *Rheologica Acta, 45*(4), 387-392.

Ajji, A., Choplin, L., Prud'homme, R. E. (1988). Rhology and phase separation in polystyrene/poly(vinyl methyl ether) blends. *Journal of Polymer Science Part B: Polymer Physics, 26*(11), 2279-2289.

Ajji, A., Choplin, L. (1991a). Rheology and dynamics near phase separation in a polymer blend: Model and scaling analysis. *Macromolecules, 24*(18), 5221-5223.

Ajji, A., Choplin, L., Prud'homme, R. E. (1991b). Rheology of polystyrene/poly(vinyl methyl ether) blends near the phase transition. *Journal of Polymer Science Part B: Polymer Physics, 29*(13), 1573-1578.

Amos, S. E., Giacoletto, G. M., Horns, J. H., Lavallee, C., Woods, S. S. (2001). *Polymer processing aids (PPA) in plastic additives*. Munich: Hanser.

Anastasiadis, S. H., Gancarz, I., Koberstein, J. T. (1988). Interfacial tension of immiscible polymer blends: temperature and molecular weight dependence. *Macromolecules, 21*(10), 2980-2987.

Archer, L. A. (2005). Wall slip: Measurement and modelling issues. In S. G. Hatzikiriakos, K. B. Migler (Eds.), *Polymer processing instabilities*. New York: Marcel Dekker.

Arraiza, A. L., Sarasua, J. R., Verdu, J., Colin, X. (2007). Rheological behavior and modeling of thermal degradation of poly(epsilon-caprolactone) and poly(L-lactide). *International Polymer Processing, 22*(5), 389-394.

Aslan, S., Calandrelli, L., Laurienzo, P., Malinconico, M., Migliaresi, C. (2000). Poly (D,L-lactic acid)/poly(ε-caprolactone) blend membranes: preparation and morphological characterisation. *Journal of Materials Science, 35*(7), 1615-1622.

Auhl, D., Kaschta, J., Munstedt, H., Kaspar, H., Hintzer, K. (2006). Molecular characterization of semi-fluorinated copolymers with a controlled amount of long-chain branching. *Macromolecules, 39*(6), 2316-2324.

Barlow, J. W., Paul, D. R. (2006). Polymer blends and alloys-a review of selected considerations. *Polymer Engineering and Science, 21*(15), 985-996.

Bernstein, B., Kearsley, E. A., Zapas, L. J. (1963). A study of stress relaxation with finite strain. *Transactions of the Society of Rheology, 7*, 391-410.

Baumgaertel, M., Schausberger, A., Winter, H. H. (1990). The relaxation of polymers with linear flexible chains of uniform length. *Rheologica Acta, 29*(5), 400-408.

Baumgaertel, M., Winter, H. H. (1989). Determination of the discrete relaxation time spectrum from dynamic mechanical data. *ANTEC 89*, 1652-1655.

Bird, R. B., Armstrong, R. C., Hassager, O. (1987). *Dynamics of polymeric liquids*. New York: Wiley.

Biresaw, G., Carriere, C. J. (2004). Compatibility and mechanical properties of blends of polystyrene with biodegradable polyesters. *Composites: Part A, 35*(3), 313-320.

Bonnet, F., Cowley, A. R., Mountford, P. (2005). Lanthanide borohydride complexes supported by diaminobis(phenoxide) ligands for the polymerization of ε-caprolactone and L- and rac-lactide. *Inorganic Chemistry, 44*(24), 9046-9055.

Bousmina, M. (1999). Rheology of polymer blends: linear model for viscoelastic emulsions. *Rheologica Acta, 38*(1), 73-83.

Bousmina, M., Lavoie, A., Riedl, B. (2002). Phase segregation in SAN/PMMA blends probed by rheology, microscopy, and inverse gas chromatography techniques. *Macromolecules, 35*(16), 6274-6283.

Brochard-Wyart, F., de Gennes, P. G. (1992). Shear-dependent slippage at a polymer solid interface. *Langmuir, 8*(12), 3033-3037.

Broz, M. E., VanderHart, D. L., Washburn, N. R. (2003). Structure and mechanical properties of poly(D,L-lactic acid)/poly(ε-caprolactone) blends. *Biomaterials, 24*(23), 4181-4190.

Buddhiranon, S., Kim, N., Kyu, T. (2011). Morphology development in relation to the ternary phase diagram of biodegradable PDLLA/PCL/PEO blends. *Macromolecular Chemistry and Physics, 212*(13), 1379-1391.

Burchard, W. (1999). Solution properties of branched macromolecules. *Advances in Polymer Science,* 113-113.

Carreau, P. J. (1972). Rheological equations from molecular network theories. *Transactions of the Society of Rheology,* 16(1), 99-127.

Carreau, P. J., Bousmina, M., Ajji, A. (1994). Rheological properties of blends: Facts and challenges. In K.P. Ghiggino, *Progress in Pacific Polymer Science 3*. Munich: Hanser.

Chen, C. C., Chueh, J. Y., Tseng, H., Huang, H. M., Lee, S. Y. (2003). Preparation and characterization of biodegradable PLA polymeric blends. *Biomaterials, 24*(7), 1167-1173.

Choi, S. J., Schowalter, W. R. (1975). Rheological properties of nondilute suspensions of deformable particles. *The Physics of Fluids*, 18(4), 420-427.

Chopra, D., Kontopoulou, M., Vlassopoulos, D., Hatzikiriakos, S. G. (2002). Effect of maleic anhydride content on the rheology and phase behavior of poly(styrene-co-maleic anhydride)/poly(methyl methacrylate) blends. *Rheologica Acta*, *41*(5), 10-24.

Chopra, D., Vlassopoulos, D., Hatzikiriakos, S. G. (1998). Shear-induced mixing and demixing in poly(styrene-co-maleic anhydride)/poly(methyl methacrylate) blends. *Journal of Rheology*, *42*(5), 1227-1247.

Cloitre, M., Vlassopoulos, D. (2012). Block copolymers in external fields: rheology, flow-induced phenomena, and applications In M. Kontopoulou (Eds.1), *Applied polymer rheology: polymeric fluids with industrial applications*. New York: John Wiley & Sons, Inc.

Coates, G. W., Ovitt, T. M. (1999). Synthesis of new poly(lactic acid) microstructures. *Abstracts of Papers of the American Chemical Society*, *218*, 207.

Cogswell, F. N. (1977). Stretching flow instabilities at exits of extrusion dies. *Journal of Non-Newtonian Fluid Mechanics*, *2*(1), 37-47.

Coleman, M. M., Serman, C. J., Bhagwagar, D. E., Painter, P. C. (1990). A practical guide to polymer miscibility. *Polymer*, *31*(7), 1187-1203.

Crescenzi, V., Manzini, G., Calzolari, G., Borri, C. (1972). Thermodynamics of fusion of poly(β-propiolactone) and poly(ε-caprolactone). Comparative analysis of the melting of aliphatic polylactone and polyester chains. *European Polymer Journal*, *8*, 449-463.

Dealy, J. M., Wissbrun, K. F. (1999). *Melt rheology and its role in plastic processing*. New York: Van Nostrand Reinhold.

Dealy, J. M., Kim, S. (2005). Gross melt fracture in extrusion. In S. G. Hatzikiriakos, K. B. Migler (Eds.1), *Polymer processing instabilities*. New York: Marcel Dekker.

Dealy, J. M., Larson, R. G. (2006). *Structure and Rheology of Molten Polymers*. Munich: Hanser.

Dell'Erba, R., Groeninckx, G., Maglio, G., Malinconico, M., Migliozzi, A. (2001). Immiscible polymer blends of semicrystalline biocompatible components: thermal

properties and phase morphology analysis of PLLA/PCL blends. *Polymer*, *42*, 7831-7840.

Dong, H., Wang, H. D., Cao, S. G., Shen, J. C. (1998). Lipase-catalyzed polymerization of lactones and linear hydroxyesters. *Biotechnology Letters*, *20*(10), 905-908.

Dorgan, J. R., Janzen, J., Clayton, M. P., Hait, S. B., Knauss, D. M. (2005). Melt rheology of variable L-content poly(lactic acid). *Journal of Rheology, 49*(3), 607-619.

Dumoulin, M. M., Utracki, L. A., Carreau, P. J. (1991). Melt rheology and morphology of linear low density polyethylene/ polypropylene blends. In L. A. Utracki, *Two-Phase Polymer Systems*. Munich: Hanser.

Easwar, N. (1992). Effect of continuous stirring on off'-critical and critical samples of a phase-separating binary liquid mixture. *Physical Review Letters, 68*(2), 186-189.

Ferri, D., Greco, F. (2006). Nonlinear stress relaxation of molten polymers: experimental verification of a new theoretical approach. *Macromolecules, 39*(17), 5931-5938.

Ferry, J. D. (1980). Viscoelastic properties of polymers. 3rd edition. New York: John Wiley & Sons, Inc.

Fischer, E. W., Sterzel, H. J., Wegner, G. (1973). Investigation of the structure of solution grown crystals of lactide copolymers by means of chemical reactions. *Colloid and Polymer Science, 251*(11), 980-990.

Flieger, M., Kantorova, M., Prell, A., Rezanka, T., Votruba, J. (2003). Biodegradable plastics from renewable sources. *Folia Microbiologica, 48*(1), 27-44.

Flory, P. J., Fox, T. G. (1954). Treatment of Intrinsic Viscosities. *Journal of the American Chemical Society, 73*, 1904-1908.

Fox, T. G., Loshaek, S. (2000). Isothermal viscosity-molecular weight dependence for long polymer chains. *Journal of Applied Physics, 26*(9), 1080-1082.

Georgiou, G. (2005). Stick-slip instability. In S. G. Hatzikiriakos, K. B. Migler (Eds.1), *Polymer processing instabilities*. New York: Marcel Dekkar.

Gharachorlou, A., Goharpey, F. (2008). Rheologically determined phase behavior of LCST blends in the presence of spherical nanoparticles. *Macromolecules, 41*(9), 3276-3283.

Gimenez, J., Cassagnau, P., Michel, A. (2000). Bulk polymerization of ε-caprolactone: Rheological predictive laws. *Journal of Rheology, 44*(3), 527-547.

Graebling, D., Muller, R., Palierne, J. F. (1993). Linear viscoelastic behavior of some incompatible polymer blends in the melt. Interpretation of data with a model of emulsion of viscoelastic liquids. *Macromolecules, 26*(2), 320-329.

Gramespacher, H., Meissner, J. (1992). Interfacial tension between polymer melts measured by shear oscillations of their blends. *Journal of Rheology, 36*(6), 1127-1141.

Gross, R. A., Kalra, B. (2002). Biodegradable polymers for the environment. *Polymer*, 297, 803-807.

Grosvenor, M. P., Staniforth, J. N. (1996). The effect of molecular weight on the rheological and tensile properties of poly(ε-caprolactone). *International Journal of Pharmaceutics, 135*(1), 103-109.

Hatzikiriakos, S. G., Dealy, J. (1991). Wall slip of molten high-density polyethylene .1. sliding plate rheometer studies. *Journal of Rheology, 35*(4), 497-523.

Hatzikiriakos, S. G., Dealy, J. (1992a). Wall slip of molten high-density polyethylenes .2. capillary rheometer studies. *Journal of Rheology, 36*(4), 703-741.

Hatzikiriakos, S. G., Dealy J. (1992b). Role of slip and fracture in the oscillating flow of HDPE in a capillary. *Journal of Rheology, 36*(4), 845-884.

Hatzikiriakos, S. G., Dealy J. (1994). Start-up pressure transients in a capillary rheometer. *Polymer Engineering and Science, 34*(6), 493-499.

Hatzikiriakos, S.G., Migler, K. B. (2005). Overview of processing instabilities In S. G. Hatzikiriakos, K. B. Migler (Eds.1), *Polymer processing instabilities*. New York: Marcel Dekker.

Hatzikiriakos, S. G. (2012). Wall slip of molten polymers, *Progress in Polymer Science, 37*(4), 624-643.

Hong, Y., Coombs, S. J., Cooper-White, J. J., Mackay, M. E., Hawker, C. J., Malmstrom, E., Rehnberg, N. (2000). Film blowing of linear low-density polyethylene blended with a novel hyperbranched polymer processing aid. *Polymer, 41*(21), 7705-7713.

Hutmacher, D. W. (2000). Scaffolds in tissue engineering bone and cartilage. *Biomaterials, 21*(24), 2529-2543.

Ikada, Y., Tsuji, H. (2000). Biodegradable polyesters for medical and ecological applications. *Macromolecular Rapid Communications, 21*(3), 117-132.

Jenkins, M. J., Harrison, K. L. (2006). The effect of molecular weight on the crystallization kinetics of polycaprolactone. *Polymers for Advanced Technologies, 17*(6), 474-478.

Kamal, M. R., Lai-Fook, R., Demarquette, N. R. (1994). Interfacial tension in polymer melts. Part II: Effects of temperature and molecular weight on interfacial tension. *Polymer Engineering and Science, 34*(24), 1834-1839.

Kanev, D., Takacs, E., Vlachopoulos, J. (2007). Rheological evaluation and observations of extrusion instabilities of biodegradable polyesters. *International Polymer Processing, 22*(5), 395-401.

Kapnistos, M., Vlassopoulos, D., Anastasiadis, S. H. (1996) Determination of both the binodal and the spinodal curves in polymer blends by shear rheology. *Europhysics letter, 34*(7), 513-518.

Kapoor, B., Bhattacharya, M. (1999). Transient shear and extensional properties of biodegradable polycaprolactone. *Polymer Engineering and Science, 39*(4), 676-687.

Kasehagen, L. J., Macosko, C. W. (1998). Nonlinear shear and extensional rheology of long-chain randomly branched polybutadiene. *Journal of Rheology*, *42*(6), 1303-1327.

Kaye, A. (1962). *College of Astronauticsournal of Rheology-Note No. 134.* Cranford UK.

Khatiwala, V. K., Shekhar, N., Aggarwal, S., Mandal, U., K. (2008). Biodegradation of poly(ε-caprolactone) (PCL) film by alcaligenes faecalis. *Journal of Polymers and the Environment*, *16*(1), 61-67.

Koleske, J. V., Lundberg, R. D. (1969). Lactone polymers. II. Hydrodynamic properties and unperturbed dimensions of poly(ε-caprolactone). *Journal of Polymer Science Part A*, *7*(5), 897-907.

Kolnaar, J. W. H., Keller, A. (1997). A singularity in the melt flow of polyethylene with wider implications for polymer melt flow rheology. *Journal of Non-Newtonian Fluid Mechanics*, *69*(1), 71-98.

Kolybaba, M., Tabil, L. G., Panigrahi, S., Crerar, W. J., Powell, T., Wang, B. (2003). Biodegradable polymers: Past, Present, and Future. *ASAE*, 1-15.

Lacroix, C., Aressy, M., Carreau, P. J. (1997). Linear viscoelastic behavior of molten polymer blends: A comparative study of the Palierne and Lee and Park models. *Rheologica Acta*, *36*(4), 416-428.

La Mantia, F. P., Valenza, A., Paci, M., Magagnini, P., L. (1989). Liquid crystal polymers (LCP) as processing aids and reinforcing agents. A study of nylon 6/LCP blends. *Journal of Applied Polymer Science*, *38*(3), 583-589.

Larson, R. G. (1999). *The structure and rheology of complex fluids*. New York: Oxford University Press.

Lopez-Rodriguez, N., Lopez-Arraiza, L., Meaurio, E., Sarasua, J. R. (2006). Crystallization, morphology, and mechanical behavior of polylactide/poly(ε-caprolactone) blends. *Polymer Engineering and Science*, *46*(9), 1299-1308.

Labet, M., Thielemans, W. (2009). Synthesis of polycaprolactone: a review. *Chemical Society Reviews, 38*(12), 3484-3504.

Macosko, C. (1994). *Rheology principles, measurements and applicationss*. New York: Wiley-VCH.

Madbouly, S. A., Ougizawa, T. (2004). Rheological investigation of shear induced-mixing and shear induced-demixing for polystyrene/poly(vinyl methyl ether) blend. *Macromolecular Chemistry and Physics, 205*(9), 1222-1230.

Malkin, A. Y. (1994). *Rheology fundamentals*. Toronto: ChemTec Publishing.

Meredith, J. C., Amis, E. J. (2000). LCST phase separation in biodegradable polymer blends: poly(D,L-lactide) and poly(ε-caprolactone). *Macromolecular Chemistry and Physics, 201*(6), 733-739.

Migler, K. B. (2005). Sharkskin instability in extrusion In S. G. Hatzikiriakos, K. B. Migler (Eds.1), *Polymer processing instabilities*. New York: Marcel Dekker.

Mitsoulis, E., Hatzikiriakos, S. G. (2003). Bagley correction: the effect of contraction angle and its prediction. *Rheologica Acta, 42*(4), 309-320.

Mohanty, A. K., Misra, M., Hinrichsen, G. (2000). Biofibres, biodegradable polymers and biocomposites: An overview. *Macromolecular Materials and Engineering, 276*(1), 1-24.

Mooney, M. (1931). Explicit formulas for slip and fluidity. *Journal of Rheology,* 2, 210-222.

Na, Y. H., He, Y., Shuai, X., Kikkawa, Y., Doi, Y., Inoue, Y. (2002). Compatibilization effect of poly(ε-caprolactone)-b-poly(ethylene glycol) block copolymers and phase morphology analysis in immiscible poly(lactide)/poly(ε-caprolactone) blends. *Biomacromolecules, 3*(6), 1179-1186.

Nair, L. S., Laurencin, C. T. (2007). Biodegradable polymers as biomaterials. *Progress in Polymer Science, 32*(8), 762-798.

Narayan, R. (2006). Biobased and biodegradable polymer materials: Rationale, drivers, and technology exemplars In C. Scholz, K. C. Khemani (Eds.1), *Degradable Polymers and Materials: Principles and Practice*. Washington D.C: Oxford University Press.

Noroozi, N., Schafe,r L. L., Hatzikiriakos, S. G. (2012). Thermorheological properties of poly (ε-caprolactone)/ polylactide blends. *Polymer Engineering and Science, 52*(11), 2348-2359.

Okada, M. (2002). Chemical syntheses of biodegradable polymers. *Progress in Polymer Science, 27*(1), 87-133.

Onuki, A., Kawasaki, K. (1979). Nonequilibrium steady state of critical fluids under shear flow: A renormalization group approach. *Annals of Physics, 121*(1), 456-528.

Oriani, S. R., Chapman, G. R. (2003). Fundamentals of melt fracture elimination using flouropolymer process aids. *ANTEC,* 22-26.

Othman, N., Acosta-Ramirez, A., Mehrkhodavandi, P., Dorgan, J. R., Hatzikiriakos, S. G. (2011). Solution and melt viscoelastic properties of controlled microstructure poly(lactide). *Journal of Rheology, 55*(5), 987-1005.

Othman, N., Jazrawi, B., Mehrkhodavandi, P., Hatzikiriakos, S.G. (2012). Wall slip and melt fracture of poly(lactides). *Rheologica Acta,* 51,357-369.

Papanastasiou, A. C., Scriven, L. E., Macosko, C. W. (1983). Integral constitutive equation for mixed flows: viscoelastic characterization. *Journal of Rheology, 27*(4), 387-410.

Park, J., Todo, M. (2011). Compressive mechanical properties and deformation behavior of porous polymer blends of poly(ε-caprolactone) and poly(L-lactic acid). *Journal of Material Science, 46*(24), 7850-7857.

Pudjijanto, S., Denn, M. M. (1994). A stable "island" in the slip-stick region of linear low-density polyethylene. *Journal of Rheology, 38*(6), 1735-1744.

Ramamurthy, A. (1986). Wall slip in viscous fluids and influence of materials of construction. *Journal of Rheology, 30*(2), 337-357.

Ramkumar, D. H. S., Bhattacharya, M. (1998). Steady shear and dynamic properties of biodegradable polyesters. *Polymer Engineering and Science, 38*(9), 1426-1435.

Ray, S., Bousmina, M. (2005). Biodegradable polymers and their layered silicate nano composites: In greening the 21st century materials world. *Progress in Materials Science, 50*(8), 962-1079.

Reddy, C. S. K., Ghai, R., Rashmi, V., Kalia, V. C. (2003). Polyhydroxyalkanoates: an overview. *Bioresource Technology, 87*(2), 137-146.

Reich, S., Cohen, Y. (1981). Phase separation of polymer blends in thin films. *Journal of Polymer Science Part B: Polymer Physics, 19*(8), 1255-1267.

Rollon-Garrido, V. H., Wagner, M. H. (2009). The damping function in rheology. *Rheologica Acta, 48*(3), 245-284.

Rosenbaum, E. E., Randa, S. K., Hatzikiriakos, S. G., Stewart, C. W., Henry, D. L., Buckmaster, M., (2000). Boron nitride as a processing aid for the extrusion of polyolefins and flouropolymers. *Polymer Engineering and Science, 40*(1), 179-190.

Sarazin, P., Li, G., Orts, W. J., Favis, B. D. (2008). Binary and ternary blends of polylactide, polycaprolactone and thermoplastic starch. *Polymer, 49*(2), 599-609.

Scholz, P., Froelich, D., Muller, R. (1989). Viscoelastic properties and morphology of two-phase polypropylene/polyamide 6 blends in the melt. Interpretation of results with an emulsion model. *Journal of Rheology, 33*(3), 481-499.

Schwach, E., Averous, L. (2004). Starch-based biodegradable blends: morphology and interface properties. *Polymer International, 53*(12), 2115-2124.

Semba, T., Kitagawa, K., Ishiaku, U. S., Hamada, H. (2006). The effect of crosslinking on the mechanical properties of polylactic acid/polycaprolactone blends. *Journal of Applied Polymer Science, 101*(3), 1816-1825.

Sentmanat, M. (2004). Miniature universal testing platform: From extensional melt rheology to solid-state deformation behavior. *Rheologica Acta, 43*(6), 657-669.

Shimao, M. (2001). Biodegradation of plastics. *Current Opinion in Biotechnology*, *12*(3), 242-247.

Simoes, C. L., Viana, J. C., Cunha, A. M. (2009). Mechanical properties of poly(ε-caprolactone) and poly(lactic acid) blends. *Journal of Applied Polymer Science, 112*(1), 345-352.

Song, G. H., Murphy, R. J., Narayan, R., Davies, G. B. (2009). Biodegradable and compostable alternatives to conventional plastics. *Philosophical Transactions of the Royal Society of London. Series B, Biological Sciences, 364*(1526), 2127-2139.

Stanlake, L. J. E., Beard, J. D., Schafer, L. L. (2008). Rare-earth amidate complexes. Easily accessed initiators for epsilon-caprolactone ring-opening polymerization. *Inorganic Chemistry*, *47*(18), 8062-8068.

Steinmann, S., Gronski, W., Friedrich, C. (2002). Quantitative rheological evaluation of phase inversion in tow-phase polymer blends with cocontinuous morphology. *Rheologica Acta, 41*(1), 77-86.

Takayama, T., Todo, M. (2006). Improvement of impact fracture properties of PLA/PCL polymer blend due to LTI addition. *Journal of Materials Science, 41*(15), 4989-4992.

Teraoka, I. (2002). *Polymer Solutions: An Introduction to Physical Properties*. New York: Wiley.

Thomas, C., Peruch, F., Bibal, B. (2012). Ring-opening polymerization of lactones using supramolecular organocatalysts under simple conditions. *RSC Advances, 2*(33), 12851-12856.

Thomson, J. A., Schafer, L. L. (2012). Yttrium (amidate) complexes for catalytic C–N bond formation. Rapid, room temperature amidation of aldehydes. *Dalton Transactions, 41*(26), 7897-7904.

Tsuji, H., Horikawa, G. (2007). Porous biodegradable polyester blends of poly(L-lactic acid) and poly(ε-caprolactone): physical properties, morphology and biodegradation. *Polymer international, 56*(2), 258-266.

Tsuji, H., Horikawa, G., Itsuno, S. (2007). Melt-processed biodegradable polyester blends of poly(L-lactic acid) and poly(e-caprolactone): Effects of processing conditions on biodegradation. *Journal of Applied Polymer Science, 104*(2), 831-841.

Tsuji, H., Ikada, Y. (1996). Blends of aliphatic polyesters. I. Physical properties and morphologies of solution-cast blends from poly(DL-lactide) and poly(ε-caprolactone). *Journal of Applied Polymer Science, 60*(13), 2367-2375.

Urakawa, O., Takahashi, M., Masuda, T., Golshan Ebrahimi, N. (1995). Damping functions and chain relaxation in uniaxial and biaxial enxtensions: comparison with the Doi-Edwards Theory. *Macromolecules, 28*(21), 7196-7201.

Utracki, L. A. (1991). Two phase polymer systems. New York: Hanser.

Vlassopoulos, D., Koumoutsakos, A., Anastasiadis, S. H., Hatzikiriakos, S. G., Englezos, P. (1997). Rheology and phase separation in a model upper critical solution temperature polymer blend. *Journal of Rheology, 41*(3), 739-755.

Wagner, M. H. (1976). Analysis of time-dependent non-linear stress-growth data for shear and elongational flow of a low-density branched polyethylene melt. *Rheologica Acta, 15*(2), 136-142.

Wang, L., Ma, W., Gross, R. A., McCarthy, S. P. (1998). Reactive compatibilization of biodegradable blends of poly(lactic acid) and poly(ε-caprolactone). *Polymer Degradation and Stability, 59*(1), 161-168.

Woodruff, M. A., Hutmacher, D. W. (2010). The return of a forgotten polymer-Polycaprolactone in the 21st century. *Progress in Polymer Science*, 35(10), 1217-1256.

Wu, S. (1971). Calculation of interfacial tension in polymer systems. *Journal of Polymer Science Part C: Polymer Symposia*, 3*4*(1), 19-31.

Wu, D., Zhang, Y., Yuan, L., Zhang, M., Weidong, Z. (2010). Viscoelastic Interfacial Properties of Compatibilized Poly(ε-caprolactone)/ Polylactide Blend. *Journal of Polymer Science: Part B: Polymer Physics*, *48*(7), 756-765.

Wu, D., Zhang, Y., Zhang, M., Zhou, W. (2008). Phase behavior and its viscoelastic response of polylactide/poly(e-caprolactone) blend. *European Polymer Journal*, *44*(7), 2171-2183.

Yang, J. M., Chen, H. L., You, J. W., Hwang, J. C. (1997). Miscibility and crystallization of poly(L-lactide)/poly(ε-caprolactone) blends. *Polymer Journal*, *29*(8), 657-662.

Zhang, R., Cheng, H., Zhang C., Sun, T., Dong, X., Han, C. C. (2008). Phase separation mechanism of polybutadiene/polyisoprene blends under oscillatory shear flow. *Macromolecules*, *41* (18), 6818-6829.

Zhang, Y., Wu, D., Zhang, M., Zhou, W., Xu, C. (2009). Effect of steady shear on the morphology of biodegradable poly(ε-caprolactone)/polylactide blend. *Polymer Engineering and Science*, *49*(12), 2293-2300.

Zhang, Z. L., Zhang, H. D., Yang, Y. L., Vinckier, I., Laun, H. M. (2001). Rheology and morphology of phase-separating polymer blends. *Macromolecules*, *34*(5), 1416-1429.

Zou, F., Dong, X., Liu, W., Yang, J., Lin, D., Liang, A., Li, W., Han, C. C. (2012). Shear induced phase boundary shift in the critical and off-critical regions for a polybutadiene/polyisoprene blend. *Macromolecules*, *45*(3), 1692-1700.

Appendix A- Linear Viscoelastic Properties of PCL homopolymers

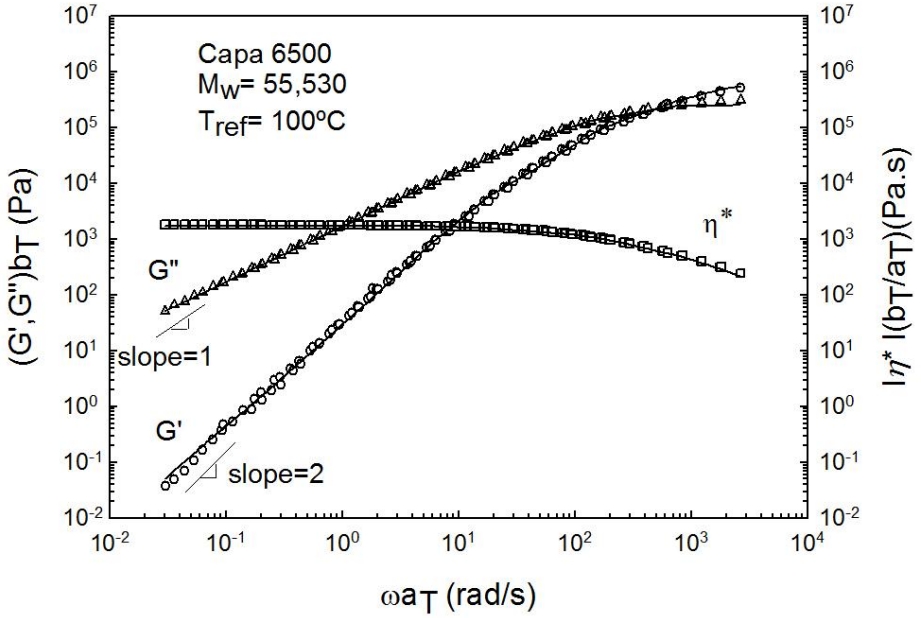

Figure A.0.1 Master curve of Capa®6500 at the reference temperature of 100°C.

Table A.1 Generalized Maxwell parameters, g_i (relaxation modulus) and λ_i (relaxation time) for Capa®6500 at 100°C.

g_i (Pa)	λ_i (s)
1.53×10^{5}	5.63×10^{-3}
3.81×10^{5}	9.22×10^{-4}
0.09×10^{5}	4.61×10^{-3}
0.00006×10^{5}	1.09×10^{0}
0.000002×10^{5}	1.07×10^{1}

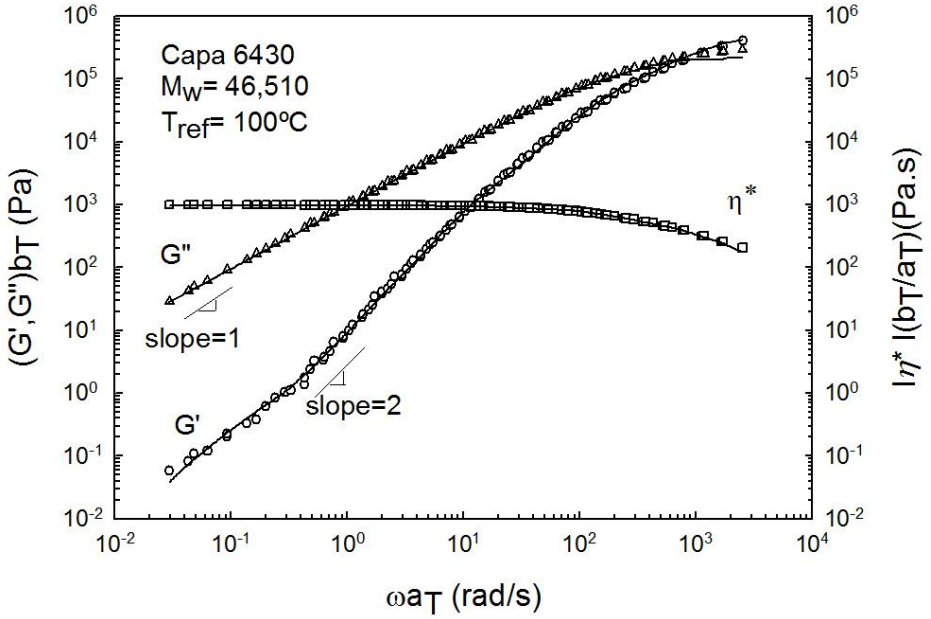

Figure A.0.2 Master curve of Capa®6430 at the reference temperature of 100°C.

Table A.2 Generalized Maxwell parameters, g_i (relaxation modulus) and λ_i (relaxation time) for Capa®6430 at 100°C.

g_i (Pa)	λ_i (s)
0.82×10^{5}	5.96×10^{-3}
3.41×10^{5}	9.49×10^{-4}
0.02×10^{5}	0.06×10^{0}
0.0×10^{5}	0.11×10^{1}
0.000003×10^{5}	1.09×10^{1}

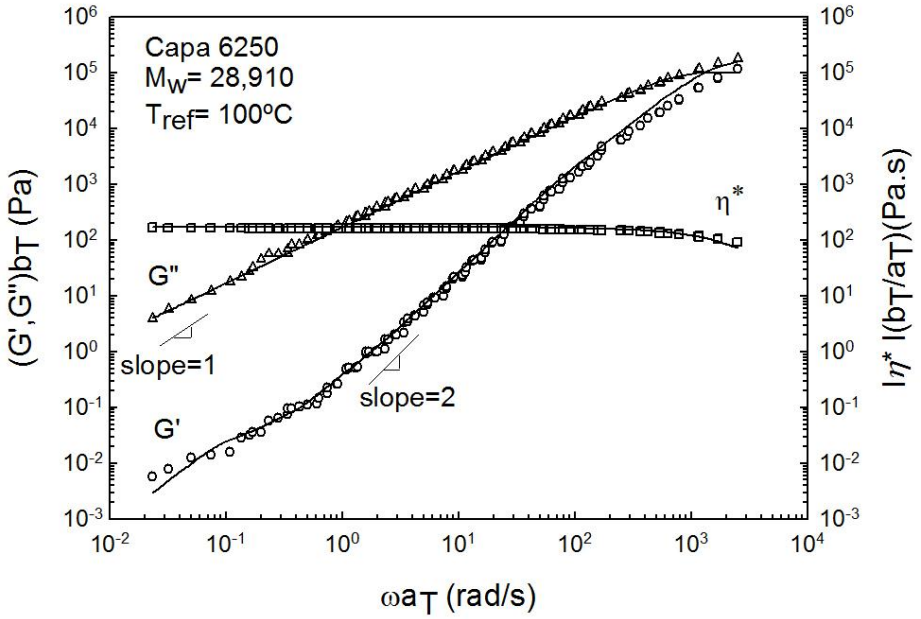

Figure A.0.3 Master curve of Capa®6250 at the reference temperature of 100°C.

Table A.3 Generalized Maxwell parameters, g_i (relaxation modulus) and λ_i (relaxation time) for Capa®6250 at 100°C.

g_i (Pa)	λ_i (s)
0.02×10^{5}	7.43×10^{-3}
1.54×10^{5}	6.61×10^{-4}
0.00001×10^{5}	1.29×10^{-1}
0.0000009×10^{5}	1.33×10^{0}
0.0000003×10^{5}	1.35×10^{1}

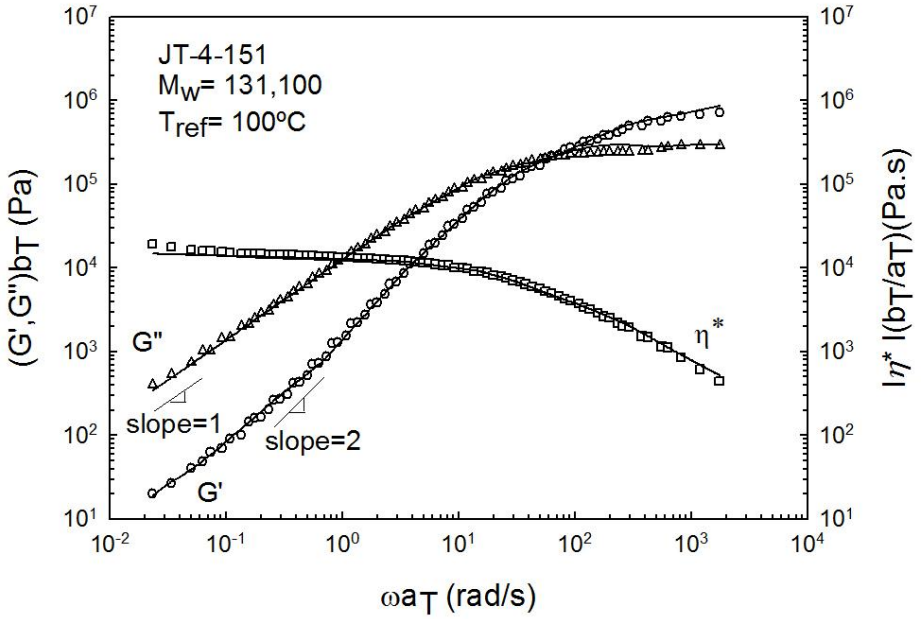

Figure A.0.4 Master curve of JT-4-151 at the reference temperature of 100°C.

Table A.4 Generalized Maxwell parameters, g_i (relaxation modulus) and λ_i (relaxation time) for JT-4-151 at 100°C.

g_i (Pa)	λ_i (s)
1.73×10^{5}	0.04×10^{0}
0.13×10^{5}	0.23×10^{0}
4.44×10^{5}	5.38×10^{-3}
0.003×10^{5}	3.85×10^{0}
0.0003×10^{5}	4.36×10^{1}

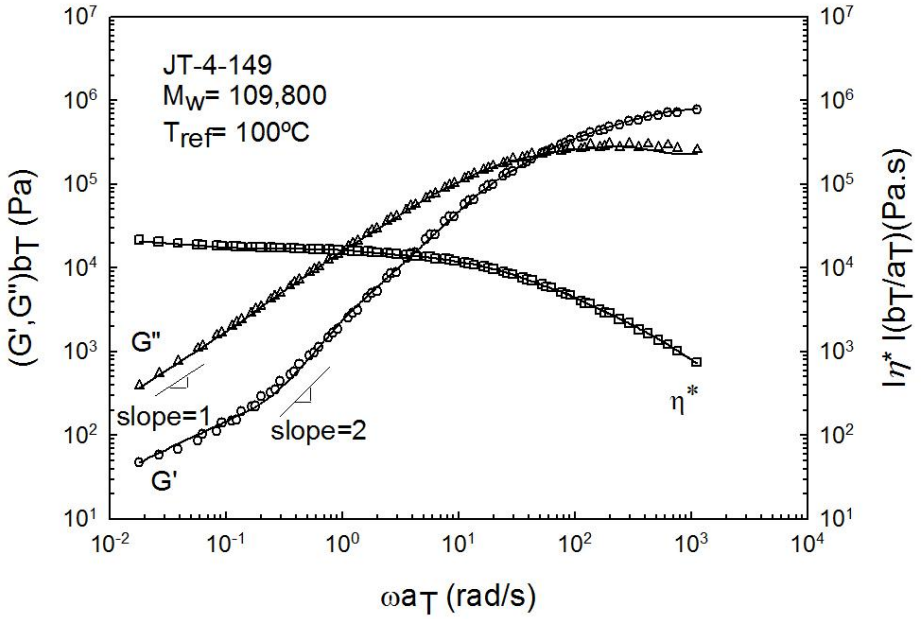

Figure A.0.5 Master curve of JT-4-149 at the reference temperature of 100°C.

Table A.5 Generalized Maxwell parameters, g_i (relaxation modulus) and λ_i (relaxation time) for JT-4-149 at 100°C.

g_i (Pa)	λ_i (s)
0.94×10^{5}	0.73×10^{-1}
0.04×10^{5}	3.19×10^{-3}
2.85×10^{5}	1.78×10^{-2}
0.06×10^{5}	6.13×10^{-1}
0.001×10^{5}	4.16×10^{1}

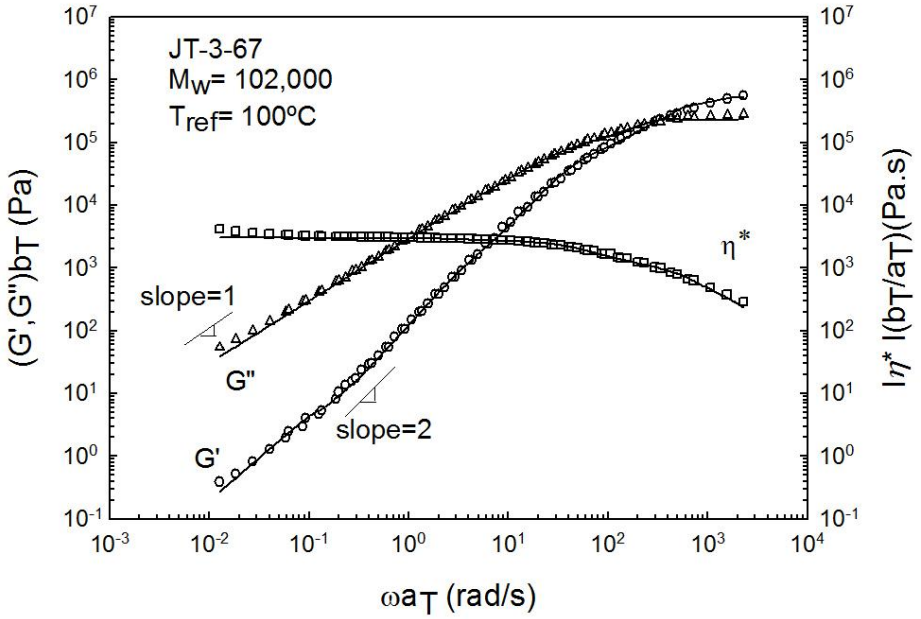

Figure A.0.6 Master curve of JT-3-67 at the reference temperature of 100°C.

Table A.6 Generalized Maxwell parameters, g_i (relaxation modulus) and λ_i (relaxation time) for JT-3-67 at 100°C.

g_i (Pa)	λ_i (s)
0.79×10^{5}	0.02×10^{0}
4.18×10^{5}	2.25×10^{-3}
0.01×10^{5}	2.52×10^{-1}
0.0001×10^{5}	2.08×10^{0}
0.00003×10^{5}	2.36×10^{1}

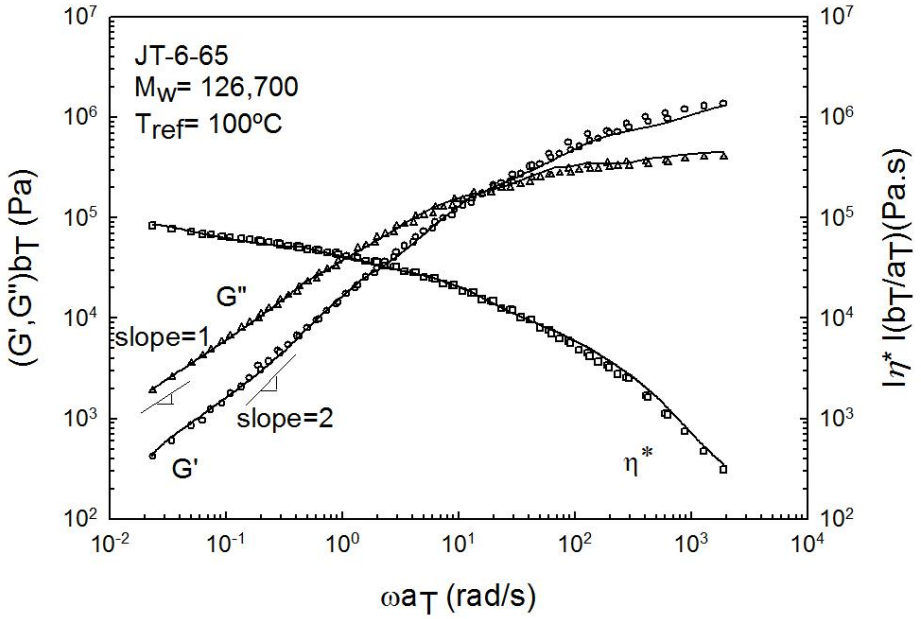

Figure A.0.7 Master curve of JT-6-65 at the reference temperature of 100°C.

Table A.7 Generalized Maxwell parameters, g_i (relaxation modulus) and λ_i (relaxation time) for JT-6-65 at 100°C.

g_i (Pa)	λ_i (s)
5.26×10^{5}	0.01×10^{0}
7.53×10^{5}	7.91×10^{-4}
1.91×10^{5}	0.11×10^{0}
0.24×10^{5}	0.11×10^{1}
0.02×10^{5}	2.14×10^{1}

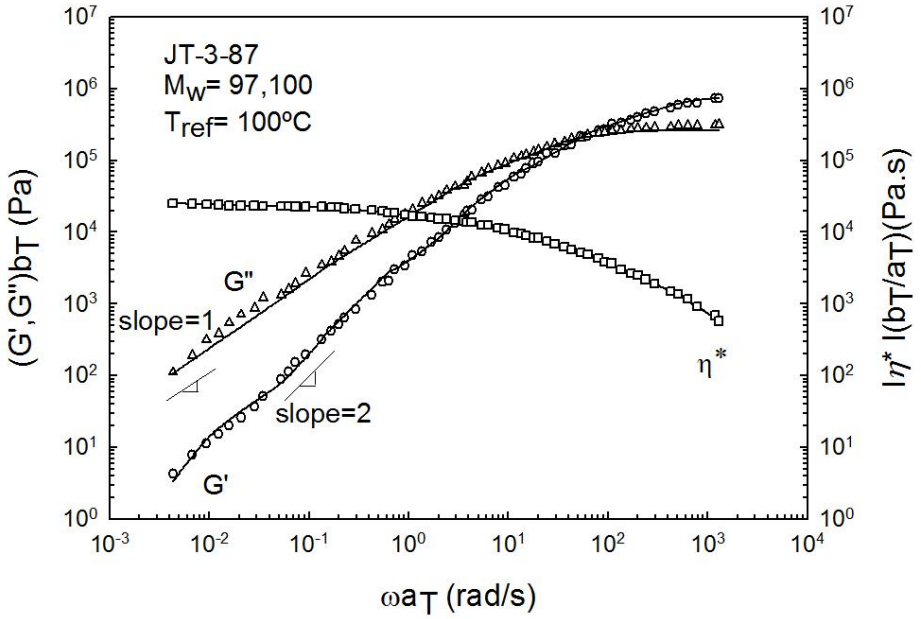

Figure A.0.8 Master curve of JT-3-87 at the reference temperature of 100°C

Table A.8 Generalized Maxwell parameters, g_i (relaxation modulus) and λ_i (relaxation time) for JT-3-87 at 100°C.

g_i (Pa)	λ_i (s)
2.63×10^{5}	0.02×10^{0}
4.08×10^{5}	2.98×10^{-3}
0.62×10^{5}	0.15×10^{0}
0.03×10^{5}	0.22×10^{1}
0.0003×10^{5}	6.86×10^{1}

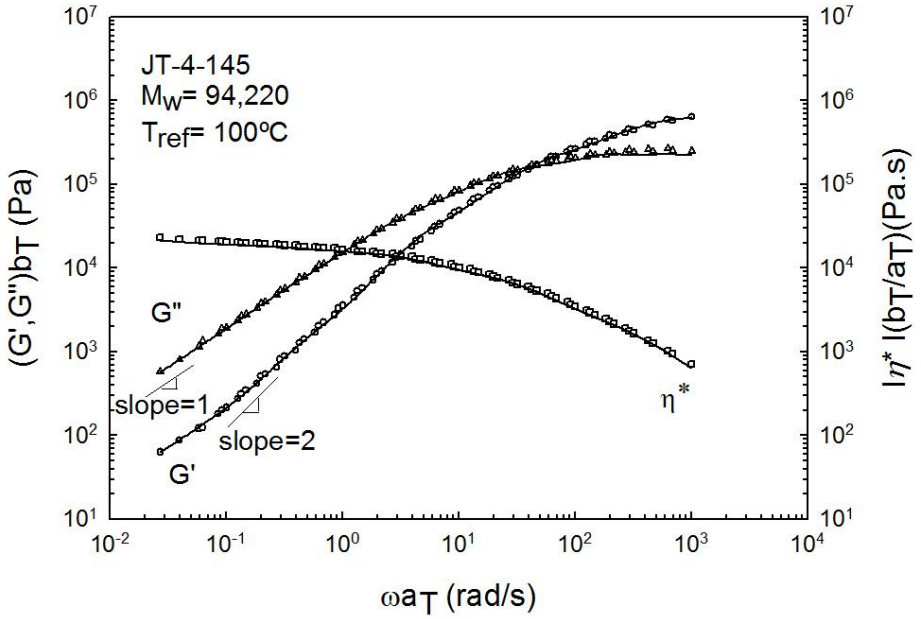

Figure A.0.9 Master curve of JT-4-145 at the reference temperature of 100°C.

Table A.9 Generalized Maxwell parameters, g_i (relaxation modulus) and λ_i (relaxation time) for JT-4-145 at 100°C.

g_i (Pa)	λ_i (s)
3.95×10^{5}	3.65×10^{-3}
1.97×10^{5}	0.03×10^{0}
0.35×10^{5}	0.22×10^{0}
0.01×10^{5}	0.24×10^{1}
0.001×10^{5}	3.29×10^{1}

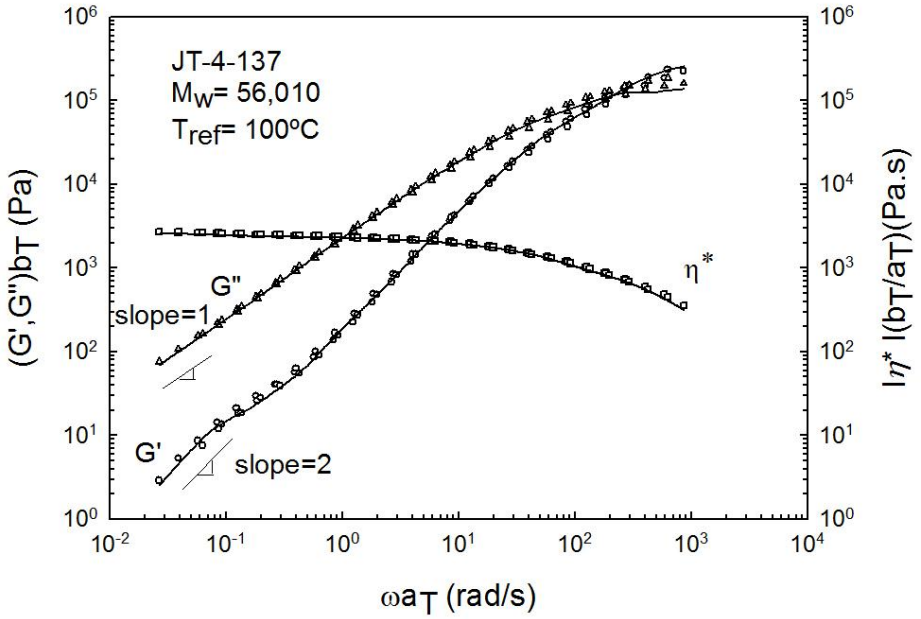

Figure A.10 Master curve of JT-4-137 at the reference temperature of 100°C.

Table A.10 Generalized Maxwell parameters, g_i (relaxation modulus) and λ_i (relaxation time) for JT-4-137 at 100°C.

g_i (Pa)	λ_i (s)
0.51×10^{5}	0.02×10^{0}
2.05×10^{5}	3.03×10^{-3}
3.95×10^{5}	1.01×10^{-1}
0.05×10^{5}	3.65×10^{-3}
0.0002×10^{5}	1.42×10^{1}

Appendix B- Capillary Rheometry

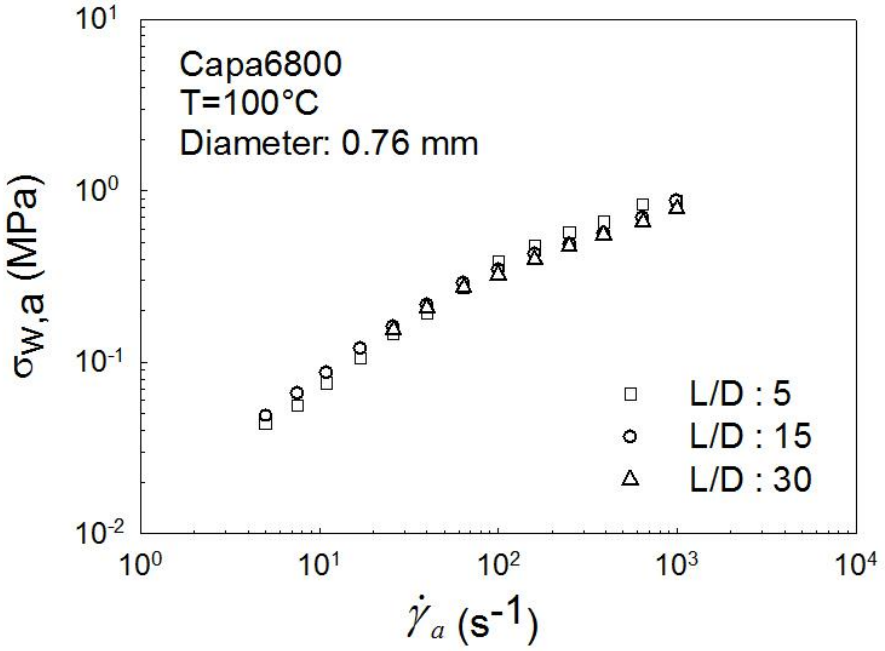

Figure B.0.1 The apparent flow curves of PCL Capa®6800 at 100°C using three capillary dies having a constant diameter of 0.76 mm and different *L*/*D* ratio to determine the effect of pressure on viscosity.

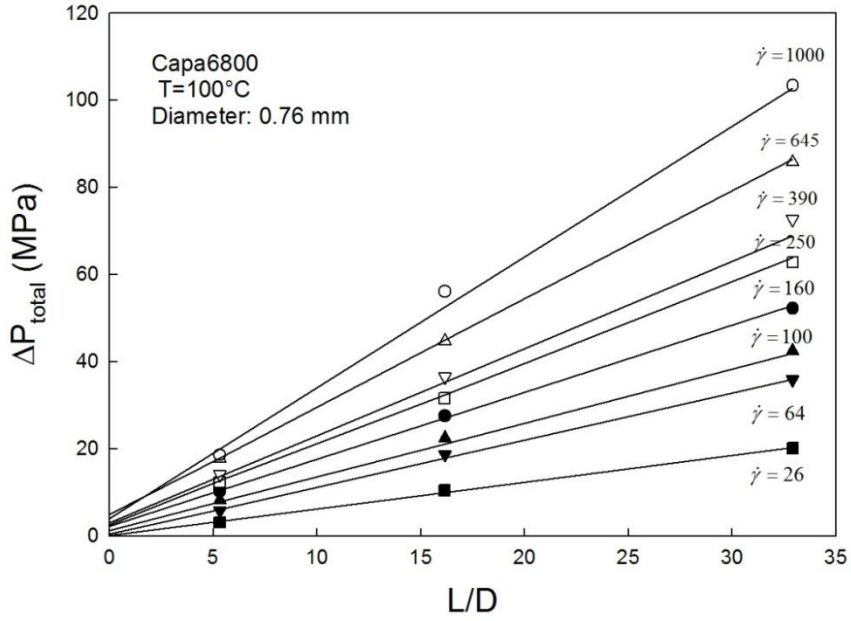

Figure B.0.2 Bagley plot to determine the end pressure for Capa®6800 at 100°C for a set of dies with a constant diameter of 0.76mm.

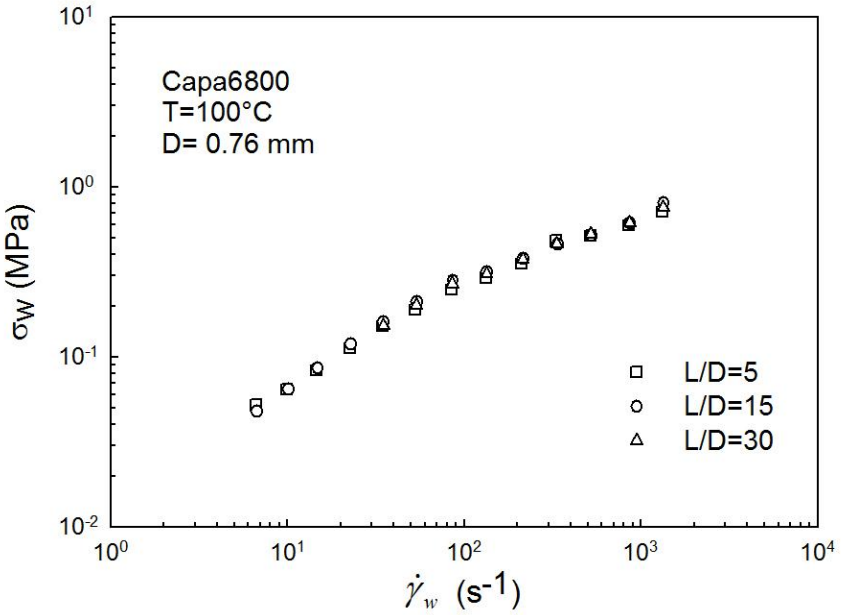

Figure B.0.3 The Bagley-corrected flow curves of PCL Capa®6800 at 100°C using three capillary dies having a constant diameter of 0.76mm and different *L*/*D* ratio. Superposition of the data implies that the effect of pressure on viscosity is insignificant.

Appendix C- Mechanical Properties

Table C.1 Mechanical properties of PCL Capa®6800/ PLA2002D blends.

PLA 2002D (wt%)	*Tensile strength (MPa)*	*Elastic modulus (GPa)*	*Elongation at break (%)*
0	14.9± 0.8	0.4±0.06	613.1±33.9
20	17.6±0.4	0.8±0.05	333.8±32.9
40	18.4±0.5	1.0±0.06	54.2±10.1
60	27.4±0.9	1.6±0.08	18.7±5.6
80	39.5±1.4	2.5±0.09	15.7±3.4
100	49.8±2.3	3.1±0.11	7.5±0.4